Synthesis, Characterization, and Self –Assembly of Size Tunable Gold Nanorods

A Dissertation
Presented to
The Academic Faculty

by
Kyoungweon Park

In Partial Fulfillment
of the Requirements for the Degree
Doctor of Philosophy in the
School of Polymer, Textile and Fiber Engineering

Georgia Institute of Technology
December 2006

Synthesis, Characterization, and Self –Assembly of Size Tunable Gold Nanorods

Approved by:

Dr. Mohan Srinivasarao, Advisor
School of Polymer, Textile & Fiber Engineering
Georgia Institute of Technology

Dr. Robert Dickson
School of Chemistry and Biochemistry
Georgia Institute of Technology

Dr. Mostafa A.El-Sayed
School of Chemistry and Biochemistry
Georgia Institute of Technology

Dr. Anselm Griffin
School of Polymer, Textile & Fiber Engineering
Georgia Institute of Technology

Dr. Jung O. Park
School of Polymer, Textile and Fiber Engineering
Georgia Institute of Technology

Dr. Laren M. Tolbert
School of Chemistry and Biochemistry
Georgia Institute of Technology

Date Approved: September 19, 2006

ACKNOWLEDGEMENTS

To my research advisor, Dr. Mohan Srinivasarao, for his support, guidance, and encouragement.

To my committee, comprised of Drs. Jung O. Park, Anselm Griffin, Mostafa El-Sayed, Robert Dickson, and Laren Tolbert, for their guidance and cooperation during my research.

To my research group, Jong Seung Park, Vivek Sharma, Matije Crne, Lulu Song , Jian Zhou, Haixia Wu and Raymond René, for great discussions and enjoyable moments.

To the members of the New Church of Marietta, for their love and prayer.

To my parents, Jae-Yoon Park and Sam-Sun Hur, and my sisters, Kyoung-Hee, Kyoung-Ah and my brother Mum-hm, for their bottomless love, support, and prayer. I could not have done this without them.

Most especially, to my son, Caleb for making my life full of delight which I have been blessed with since he was born.

TABLE OF CONTENTS

LIST OF TABLES

LIST OF FIGURES

LIST OF SCHEMES

Summary

The successful applications of nanoparticles require the ability to tune their properties by controlling size and shape at the nanoscale. In metal nanomaterial research, the optical properties have been of interest especially because of the applications to medical diagnostics and nanooptics. It is important to prepare nanoparticles of well-defined shape and size for properly characterizing the optical properties.

We describe improved seed mediated synthesis of gold nanorods (GNRs) producing a high yield of NRs with low polydispersity and few byproducts. The efficient separation of GNRs from mixture of shapes is achieved by understanding the hydrodynamics of nanoparticles undergoing centrifugation. The optical properties of resulting refined GNRs are compared to predictions of existing theories, and the main parameters affecting them are discussed.

GNRs with well defined aspect ratios are introduced into a polyvinyl alcohol matrix by means of solution-casting techniques. The film is drawn to induce the uniaxial alignment of GNRs to be used as color polarizing filters. We prepare GNR polarizing filter with different peak positions ranging from visible to near infra red by

using different aspect ratio of NRs.

To utilize GNRs to make nanoscale devices, spatial organization is required. We characterize the self-assembly of GNRs observed on a TEM grid. The drying process is accompanied by complex hydrodynamic and thermodynamic events, which create rich range of patterns observed. Being anisotropic in shape, the rods can form liquid crystal (LC) assemblies above a certain concentration. We observed LC phase of GNRs by resorting to an evaporation of aqueous NR solution. The convective flow caused by the solvent evaporation carries NRs from the bulk solution to solid-liquid-air interface, which makes the solution locally very concentrated driving the phase transition of NRs. We calculate the order parameter from various assemblies observed, and compare the observed phase behavior to the one expected on the basis of theory.

Chapter I

Introduction

Gold nanoparticles (NPs) have been known as "colloidal gold" long before the development of modern gold chemistry. It dates back to the time when colloidal gold was used as a colorant to make ruby glass and ceramic in the 5th century B.C.[1] However, Faraday was the first to recognize that the brilliant color is due to the presence of the metallic gold in colloidal form in 1857[2]. He reported the formation of deep red solutions of colloidal gold by reduction of an aqueous solution of chloroaurate ($AuCl_4^-$) using phosphorus in CS_2 (a two-phase system). In the 20th century, various methods for the preparation of gold colloids were reported [3,4,5]. The most popular one for a long time has been using citrate reduction of $HAuCl_4$ in water, which was introduced by Turkevitch in 1951[3].

With the advent of nanotechnology, gold NPs have turned out to play an important role in the field because they have the potential to serve as building blocks for putting nanotechnology to practical use[6,7].

Much progress has been made in the synthesis of spherical gold NPs in the past decades, and the influence of particle radius on the physical, chemical, optical, electronic and catalytic properties of the material have been broadly studied[8].

By suitable choice of experimental conditions and additives, non-spherical

shape of NPs such as rods, wires, tubes and concentric core-shell structures have been successfully synthesized and they are found to possess properties which depend not only on the size but also on other topological aspects[9]. Nanorods (NRs) have drawn the most attention because they can be synthesized using a relatively simple process such as wet chemical methods and the rational control over the aspect ratio is possible. Gold NRs show different color depending on the aspect ratio, which is due to the two intense surface plasmon resonance peaks (longitudinal surface plasmon peak and transverse surface plasmon peak corresponding to the oscillation of the free electrons along and perpendicular to the long axis of the rods)[9]. The color change provides the opportunity to use gold NRs as novel optical applications. There have been many applications utilizing this intense color and its tunablity[10]. One of them is in the field of biological system. NRs bind to specific cells with greater affinity and one can visualize the conjugated cell using a simple optical microscope due to the enhanced scattering cross section[11]. This is how gold NRs are used in molecular biosensor for the diagnosis of diseases such as cancer.

NRs show enhanced fluorescence over bulk metal and nanospheres, due to the large enhancement of the longitudinal plasmon resonance[12], which will prove to be beneficial in sensory applications. The increase in the intensity of the surface plasmon resonance absorption results in an enhancement of the electric field and

surface enhanced Raman scattering of molecules adsorbed on gold NRs[13].

All theses properties make gold NR a good candidate for future nanoelectronics, once appropriate techniques allow for the generation of artificial structures in 2D or 3D. All of these properties have lead to a dramatic growth in the publications related to gold NRs.

The key issue in the successful applications of NPs is how to organize individual NP into a well defined macroscopic structure having a particular configuration which shows interesting new collective physical properties that are different from those of the NPs as well as the original bulk materials. And the ability to tune their properties by controlling size, shape and surface modifications of individual particles is very important.

While the number of publications on gold NR research, to date, has been increasing dramatically, the specific mechanisms governing the morphology and geometry control over particle growth are still far from being well understood, and the reproducibility of the synthesis is poor. Therefore, the application is often demonstrated without the proper characterization of the sample, thus leading to results that are not necessarily reproducible by various research groups.

In this study, we have to carefully re-examine the process of synthesis, characterization and application of gold NR to have better understanding and insight of gold NR research. The objective of this study can be summarized as following.

- To gain a better understanding of growth mechanism of gold NRs.
- To achieve the ability to tune the shape and size of gold NRs, quite reproducibly.
- Proper characterization of optical properties, with well characterized samples, obtained by understanding the principles behind the shape separation of particles.
- To fabricate superstructures using well defined gold NRs.

Following this introduction, Chapter 2 describes the modified seed-mediated synthesis of gold NRs by which the morphology, mainly the aspect ratio of gold NRs can be controlled by the choice of experimental conditions and additives. The parameters such as the type, concentration and combination of surfactants, reducing agent, temperarture, and additives are extensively discussed. We also describe the manipulation of the synthesis steps to obtain a desired aspect ratio of gold NRs. In chapter 3, growth mechanism of gold NRs will be proposed based on the data in literature and our experimental results in chapter 2. Chapter 4 describes the hydrodynamic behavior of NPs of various shapes to identify the parameters to achieve efficient separation of NRs from other shape of NPs. Chapter 5 and 6 are devoted to

the optical properties of gold NRs in various dielectric media including polymer matrix, and the potential application of polarizing color filter is described. In chapter 7, we demonstrate and analyze varied range of structured aggregates and spatial patterns formed by the drying of thin gold NRs solution films. In chapter 8, we accomplish the experimental observations of lyotropic liquid crystalline phases of colloidal gold NRs by achieving the phase transition volume fraction through the convective flow resulting from the solvent evaporation.

References

[1] Pollard, A.P.; Heron, C. “Archaeological Chemistry” Royal Society of Chemistry, **1996;** Chapter 5.

[2] Faraday, M. “Experimental Relations of Gold (and other metals) to Light” *Philos. Trans.* **1857**, *147*, 145.

[3] Turkevitch, J.; Stevenson, P. C.; Hillier, J. “Nucleation and Growth Process in the Synthesis of Colloidal Gold” *Discussions of the Faraday Society* 1951, *11*, 55.

[4] Frens, G. “Controlled Nucleation for the Regulation of the Particle Size in Monodisperse Gold Suspensions. *Nature: Phys. Sci.* 1973, 241, 20.

[5] Hayat, M. A. “Colloidal Gold, Principles, Methods and Applications” Academic Press: New York, 1989.

[6] Pellegrino,T.; Kudera, S.; Liedl,T.; Javier,A.M.; Manna,L.; Parak,W.J. “On the Development of Colloidal Nanoparticles towards Multifunctional Structures and their Possible Use for Biological Applications” *Small* **2005**,*1*,48.

[7] Elghanian, R.; Storhoff, J.J.; Mucic, R.C.; Letsinger, R.L.; Mirkin, C.A. “Selective colorimetric detection of polynucleotides based on the distance-dependent optical properties of gold nanoparticles” *Science* **1997**, *277*,1078.

[8] Marie-Christine,D.; Didier,A. “Gold nanoparticles: assembly, supramolecular chemistry, quantum-size-related properties, and applications toward biology, catalysis, and nanotechnology” *Chemical reviews* **2004,** *104*, 293 and references therein.

[9] Kelly, K. L.; Coronado, E.; Zhao, L. L.; Schatz, G. C. “The optical properties of metal nanoparticles: The influence of size, shape, and dielectric environment” *J. Phys.Chem. B.* 2003, *107*, 668.

[10] Pérez-Juste,J.; Pastoriza-Santos ,I.; Liz-Marzán ,L.M.; Mulvaney, P. “Gold nanorods: Synthesis, characterization and applications” *Coordination Chemistry Reviews* **2005**, *249*, 1870.

[11] El-Sayed,I.H.; Huang,X.; El-Sayed,M.A., “Surface Plasmon Resonance

Scatteringand Absorption of anti-EGFR Antibody Conjugated Gold Nanoparticles in Cancer Diagnostics: Applications in Oral Cancer" *Nano Lett.*, **2005,** *5*, 829.

[12] Eustis,S.; El-Sayed, M.A., "Aspect Ratio Dependence of the Enhanced Fluorescence Intensity of Gold Nanorods: Experimental and Simulation Study" *J. Phys. Chem. B* **2005**, *109,* 16350.

[13] Nikoobakht, B.; Wang, J.; El-Sayed, M. A., "Surface-enhanced Raman scattering of molecules adsorbed on gold nanorods: off-surface plasmon resonance condition" *Chemical Physics Letters* 2002, 366, 17.

Chapter II

Synthesis of Refined Gold Nanorods in Binary Surfactant System

Abstract

The morphology of gold nanorods(NRs) is controlled by manuplating the reduction condition thus changing the reduction kinetics and the adsorption kinetics of the surfactant on the surface of growing NR. The parameters affecting the adsorption kinetics such as types, and concentration of surfactant can also affect the reduction kinetics. Hexadecyltrimethylammonium bromide (CTAB) forms the precusor of gold-surfactant complex which has a lower redox potential to influence reduction reaction. Benzyldimethylhexadecylammonium chloride (BDAC) as a cosurfactant lowers the 1^{st} and 2^{nd} critical micelle concentration(CMC) of the surfactant solution promoting the formation of bigger micelle with anisotropic shape which is benefitial to keep the precursor inside to prevent instant reduction and the efficient confinement of growing surface of gold NR. Our results show that the adsorption competes with the reduction of gold ion on the same surface of NR. When reduction rate is slower, long NRs with smaller diameter are obtained while when reduction is faster, short NRs with larger diameter are obtained.

2.1. Introduction

A common top down technique to prepare gold nanorods (NRs) is electron beam lithography [1]. This technique has the advantage of preparing highly monodisperse NRs but it can only create a 2-dimensional structure in a single step and the instrumentation is expensive. For bottom up techniques, two different approaches are available to synthesize gold NRs. One is using hard templates to physically confine the growth such that gold ions are only reduced inside this template[2]. The growth mechanism is straightforward and the size and shape of the NRs are predetermined by the size and shape of the template. This method has advantages for obtaining monodisperse particles. But large scale synthesis is limited since it requires nanoporous templates. In the other method, the gold ions are reduced in the presence of capping materials (also called stabilizers since it stabilizes the colloidal NPs) which bind to the surface of growing nanoparticle to direct the formation of NRs (we will call this method as a single batch preparation). As for the reduction path, one can choose photochemistry (UV-irradiation), electrochemistry, bio-reduction or chemical reduction. The size and shape of the NRs are determined by the various experimental parameters that affect the growth mechanism. However, the specific mechanisms governing morphology and geometry control over particle growth are not yet explicitly understood.

We have been particularly interested in the single batch preparation of gold NRs where various experiment parameters such as concentration of reactants and temperature have an effect on the morphology of NRs.

In the following, we summarize the most commonly used methods to grow gold NRs by chemical reduction.

Gold nanoparticles (NPs) has bee known as colloidal gold for centuries. This dates back to the time when colloidal gold was used as a colorant to make ruby glass and ceramic in the 5th century B.C.[3] However, Faraday was the first to recognize in 1857[4] that the brilliant color is due to the presence of the metallic gold in colloidal form. He reported the formation of deep red solutions of colloidal gold by reduction of an aqueous solution of chloroaurate ($AuCl_4^-$) using phosphorus in CS_2 (a two-phase system). In the 20th century, various methods for the preparation of gold colloids were reported and reviewed[5,6]. The most popular one for a long time has been using citrate reduction of $HAuCl_4$ in water, which was introduced by Turkevitch in 1951[7].

Since rod-like gold particles were observed as a byproduct of spherical NPs in 1992[8], many efforts have been made to move beyond conventional spherical growth to achieve shape control.

In the first observation of rod-like gold particles, UV-irradiation was used as a

reduction path and with alkyltrimethylammonium chlorides as a stabilizer. Synthesis condition such as type and concentration of surfactant and duration of UV-irradiation has been modified to prepare NRs in majority[9,10,11]. However, the results have been rather unsuccessful. Kim et al. also used UV-irradiation to produce NRs [12]. They changed the type of stabilizer to hexadecyltrimethylammonium bromide (CTAB) and tetradodecylammonium bromide. They were able to prepare NRs as the major component with the aspect ratio up to 5. The aspect ratio of the rods was controlled by the amount of silver ions (of $AgNO_3$) added to the system. More recently, combination of chemical reduction of tetrachloroaurate by ascorbic acid and subsequent UV-irradiation resulted in the quick generation of gold NRs[13]. By UV-irradiation method, gold NRs having aspect ratio less than 5 are obtained. However, this method has a limitation to produce a large quantity of NRs since the reactor size is limited.

Meanwhile, an electrochemical method was developed by Yu et al. in which the gold ions were reduced on a platinum electrode in the presence of a solution of surfactant mixture[14]. CTAB and tetraoctylammonium bromide (hydrophobic) were used as surfactants above their critical micelle concentration (CMC). This method is simple, and NRs can be prepared in a short time.

Jana et al. [15] modified the seed-mediated synthesis of nanospheres[16] to obtain NRs by changing the concentration of surfactant and adding $AgNO_3$. Gold nanospheres are made by chemical reduction of a gold salt with a strong reducing agent (such as sodium borohydride). These seeds are then added to a growth solution of gold salt, a weak reducing agent and CTAB. No metal salts are reduced to metal unless the seeds are present where the seeds serve as nucleation sites for NRs.

The seed-mediated synthesis of gold NRs provides rods with higher aspect ratios than those prepared by other methods. This method was further developed into sequential growth method in which NRs grown from the previous synthesis were used as seed to grow longer NRs(eg., the aspect ratio of 25)[17].

Besides the methods mentioned above, various other approaches have been attempted to produce gold NRs, such as bio-reduction[18] and growth of gold NRs directly on mica surface[19].

In any case, the ultimate aim of the research has been to obtain controlled size and shape of NRs with less byproduct and to understand the effect of various experimental parameters on the growth mechanism and finally on the morphology of NRs.

2.1.1. The effect of surfactants

The role of surfactant in NRs formation is critical since both the growth and

the shape of the particles are greatly controlled by the condition of surfactant used. At first, it was believed that the rod-like micelle formed by surfactant provides soft template for rod formation[13]. But recently many researchers concluded that surfactant monomer adsorption takes place preferentially on specific faces so that the growth in the diameter direction is constrained promoting the growth in the length direction[20] . In fact, the concentration of CTAB used in most synthesis is lower than the 2nd CMC above which the micelle becomes rod shape[21].

CTAB is widely used in the synthesis of NRs (or NPs) in all reduction paths. The concentration of CTAB determines the shape of NPs. Below CMC, the reduction primarily results in nanospheres[22]. Only above CMC, anisotropic shape develops as the major product[15].

Binary surfactant system was originally used in electrochemical method[14] and later adapted for other reduction paths. Surfactants which have much more hydrophobic head groups were usually used as cosurfactant to induce the rod shape.

Babak et al. were the first to introduce binary surfactant system in the seed-mediated method[20]. In this case, more hydrophobic surfactant (benzyldimethylammonium chloride (BDAC)) was used along with CTAB. By increasing the ratio of BDAC/CTAB from 2 to 16, the aspect ratio of NRs increased. Thus, this approach provides rods with fairly good uniformity, higher yield, and yet

little byproduct. However, the role played by the cosurfactant was not clearly understood.

The role of CTAB in the synthesis of NRs has been extensively discussed [15,17,20] and the consensus is that CTAB adsorbs preferentially on to the specific crystal facet of the gold NPs, thus confining the growth direction.

2.1.2. The reduction

In most methods of synthesis of gold NPs, the chemical principle is the reduction of gold (III) derivatives, chloroaurate ($AuCl_4^-$) in an aqueous solution. Reduced gold atoms start to form small sub-nanometer particles (nucleation). The gold atoms that appear later stick to the existing particles (growth). To prevent the particles from aggregating, the solution is stirred vigorously and a stabilizing agent is usually added to the mixture.

In UV-irradiation and electrochemical reduction, Au^{+3} is reduced to Au^0. In the seed-mediated method, ascorbic acid (AA) is often used as a mild reducing agent to reduce the gold ion from Au^{+3} to Au^{+1}, and then the reduction to Au^0 only begins when the seed solution is added. The amount of AA added was not the same in scattered reports and the variation in the size and shape of the NPs produced was not trivial [15,20]. The effect of the type and concentration of reducing agent on the size and shape of spherical gold particle was investigated[23,24]. But little attention has

been devoted to the effect of reducing agent on the formation of NRs.

The driving force for the reaction is the difference between the redox potentials (ΔE) of the two half cell reactions (reduction of gold ion and oxidation of reducing agent). An increase in the value of ΔE translates into a more spontaneous reaction. The kinetics of reaction is also governed by the concentration of reactants, temperature and pH. Therefore, by changing the type of reducing agent, pH, temperature, and the concentration of reactants, one can exert control on the size, shape and morphology of the particle. As for the spherical particles, it is not so complicated to relate the parameters that affect the reaction kinetics to the final morphology. For example, strong reducing agents such as $NaBH_4$ or phosphorus produce small gold particles while mild reducing agents like ascorbic acid produce larger gold particle which can be explained by decreasing ΔE. Decreasing the particle size upon increasing the concentration of the stabilizing agent can be explained by better stabilization[24]. A mechanism for anisotropic particle formation is still a problem awaiting complete solution.

In attempting to provide a mechanism for the synthesis of gold NRs, the key issue is why the particle grows faster in one direction in comparison to the other direction. The role of CTAB in the synthesis of NRs has been extensively discussed [15,17,20] and the consensus is that CTAB adsorbs preferentially on to the specific crystal

facet of the gold NPs, thus confining the growth direction. Then the adsorption and reduction kinetics should greatly affect the morphology of NR as has been found in the literature[9-20]. Then in order to control the growth of NPs, one should be able to manipulate the adsorption and reduction kinetics so that the gold particles grow slowly, while the stabilizing agent can exert control over the growth direction. In this chapter, we focus on the parameters which we believe exert control over the rate of reduction and adsorption.

We prepared NRs by the modified seed-mediated method[20]. As has been noted above, this method provides rods with high aspect ratios (up to L/d=25), fairly good uniformity, higher yield, and with fewer byproducts, thus allowing us to focus on establishing the growth mechanism of NRs. Primitive gold NPs were made by the chemical reduction of a gold salt with a strong reducing agent such as sodium borohydride. These seeds are then added to a growth solution that contains gold salt, a weak reducing agent, surfactants and $AgNO_3$. CTAB was used as stabilizer in both the seed and the growth solution.

2.2. Experimental

CTAB and BDAC (chemical structures are shown in Scheme 2.1) were purchased from TCI America. The quality of the CTAB and BDAC is critical because the minor impurities (most likely cetyldimethylamine) can result in much faster rates of reduction preventing the reproducible preparation of NPs[25]. The chemicals purchased from other company do not give reproducible result even after multiple recrystallization procedures.

All other chemicals were purchased from Sigma-Aldrich. Deionized water (18 MΩ) was used in all the experiments. For preparation of NRs, seed and growth solutions were made as described below.

CTAB BDAC

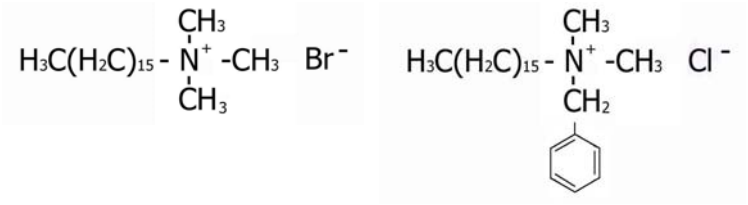

Scheme 2.1. Structures of hexadecyltrimethylammoniumbromide (CTAB) and benzyldimethylammoniumchloride (BDAC). The latter has a bulkier head group.

2.2.1. Preparation of the seed solution

Seed solution was prepared by mixing CTAB solution (5.0 mL, 0.20 M) with 5.0 mL of 0.00050 M $HAuCl_4$. To the stirred solution, 0.60 mL of ice-cold 0.010 M $NaBH_4$ was added, which resulted in the formation of a brownish yellow solution.

Vigorous stirring of the seed solution was continued for 2 min, then the solution was stirred, it was kept at 25 °C without further stirring.

2.2.2. Preparation of the growth solution

2.2.2.1. Variation of surfactant

The growth solution was prepared by mixing 5 mL of the solution at a known concentration of surfactant (CTAB, hexadecyltrimethylammonium chloride (CTAC), BDAC) to 5 mL of 0.001M $HAuCl_4$ solution. 200 µl of 0.0040 M $AgNO_3$ solution was added to the solution at 25 °C. After gentle mixing of the solution, 60µl of 0.10M ascorbic acid was added to the test tube. The color of the growth solution changes from dark yellow to colorless. The final step was the addition of 10 µl of the seed solution to the growth solution. The color of the solution changes over the period of time depending on the final size of the NRs.

2.2.2.2. Variation of the amount of ascorbic acid

Seven test tubes of growth solutions were prepared. Each tube contained 10 mL of an aqueous solution of 0.10 M CTAB and 0.495 mg/mL of BDAC. 200 µl of 0.0040 M $AgNO_3$ solution was added to this solution at 25 °C. To this solution, 50 µl of 0.10 M $HAuCl_4$ was added, and after gentle mixing of the solution 50, 55, 60, 65, 70, 75 and 80µl (corresponding ratio of the molar concentration of the reducing

agent to the concentration of the gold cations is 1.0, 1.1, 1.2, 1.3, 1.4, 1.5 and 1.6, repectively) of 0.10M ascorbic acid was added to each tube. All seven growth solutions above were identical except for their AA content. The color of the growth solution changes from dark yellow to colorless. The final step was the addition of 10 μl of the seed solution to the growth solution. The temperature was kept at 25°C during the growth process. The growth rate was found to level off within about 12 hrs.

For reinitiating the growth, 50ml of bulk NPs solution was made as described above with AA/Au molar ratio of 1.1. After 48 hrs, the bulk solution was divided into 5 tubes each containing 10ml of NPs solution. 10,30,50,100 μl of 0.10M of ascorbic acid were added to each tube, which makes the final molar ratio of AA to Au as 1.3, 1.7, 2.1, and 3.1. Additional ascorbic acid reinitiates the growth within a few minutes as detected by the change of UV-Vis-NIR spectrum and the growth rate levels off within 3 hrs.

All the resulting solutions were centrifuged at 5600G for 30 min to remove the surfactants. The clear supernatant liquid which mainly contains surfactants was removed, then the concentrated NP solution was collected and redispersed in deionized water. This process was repeated for further purification. No process for

separating shapes and size was done. The process for separating the shapes and sizes is decribed in chapter 4.

2.2.3. Instrumentations

UV-Vis-NIR spectra were acquired with a Cary 5G UV-Vis-NIR spectrophotometer. Morphology and the mean size of NPs were examined by TEM (JEOL100 at 100 KV). For each sample, the size of more than 300 particles were measured to obtain the average size and the size distribution.

2.3. Results and Discussion

2.3.1. The role of CTAB in enhancing the formation of anisotropic shape of gold NRs.

Alkyltrimethylammonium surfactant is a prerequisite as a stabilizer for the formation of anisotropic shape of gold NPs for all reduction paths. CTAB has been shown to be most effective to produce longer NRs in a larger fraction among other alkyltrimethylammonium bromide surfactants having different hydrocarbon tail[26].

Hexadecyltrimethylammonium chloride (CTAC) was used only for the UV-irradiation method only to produce NRs in minority[8]. Since CTAC has never been used as a single component in other reduction paths, we want to probe how the difference of counter ion affects the morphology of resulting NRs.

When only CTAC was used, only spherical particles were obtained. Short NRs were obtained in majority with CTAB (Figure 2.1).

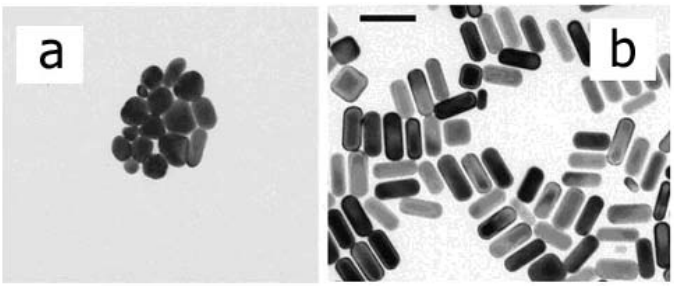

Figure 2.1. Influence of the type of surfactant used in growth solution on the morphology of the gold NRs: a) CTAC and b) CTAB . Scale bar is 50nm.

Since CTAB and CTAC have the same hydrophobic group, the difference in the morphology of gold NRs can be attributed to different counter ions, Br and Cl respectively. The observation brings the question, "how does Br ion promote the growth of NRs over Cl ion?".

Transition metal complexes such as $[PdCl_4]^{-2}$ and $[AuCl_4]^-$ show specific interactions with oppositely charged surfactants [27]. The complex of $[AuCl_4]^-$ and CTAC was studied[8]. Upon mixing $HAuCl_4$ solution to CTAC solution, brilliant yellow-white fine crystals of gold surfactant complex were produced. The binding originates from electrostatic attractions between the complex anions and the organic cations and the existence of 1:1 stoichiometry of CTAC and $[AuCl_4]^-$ has been reported[8]. Above CMC of CTAC, the complex is solubilized and the solution became clear.

Our visual observations during the preparation of gold NRs also indicated that $[AuCl_4]^-$ interacts with CTAB before the reduction process is induced. But the change of color is more pronounced than that of CTAC and $[AuCl_4]^-$ mixture. Upon addition of CTAB to the pale-yellow solution of $HAuCl_4$, orange color precipitate forms. As the concentration of CTAB increases, the precipitation disappears and the color of the solution becomes orange. In the later stage, water-insoluble gold-surfactant complex is solubilized into micelles.

The UV-Vis spectrum of $HAuCl_4$ solution has two peaks at 220 and 300 nm due to the ligand metal charge transfer[28]. By mixing $HAuCl_4$ solution with different surfactant, the peak position is shifted depending on the interaction between the surfactant and $[AuCl_4]^-$. Therefore the complex can be characterized by the peak shift. When $HAuCl_4$ solution is mixed with CTAB solution, the ligand metal charge transfer peaks are shifted to 260 and 380nm which are very close to the peaks of $[AuBr_4]^-$ as compared in the Figure 2.2. The change is caused by the change of ligand X in $[AuX_4]^-$ from Cl to Br, since it is easier to oxidize Br than Cl [28].

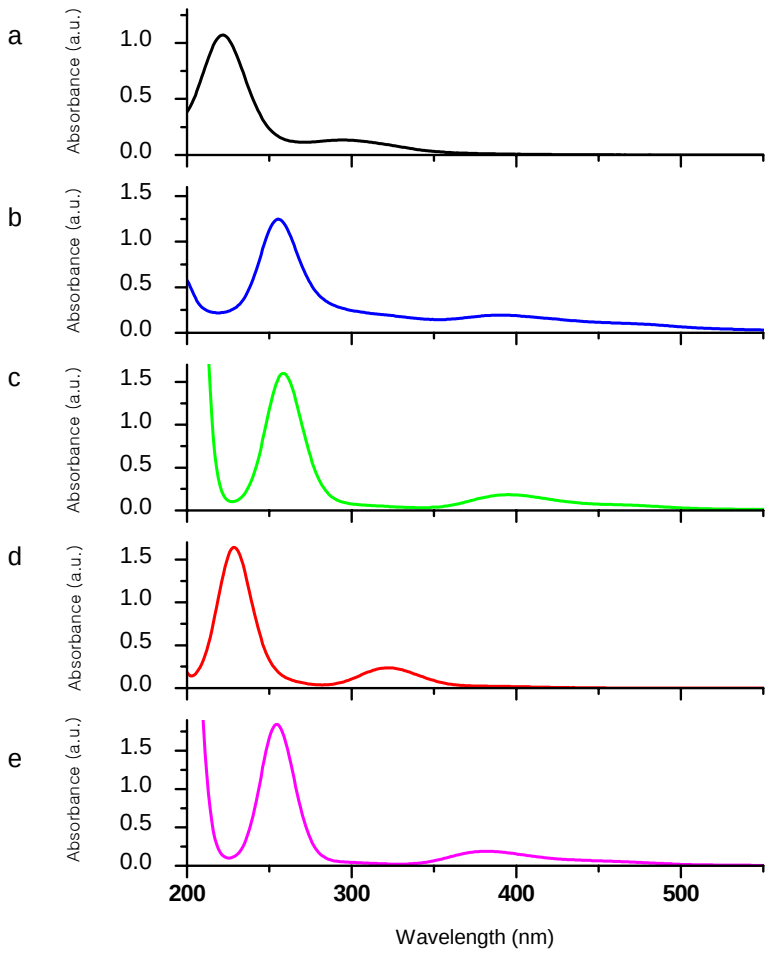

Figure 2.2. The spectral change in aqueous solutions of $HAuCl_4$ upon adding different surfactants. $[HAuCl_4] = 5\times10^{-4}$ M for all solutions and [surfactant]= 5×10^{-2} M if added. a) $HAuCl_4$, b) $HAuBr_4$, c) $HAuCl_4$/CTAB, d) $HAuCl_4$/CTAC, and e) $HAuCl_4$/KBr(0.05M) mixture.

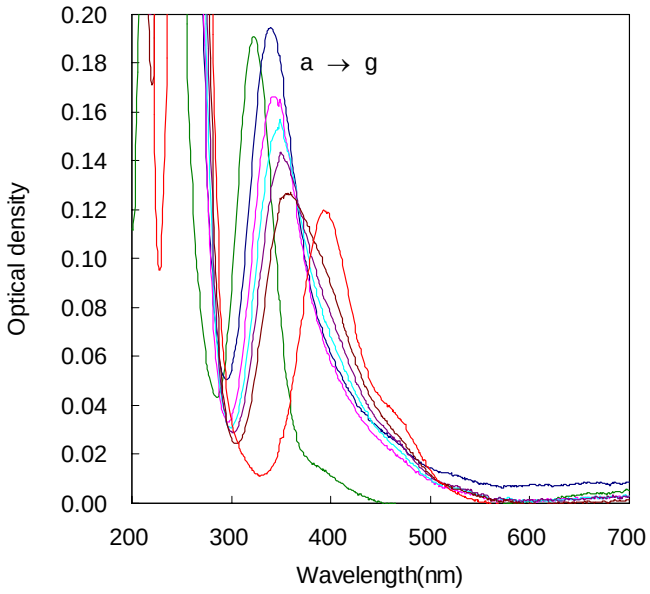

Figure 2.3. The spectral change in aqueous solutions of $HAuCl_4$ upon adding increasing amount of 0.1M of KBr solution. $[HAuCl_4] = 5\times10^{-4}$ M for all solutions and $[CTAC]= 5\times10^{-2}$ M, [KBr]= a: 0, b: 0.003M, c: 0.004M, d: 0.005M, e: 0.006M , f: 0.008M, and g: 0.035M. As the concentration of KBr increased, the characteristic peak of 220 and 300nm shifted gradually to 260 and 380nm.

For comparison, we added KBr to the solution of $HAuCl_4$ and examined the spectral changes. As the concentration of KBr increased, the characteristic peaks at 220 and 300nm shifted gradually to 260 and 380nm (Figure 2.3).

Therefore the net interaction between CTAB and $HAuCl_4$ in aqueous solution results in the formation of [CTA]-[$AuBr_4$], while CTAC and $[AuCl_4]^-$ form a complex without the change of ligand. This organic salt is solubilized by the surfactant micelles to produce "metallomicelles".

$$[AuCl_4]^- + 4\,CTAB \leftrightarrow CTA\text{-}[AuBr_4] + 4Cl^- + 3CTA^+$$

So, one is left to wonder, "why is it important to have $[AuBr_4]^-$, instead of

$[AuCl_4]^-$, and metallomicelles regarding the formation of NRs?" If metallic species are involved in the formation of solute complexes or compounds, the standard redox potential will be lower since the complex is more stable than the gold ion. In Table 2.1, the standard potentials of gold ion and gold complex are shown[29].

Table 2.1. Standard potentials in aqueous solutions[29]

Half reaction	Standard potential(V)
Au(III)/Au(I)	
$Au^{3+} + 2e^- \rightarrow Au^{1+}$	+1.40
$AuCl_4^- + 2e^- \rightarrow AuCl_2^- + 2Cl^-$	+0.926
$AuBr_4^- + 2e^- \rightarrow AuBr_2^- + 2Br^-$	+0.805
Au(I)/Au(0)	
$Au^+ + e^- \rightarrow Au$	+1.71
$AuCl_2^- + e^- \rightarrow Au + 2Cl^-$	+1.154
$AuBr_2^- + e^- \rightarrow Au + 2Br^-$	+0.962
Ascorbic acid $C_6H_6O_6 + 2H^+ + 2e^- \rightarrow C_6H_8O_6$	+0.13

The potential of gold complex is lower than that of gold ion. On top of it, $[AuBr_4]^-$ has a lower potential compared to $[AuCl_4]^-$ as does $[AuBr_2]^-$ in comparison to $[AuCl_2]^-$. It can be deduced that reduction is harder for the Br complex than Cl complex. In the growth solution, $[AuBr_4]^-$ exists as CTA-$[AuBr_4]^-$ which is expected to be even more stable. This is why a weak reducing agent such as ascorbic acid (AA) cannot reduce the complex to gold atom while AA easily reduces the $[AuCl_4]^-$ to gold atom to produce spherical particles. AA can only reduce $[AuBr_4]^-$ in the metallomicelles to $[AuBr_2]^-$. So the nucleation can be withheld until

the seed solution is added. With the catalytic action of the seeds, Au^{+1} ion in the metallomicelle is reduced to gold atom. Therefore the effectiveness of CTAB comes from the lower redox potential of Br complex.

To demonstrate the effect of Br substitution on the formation of NRs, KBr was added to the growth solution prepared with CTAC. When KBr was added to CTAC, short rods were obtained in significant fraction (Figure 2.4and Figure 2.5). This result comfirms that the form of precursor is important in determining the morphology of the particle.

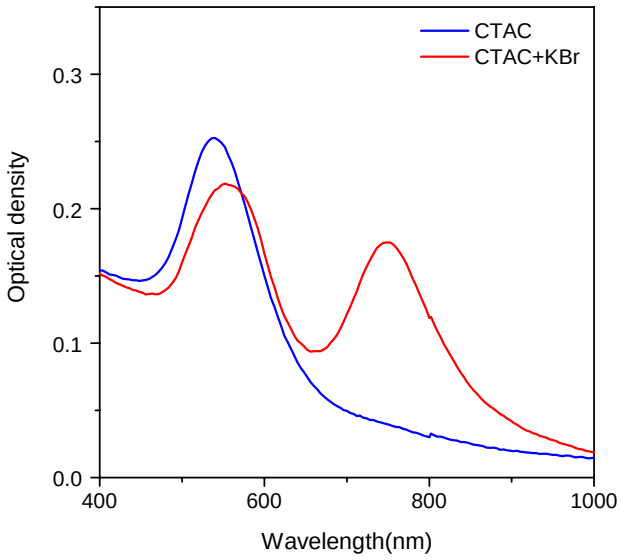

Figure 2.4. UV-Vis-NIR spectrum of gold NR solution. Effect of KBr on the formation of NR in the growth solution containing CTAC.

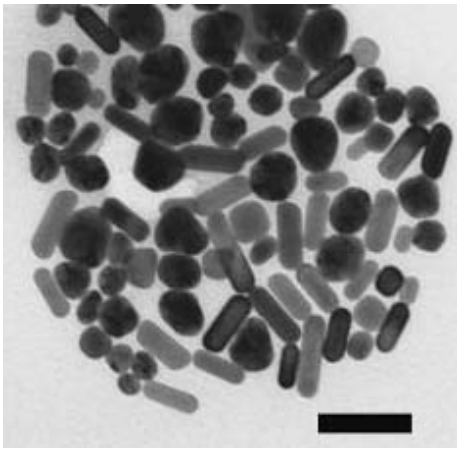

Figure 2.5. A TEM image showing that significant amount of short rods are obtained when KBr is added with CTAC. Scale bar is 50nm.

In synthesis of gold NPs, chloroaurate was dominantly used as starting gold salt. From our results, it is found that chloride is substituted by bromide in the final precursor form. We examined the possibility of using bromoaurate instead of chloroaurate and indeed succeded to prepare gold NRs of aspect ratio equivalent to or larger than those prepared by chloroaurate(Figure 2.6).

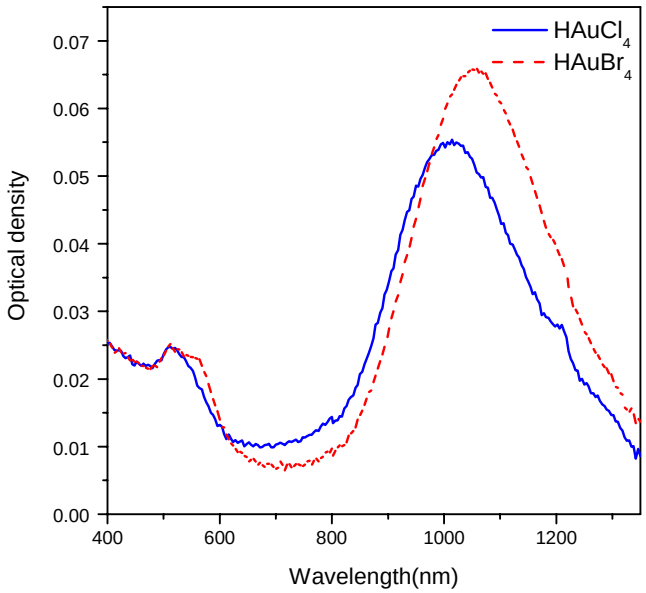

Figure 2.6. UV-Vis-NIR spectra of gold NR solution prepared by different gold salts.

Different morphology of gold NRs prepared by CTAB and CTAC may result from different adsoprtion behavior of the two surfactant. Adsorption occurs initially via attractive electorstatic interactions between the cationic headgroup and the anionic surface of growing gold NPs. Once the original charge of the surface is neutralized by the adsorption of oppositely charged surfactant ions, adsorption continues via interactions between the hydrophobic tails, leading to surfactant self assembly on the surface. Counterions affect the structure of this assembly by screening the electrostatic repulsions between the ionic headgroups. It has been reported that bromide ions have a 5-fold greater binding affinity for CTA^+ than that of chloride ions[30,31]. Above the CMC, the surface excess concentration of CTAB is 60% greater than that of CTAC making the structure of the adsorbed surfactant as densely

packed wormlike micelle(Figure 2.7). Below the CMC, the counterion has only a small effect on the srtucture of the adsorbed layer.

The structure of adsorbed CTAB on the surface of gold NRs was found to be bilayer[32]. The bilayer can result from the adsorption of the micelle on the surface as suggested by the high resolution TEM study[33]. Considering the concentration of CTAB in the growth solution is above CMC, we believe that the densely paked wormlike micelle adsoption of CTAB on the growing gold NPs efficiently promote the directional growth of particle resulting in the rod shape.

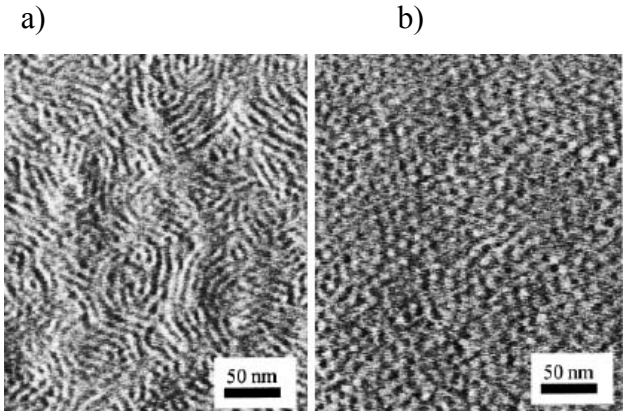

Figure 2.7. AFM images of adsorbed surfactant layers on silica observed at 10×CMC [30]. a) CTAB and b) CTAC.

The concentration of CTAB is the dominant factor to induce the anisotropic shape of NRs. The range of concentration of CTAB used to prepare NRs is from just above CMC to 0.1M in the literature. However, the effect of the concentration of CTAB on the formation of gold NRs was not studied.

We found that as the concentration of CTAB increases, the yield of NRs

increases which can be seen from the decreasing transverse surface plasmon (TSP) intensity and increasing longitudinal surface plasmon (LSP) intensity (Figure 2.8).

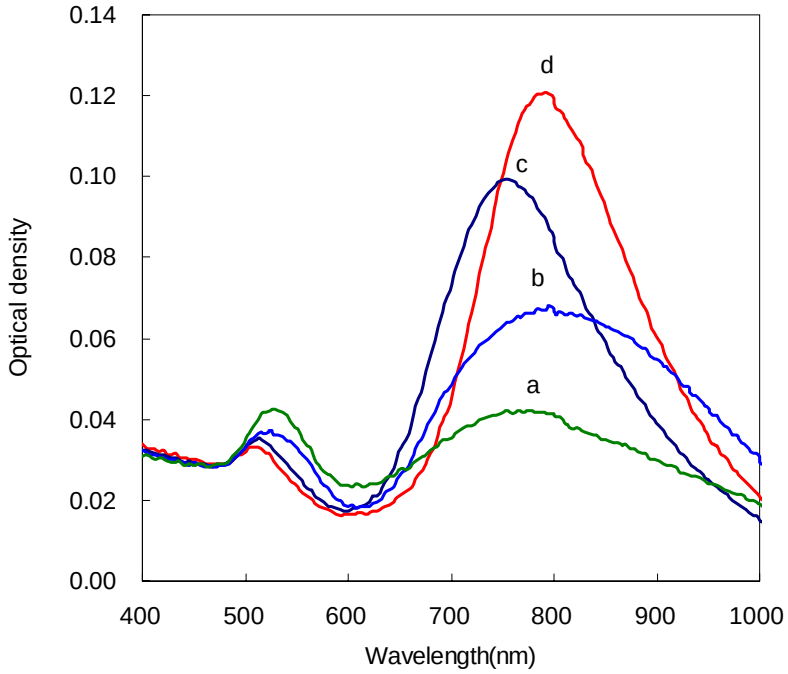

Figure 2.8. The effect of CTAB concentration on the formation of gold NRs. a: [CTAB]=0.02M, b: 0.05M, c: 0.08M, and d: 0.1M.

This result can be explained by the enhanced CTAB adsorption on the surface of the growing particle. The adsorption of surfactant onto an interface involves the straightforward processes of diffusion of surfactant molecule (monomer) from the bulk to the surface. The adsorption of monomer onto the surface disturbs the monomer/micelle equilibrium and micelles can kinetically break up releasing monomer which can then diffuse and kinetically adsorb onto the surface. Also, micelles can directly adsorb onto the surface. Therefore, by increasing CTAB concentration, the preferential adsorption on the growing gold particles can be

promoted to produce more NRs than spherical particles.

2.3.2. The role of BDAC in enhancing the formation of anisotropic shape of gold NRs.

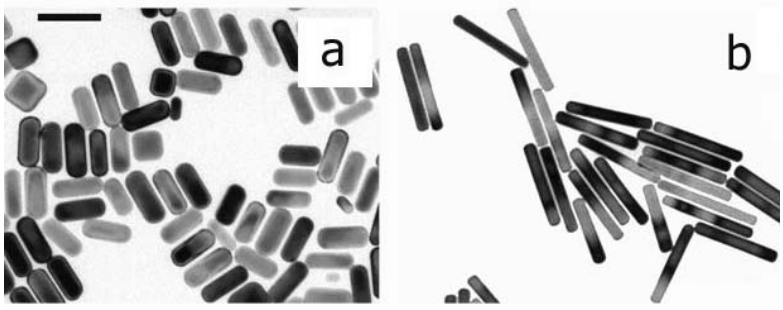

Figure 2.9. TEM images of gold NRs synthesized in a) CTAB and b) CTAB/BDAC. Scale bar is 50nm.

Figure 2.9 shows the effect of BDAC for preparing longer NRs. When BDAC is used along with CTAB, longer NRs were made. This result was attributed to a more flexible template made by surfactant mixture and the different affinity of CTAB and BDAC on the facet of growing gold NRs [20].

We took different approach to explain the role of BDAC by focusing the precursor stage of the growth solution.

The precursor in the growth solution of CTAB and BDAC shows the characteristic peaks of $[AuBr_4]^-$ instead of $[AuCl_4]^-$, indicating that CTAB is used for forming precursor (Figure 2.10).

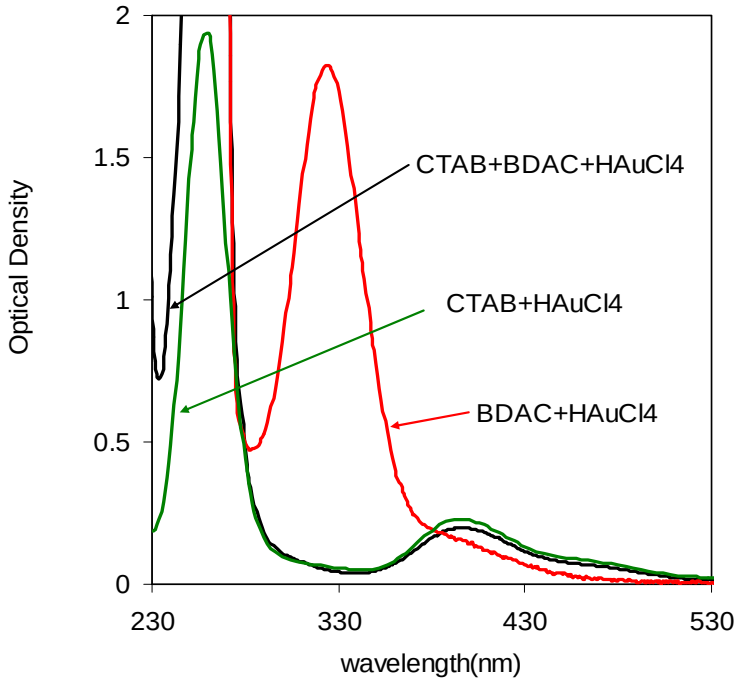

Figure 2.10. The spectral change in aqueous solutions of $HAuCl_4$ upon adding different surfactant. $[HAuCl_4] = 5\times10^{-4}$ M for all solutions and [surfactant] = 5×10^{-2} M.

As previously mentioned, the solubilizability of the complexes can be mapped at room temperature by visual inspection. To analyze the solubilizability quantitatively, a series of vials containing $HAuCl_4$ at constant concentration were prepared and the concentration of surfactant was successively increased until the turbidity disappeared. The solutions were sonicated for an hour after which the UV-Vis spectra were taken. The change in turbidity can be monitored by the change of absorbance. The absorbance at the wavelength 600 nm was chosen because this peak is not related to any of the characteristic peaks of the solution. The absorbance was plotted as a function of the concentration of surfactant. It is clearly shown in Figure 2.11 that by using the binary system, the solution starts to solubilize the

complex at a much lower concentration than by using CTAB alone. This result is consistent with the report that in a mixed surfactant system of BDAC and CTAB, the first CMC was dropped from 0.001 to 0.0005M and the second CMC was also dropped dramatically from 0.28 M to 0.0014M over all mixing ratios[34].

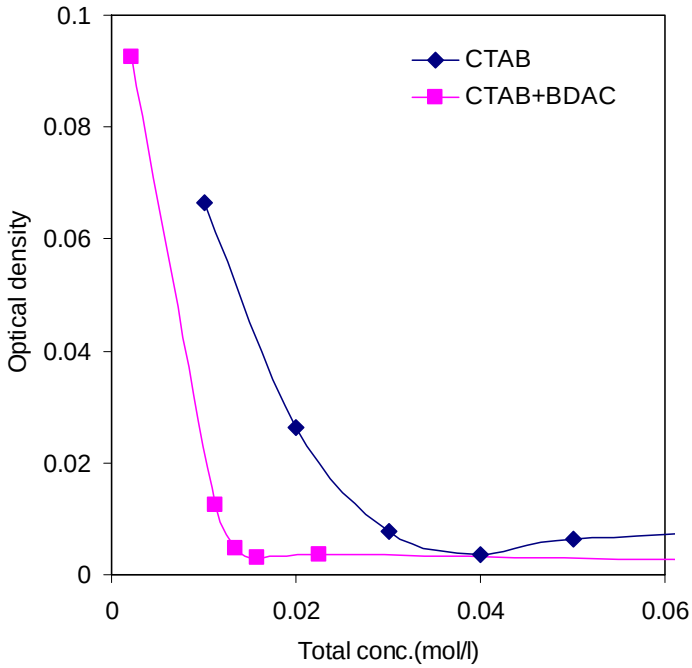

Figure 2.11. Change of the absorbance of the surfactant-$HAuCl_4$ mixture solution at 600nm as a function of total surfactant concentration. The concentration of $HAuCl_4$ was fixed at 5×10^{-4} M. The absorbance at 600nm is not related to any of the characteristic peak of the solutions and is an indicative of the turbidity.

Since 2nd CMC is lowered by BDAC, the size of micelle is expected to become even bigger through structural transitions from spherical micelle to rod shaped micelle[35].

Therefore, we reasoned that the bigger micelles accomodate the precursor facilely preventing immediate reduction which may lead to the formation of spherical particles.

Since we found that the higher concentration is also effective in making longer NRs in the case of binary surfactant system (Figure 2.12), we decided to investigate the optimum ratio of CTAB/ BDAC at higher concentration. We fixed the BDAC concentration to 0.125 M and narrowed down the range of ratio (between 0.2 and 1) by changing the amount of CTAB.

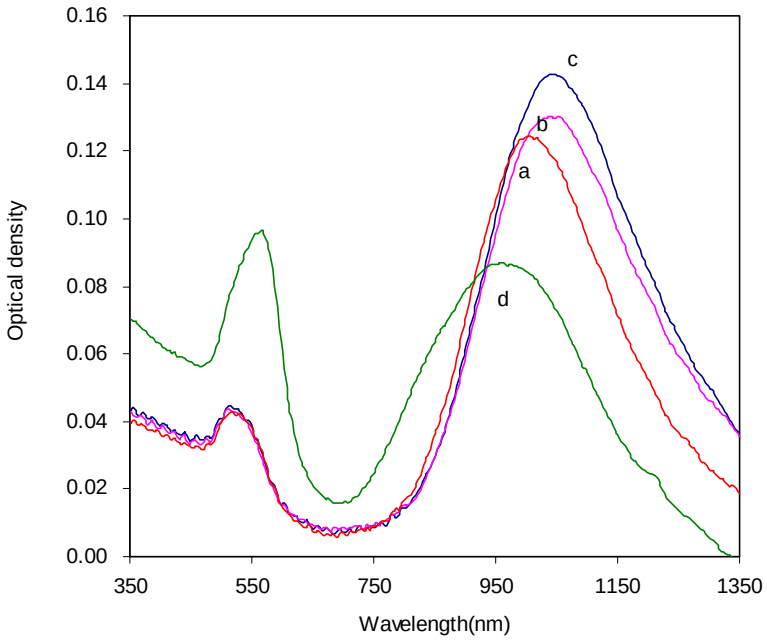

Figure 2.12. UV-Vis-NIR spectra of gold NR solutions having different total concentration of surfactant. The ratio of CTAB/ BDAC was 0.5. The total concentration of surfactants was a) 0.135M, b) 0.180M, c) 0.225M, and d) 0.270M.

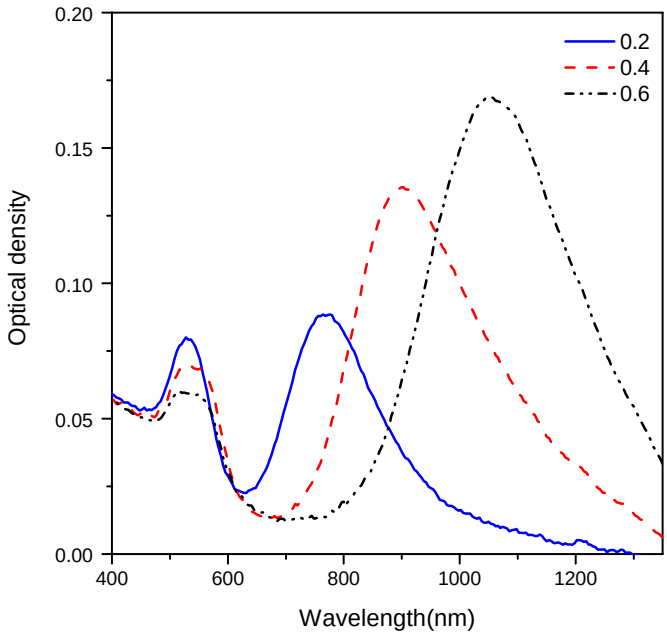

Figure 2.13. UV-Vis-NIR spectra of gold NR solutions with increasing ratio of CTAB/BDAC when the concentration of BDAC is fixed at 0.125M.

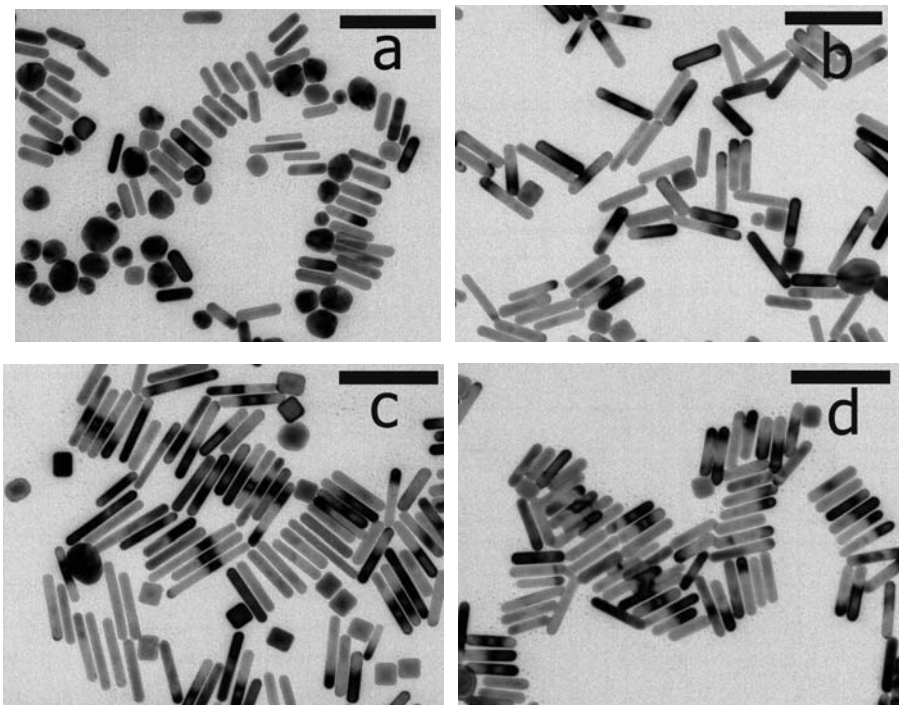

Figure 2.14. TEM images of gold NRs with the ratio of CTAB/ BDAC a) 0.2, b) 0.4 c) 0.6, and d) 1. The concentration of BDAC is fixed at 0.125M. The scale bar is 100nm.

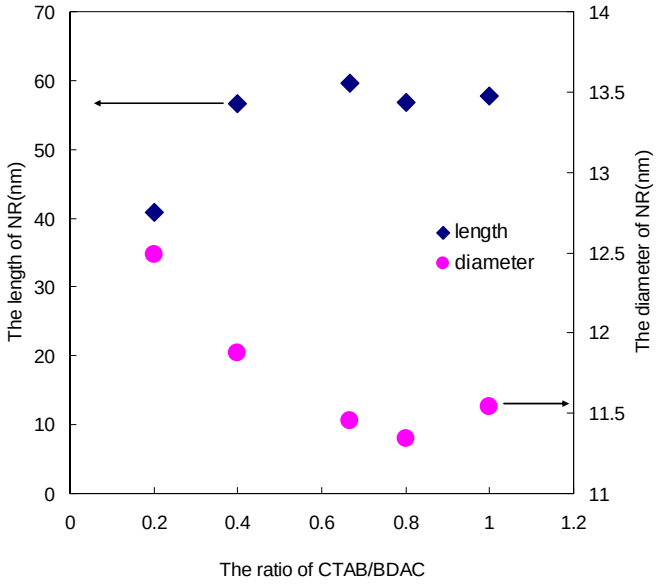

Figure 2.15. The effect of the ratio of CTAB/BDAC on the size of NRs. The concentration of BDAC is fixed at 0.125M. It can be seen that as the CTAB fraction increases, the length of NRs increases and the diameter of NRs decreases.

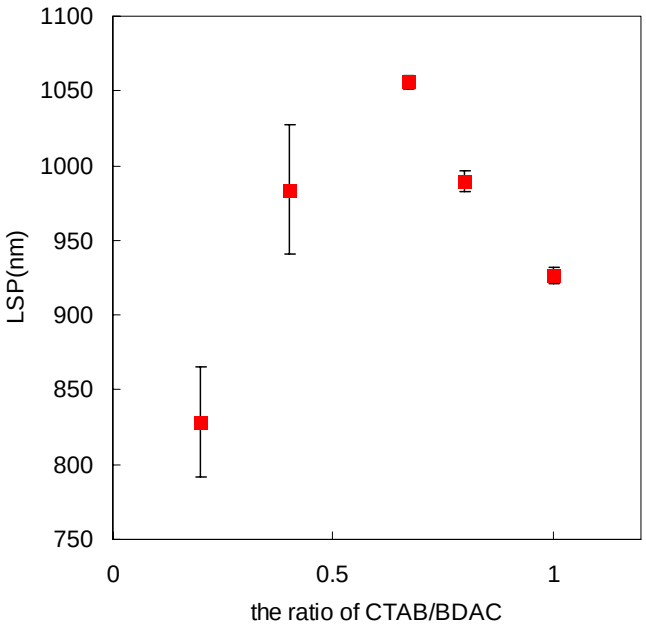

Figure 2.16. The effect of the ratio of CTAB/BDAC on LSP of the growth solutions. The concentration of BDAC is fixed at 0.125M. It can be seen that as the CTAB fraction increases, the LSP of NRs reaches maximum at the ratio of 0.67 and decreases. The reproducibility increases with increasing ratio.

From the UV-Vis-NIR spectra (Figure 2.13) and TEM images (Figure 2.14), it can be seen that as the ratio was increased, the NRs became longer and uniform (Figure 2.15), and the fraction of the byproduct significantly decreased. But on further increasing beyond 0.6, the aspect ratio of NRs became smaller, as seen from a shift of the LSP to lower wavelengths. Also reproducibility is increased by increasing the amount of CTAB (Figure 2.16).

In this experiment, the concentration of BDAC was fixed and the concentration of CTAB was changed to obtain given ratios. The amount of CTAB is critical, because it is used as a precursor in making complex with gold ion and as a stabilizer to confine and direct the growth of NRs. Therefore increasing aspect ratio could be mainly due to the increasing concentration of CTAB.

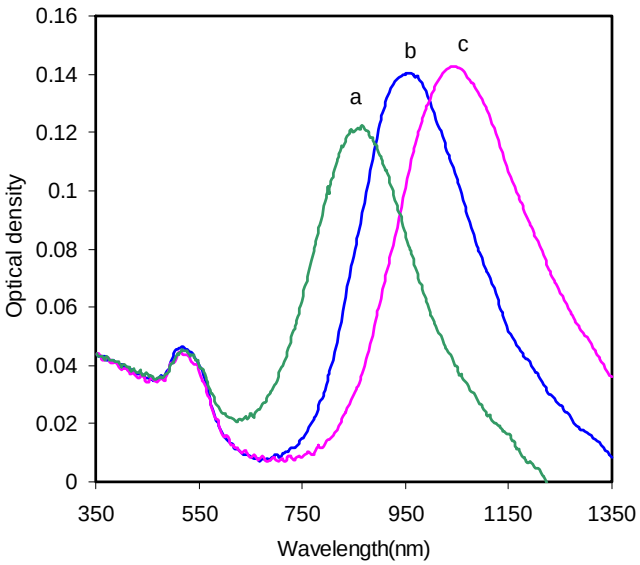

Figure 2.17. UV-Vis-NIR spectra of the gold NRs solutions with decreasing ratio of BDAC/CTAB when the concentration of CTAB is fixed at 0.1M. The concentration of BDAC is a) 0.03M b) 0.075M, and c) 0.125M.

To exclude the effect of the concentration of CTAB, a similar experiment was done by fixing CTAB concentration and changing BDAC. Up to a certain point, as the amount of BDAC increases, the aspect ratio increases (Figure 2.17). In both cases, aspect ratio of NRs increases with increasing surfactant concentration and shows a maximum at some surfactant concentration.

The number of micelles increases with increasing surfactant concentration. When the number of micelles exceeds that required to solubilize all of the substrate, there is a dilution of the concentration of substrate per micelle as the surfactant concentration is further increased. This causes the drop in reduction rate. Also, the number of monomer in the solution is increased by the increasing concentration of surfactant which causes more efficient adsorption of surfactant on the growing surface. Therefore more NRs can be made due to decreasing reduction rate and increasing adsorption efficiency.

We conclude the role of surfactant in the formation of gold NRs as follows:

1) to make complex with gold salt which is more stable so that the reduction renders slower.
2) to capture the complex inside the micelle so that it can protect gold ion from being instantly reduced.

3) to adsorb on the surface of growing NRs so that it can confine the direction of growth.

4) The role of BDAC as cosurfactant is to lower the 2nd CMC to promote effective formation of metallomicelle and preferential adsorption on the growing surface of gold NR.

2.3.3. The reduction

In the seed-mediated method, ascorbic acid (AA) is used as a mild reducing agent. When a strong reducing agent ($NaBH_4$) is used, the growth solution became deep purple within several minutes. In this case, only nanospheres are produced (Figure 2.17). When the stoichiometric ratio of AA was added without seed solution, there was no color change for 24 hrs. But when the solution was kept for over a week, pale purple color developed. But UV-Vis spectrum shows no significant NPs formation. Only when AA was added to seed solution, NR was produced as a main product.

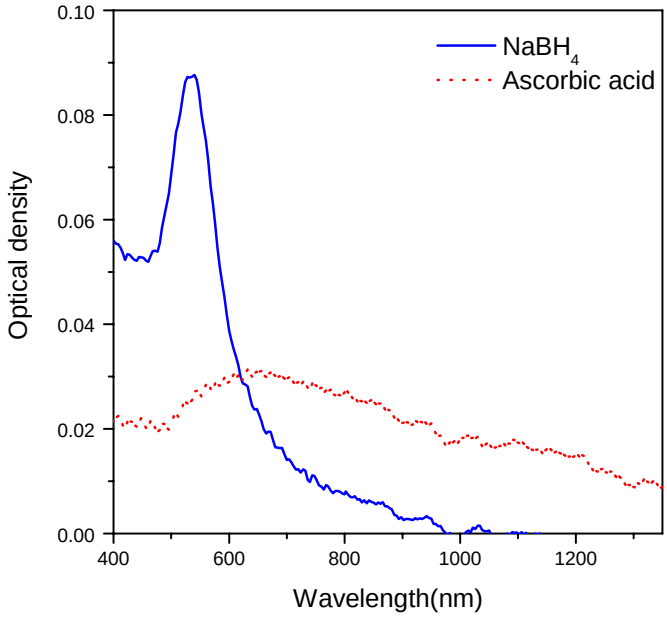

Figure 2.18. The effect of reducing agent on the formation of gold NRs.

From this result, it is apparent that weak reducing agent is essential for the formation of rod shape. Also, the seed solution is a necessity as a growth reagent inducing the second reduction process.

The reduction process of the gold ion by AA can be described as

$$\text{First reduction : } Au^{+3} \rightarrow Au^{+1}$$

$$CTA - AuBr_4 + C_6H_8O_6 \rightarrow CTA - AuBr_2 + C_6H_6O_6 + 2H^+ + 2Br^-$$

$$\text{Second reduction : } Au^{+1} \rightarrow Au^{0}$$

$$2CTA - AuBr_2 + C_6H_8O_6 \rightarrow 2Au + C_6H_6O_6 + 2CTA^+ + 2H^+ + 4Br^-$$

The first reduction is confined in the metallomicelles. The second reduction only begins after the seed solution is added. The overall reaction is

$$2CTA - AuBr_4 + 3C_6H_8O_6 \rightarrow 2Au + 3C_6H_6O_6 + 2CTA^+ + 6H^+ + 8Br^-$$

We calculated the stoichiometry of this reduction reaction by considering the ionization of AA and pH of the growth solution. That turns out to be 1.6. So for the complete reduction, molar ratio has to be greater than 1.6.

Recently, the effect of AA concentration on the morpholgy of short NRs has been reported[36]. The specific ratios of 1.6 and 7.5 were investigated. It was said that when the ratio was high, the rod length decreased. But the reaction condition was different for both of the experiments (1.6 with $AgNO_3$ and 7.5 without $AgNO_3$), thus making it difficult to draw any general conclusions.

We studied the effect of the concentration of AA on the growth of NRs. In particular, we investigated how the reduction rate affects the morphology of NRs. The molar ratio of AA to gold ion was changed from 1 (which is the ratio required to reduce Au^{+3} to Au^{+1}) to 1.9.

When the molar ratio was 1, no NPs were obtained. As the molar ratio increased from 1.1 to 1.9, the absorbance at the peaks increased indicating higher yield of particles formation. As the molar ratio increased from 1.1 to 1.3, LSP shifts to longer wavelength but upon further increasing the molar ratio, LSP shifted back to shorter wavelength (Figure 2.19). As it can be seen in the TEM images (Figure 2.20), the initial red-shift can be related to the aparent increase in the length of NR resulting

in the increasing aspect ratio. Later the growth of the diameter overtook the growth of the length resulting in decreasing aspect ratio.

When the ratio is above 1.6, the shape of NRs is no longer a spherocylinder. The growth in diameter direction was greatest at the ends and progressively slower towards center, giving a taper shape as shown in Figure 2.20(c).

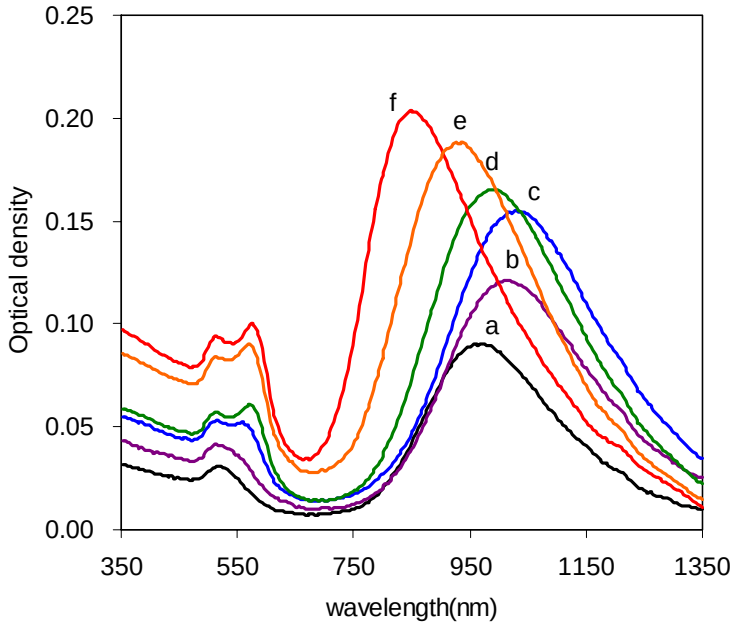

Figure 2.19. UV-Vis-NIR spectra of 6 identical growth solutions in which the ascorbic acid(AA) contents increased from a to f. The ratio of AA:gold ion was a) 1.1, b)1.2 , c) 1.3, d)1.4, e) 1.5, and f) 1.6. The spectra were taken from the as-made solutions after the growth was ended (measured in 1mm path quartz cell).

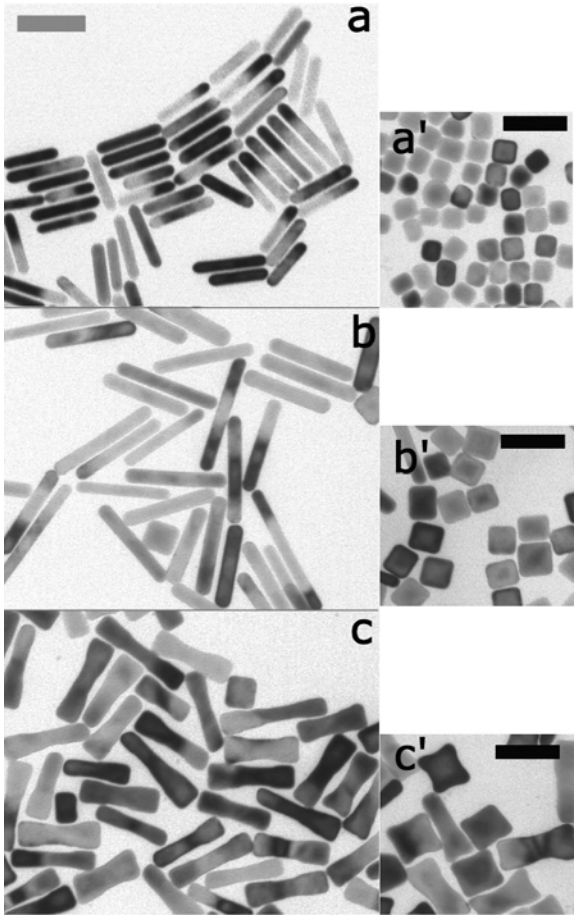

Figure 2.20.Changing morphology of NRs by varying the molar ratio of AA to Au^{+3}. a: 1.1, b: 1.3, and c: 1.6 (a′, b′, and c′ show the byproduct from the same solution). Scale bar is 50 nm.

Nanocubes were obtained as a byproduct. The fraction of nanocubes in the solution increased from 17% to 50% as AA increased. The size of nanocube increased continuously by increasing the amount of AA. The edge length reached 31nm. The broad transverse band as a result was caused by the size difference between the width of NR and the edge length of nanocube. They contributed to the plasmon bands at 512nm and 550 nm, respectively.

.

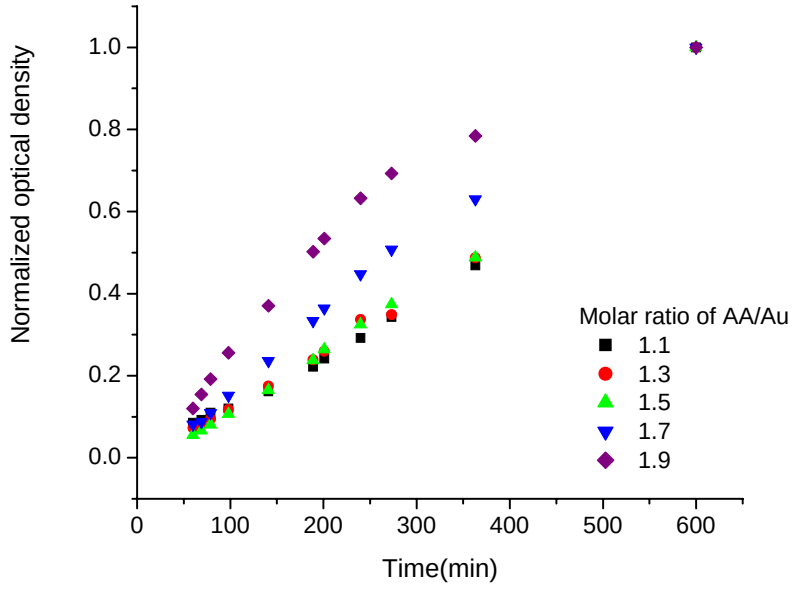

Figure 2.21. The effect of ascorbic acid(AA) on the growth kinetics of gold NRs. The molar ratio of AA to gold ion was changed from 1.1 to 1.9. The intensity at LSP was taken and normalized by the final intensity.

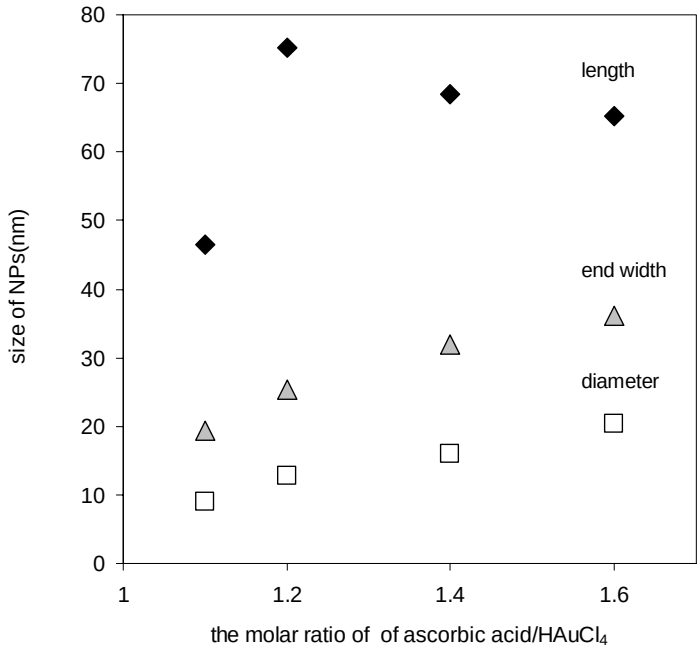

Figure 2.22. Effect of ascorbic acid(AA) on the size of NRs and nanocubes(NCs). The lenght of the NRs first increases and then decreases with increasing amount of AA. The diameter of NRs and the size of NCs increases as the amount of AA increases.

The reduction rate depends on the concentration of the reducing agent. As the amount of AA increases, the reduction of gold ion becomes rather faster (Figure 2.21). As a result, the reduction takes place before surfactants confine the growth direction. Taper shaped NRs as well as the bigger nanocubes are obtained.

When the molar ratio of AA to gold ion is less than the stoichiometric ratio, gold cations remain in the growth solution after the growth stops. The NR solution was centrifuged. After taking the concentrated NR solution at the bottom, clear supernatant was kept in a test tube. UV-Vis spectrum of this supernatant showed that supernant contains very little amount of NRs. When AA was added to this supernatant, the color of the solution changed indicating the formation of particles.

We expected that the reduction can be reinitiated by adding extra AA to the NPs solution after the initial growth stops so that remaining gold ions can be further reduced. We studied how the extra AA can reinitiate the reduction process and change the size and shape of the original NPs.

The bulk NR solution was made. The ratio of AA to Au^{+3} was 1.1. After 48 hours, the solution was divided into 5 test tubes. Different amount of extra AA was added to each test tube except one tube for comparison. As the amount of extra AA increased, the optical density became higher. LSP shifted to longer wavelength indicating the growth of NRs and TSP broadened as shown in Figure 2.23.

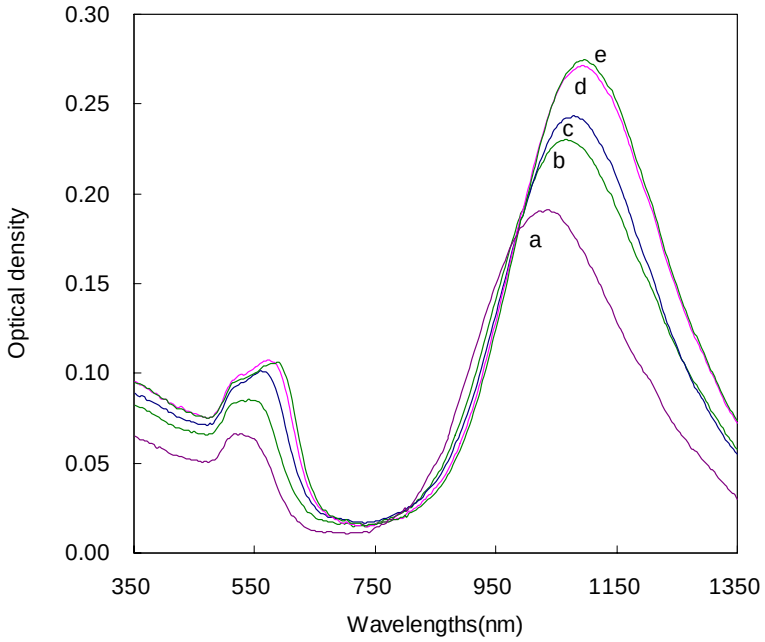

Figure 2.23. UV-Vis-NIR spectra of the NR solutions before and after adding extra ascorbic acid(AA) to the mother solution which was initially made with the molar ratio of AA to Au^{+3} is 1.1 (a: mother solution, b:adding 10μl, c:30μl, d: 50μl, and e: 100μl).

The TEM images (Figure 2.24) show the growth of NRs in the length with increasing AA. The width of NRs first increased a little and only the end of NRs became fatter while the middle of NRs did not change much (Figure 2.24). The broad transverse peak resulted from the bigger nanocubes and the fatter end of the NRs. When the largest amount of AA was added, we observed bone shaped NPs with split ends and boomerang shaped NPs. Nanocubes also became bigger and the 4 corners of nanocubes began to bulge (Figure 2.26). In all solutions, the fraction of byproducts is 20% indicating little additional nucleation.

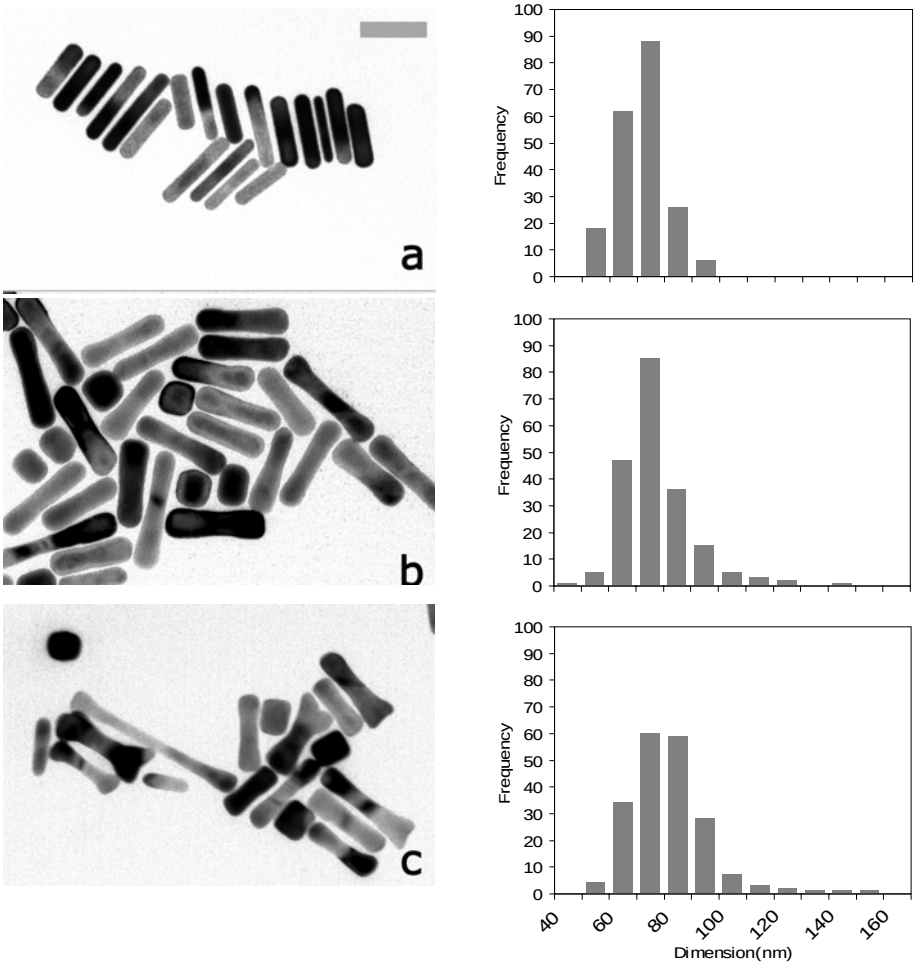

Figure 2.24. TEM images of gold NRs and the size distribution of each sample; a) from batch solution, b) grown from the batch solution (10ml) by adding 30 ul of extra AA, and c) grown from the batch solution (10ml) by adding 50 ul of extra AA. Scale bar is 50nm.

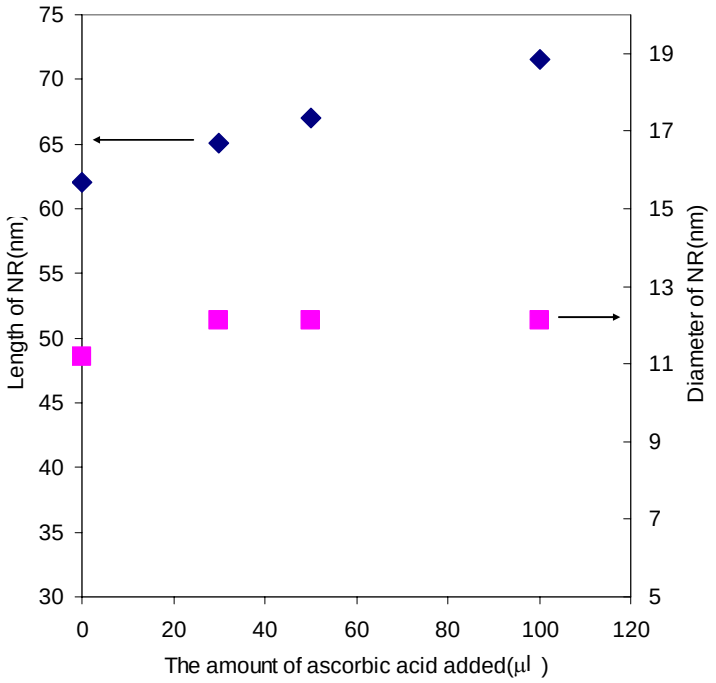

Figure 2.25. The growth of NRs by reinitiating the reducing process. The length of the NRs was increased with increasing amount of extra AA added after the first growth was completed. The width in the middle didn't change significantly, while the width in the end increases as the amount of AA increases.

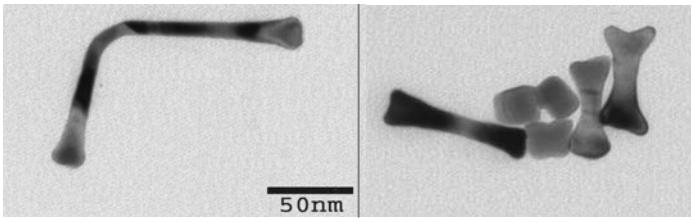

Figure 2.26.TEM images of gold NRs grown from mother solution by adding extra amont of AA. Bone shaped NPs as well as boomerang shaped NPs were obtained when the largest amount of AA was added.

When the growth resumes by reinitiating the reduction by adding extra AA, the length of NRs becomes longer and only the ends of NRs becomes bulged. This

happens because after the initial growth is completed, the side of NRs is mostly adsorbed by surfactant which restricts the growth in diameter.

Therefore reduction mainly occurs at the end of NRs. When the largest amount of extra AA is added, forced reduction makes the NRs take on the shape of a bone[37]. We believe that facets consisting the end have different reactivity with each facet having a distinct reduction rate different from other facets. Each facet grows at a different rate so that we observe asymmetric branches with 2 or 3 branches.

It is interesting to compare the NRs made by adding the same amount of AA but using different time scale. One solution is made by adding 100ul of 0.1M AA initially while the other is made by adding 70ul of 0.1M AA in the beginning and adding 30ul of 0.1M after 24 hrs. In the former case, the diameter of the NRs gradually becomes bigger from the center to the end (Figure 2.27 a).

a) b)

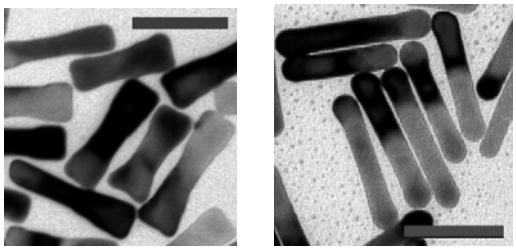

Figure 2.27. The different morphology of gold NRs. a) 100ul of 0.1M AA was added initially, and b) 70ul of 0.1M AA was added in the beginning and 30ul was added after 24 hrs. Scale bar is 50nm.

The length of NRs is 65nm and the diameter in the middle is 20nm. In the latter case, longer NRs with smaller diameter were obtained and only the ends of the NRs became bulged (Figure 2.27 b).

Temperature is one of the major control parameters which affects the reduction rate. To further investigate the effect of reduction rate on the morphology of gold NRs, the reaction temperature was varied while all other experimental conditions were kept the same. TEM images of gold NRs grown at different temperatures between 20°C and 50 °C are shown in Figure 2.28. With decreasing temperature, the aspect ratio increased from 3 to 6. It is worth noting that this increase in aspect ratio is due to the decrease in diameter of the NRs as shown in Table 2. The decreasing diameter of the NRs can be ascribed to the effective confinement of the growth in diameter direction at low temperature which renders low reduction rate.

a) b) c)

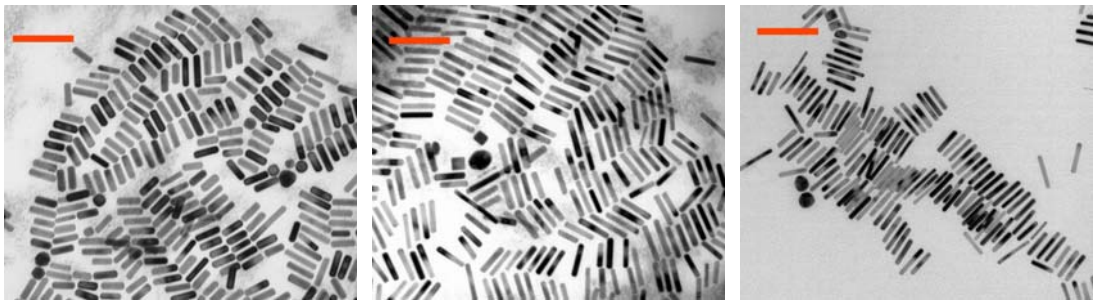

Figure 2.28. Changing morphology of NRs by varying the reaction temperature. a) 50°C, b) 30°C and c) 20°C. All other experimental parameters are the same. The scale bar is 100nm.

Table 2.2. Maximum LSP(λ_{max}), length, diameter and aspect ratio of gold NRs synthesized at different temperature.

Temperature(˚C)	λ_{max}(nm)	average length(nm)	average diameter(nm)	aspect ratio
20	732	46.8	7.9	6.0
30	954	53.4	10.0	5.6
50	1020	40.7	12.6	3.3

The reduction process in the synthesis of gold NRs can be summarized as follows: Equimolar amount of AA is necessary to reduce Au^{+3} to Au^{+1}. unconsumed AA reduces Au^{+1} to Au^{0} with the catalytic effect of the seed solution. Hence, as AA concentration increases, NRs can be obtained in higher yield. The molar ratio of gold ion to AA should be greater than 1.5 to ensure the complete reduction of gold ion. The unreacted precursor can be reduced by reinitiating the reduction which results in changing the morphology of existing NRs.

2.3.4. Tuning the aspect ratio of NRs by kinetically controlled growth

To obtain higher aspect ratio of NRs, we manipulate the reduction steps. First we prepared mother solution using lower molar ratio (1.1). The aspect ratio is about 6 and the diameter is small. The solution contains a small amount of byproducts.

After the first growth leveled off we added extra AA every 150min to balance the reduction and the adsorption. We repeated this 6 times (Table 2.3) and successfully synthesized NRs with higher aspect ratios with mainly lengthwise growth and little byproduct. Aspect ratio up to 9 can be obtained by this procedure.

Table 2.3. The modified reduction steps to obtain higher aspect ratio of gold NRs.

Addition time(min)	0	180	330	480	630	780	930
amount of AA(μl)	550	50	50	50	50	50	50
stoichiometric ratio	1.1	1.2	1.3	1.4	1.5	1.6	1.7
LSP(nm) (L/d)	1000 (**6.4**)	1040 (6.9)	1070 (7.3)	1080 (7.4)	1090 (7.5)	1120 (7.9)	1140 (**8.2**)

a) b)

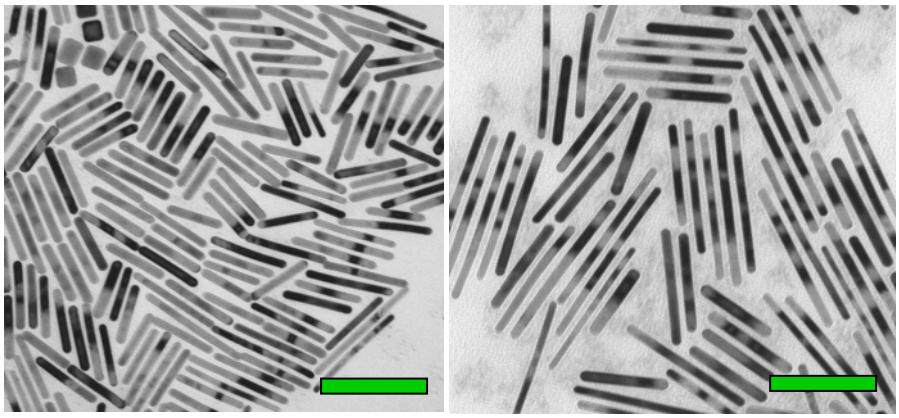

Figure 2.29. TEM images of (a) gold NRs from mother solution and (b) gold NRs grown by adding small amount of ascorbic acid step by step. The scale bar is 100nm.

The main difference of controlling aspect ratio in our synthesis method is that the procedure is rather simple. Usually obtaining higher aspect ratio of NRs often involves the preparation of many growth solutions and growth can be done by taking multiple steps which prevents to prepare low polydispersity NRs[15]. Separation of the byproduct through many rounds of centrifugation is also required.

In our approach, the desired size and shape of the NRs was obtained in high yield in a single growth solution by adding just more reducing agent step by step.

2.3.5. The effectiveness of seed-mediated method

The advantage of seed-mediated method is to separate nucleation and growth. This separation is supposed to minimize the further nucleation and decrease the size distribution. We probed the effectiveness of seed-mediated method by preparing the gold NRs without adding seed solution.

Instead of adding seed solution, we added a very small amount of $NaBH_4$ solution to the growth solution (which is equivalent to the amount of $NaBH_4$ in the seed solution) expecting that a small amount of strong reducing agent will serve as nucleating agent.

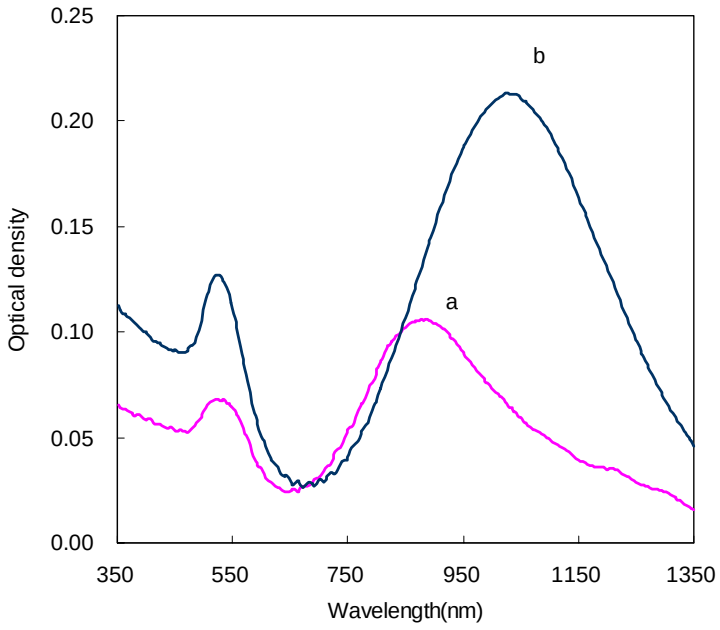

Figure 2.30. UV-Vis-NIR spectra of the NR solution grown without seed solution. A very small amount of $NaBH_4$ solution equivalent to the amount of $NaBH_4$ in the seed solution was added instead of adding the seed solution. In 24hrs, only short NRs were produced and the yield was very low (a). After 1 month , they grew longer and the yield became higher (b).

Figure 2.30 shows the UV-Vis-NIR spectrum of the growth solution over a long time period. After 1 day, we observed that short NRs were formed with significant amount of byproduct (50%). The NRs grew very slowly over 1 week and became longer (aspect ratio 7).

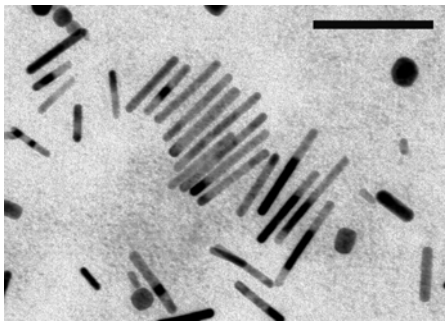

Figure 2.31. TEM image of gold NRs grown without seed solution. The scale bar is 100nm.

The growth is slow because there should be an induction period to form nuclei from which NRs can be grown. The amount of byproduct is higher than the seed grown case because nucleation and growth take place at the same time. Figure 2.31 shows a TEM image of gold NRs grown by adding $NaBH_4$ as a nucleating agent. Since the growth is slow, the surfactant can effectively confine the growing direction, the diameter of NRs is smaller than the diameter of NRs grown by adding seed solution (average diameter of NRs grown without seed solution< 8 nm, average diameter of NRs grown with seed solution > 8 nm). Therefore, the seed solution must act as a catalyst for the reduction of $AuBr_2^-$ ions by the unconsumed AA due to particle-mediated electron transfer from AA to $AuBr_2^-$ [38].

2.4. Conclusions

In summary, we have shown that the morphology of gold NRs is controlled by manuplating the reduction rate and the adsorption kinetics of the surfactant. The choice of surfactant is important not only because of its adsorption on the surface of the growing particles but also because the precusor of gold-surfactant complex has significant influence on determining ΔE of reduction reaction. Our results show that the adsorption competes against the reduction of gold ion on the same surface of the NR. When reduction rate is slower, long NRs with smaller diameter are obtained while when reduction is forced, short NRs with larger diameter are obtained. Therefore, by scheming the addition of AA in multiple steps, tuning the aspect ratio and the shape of the NRs can be achieved.

References

[1] Shalaev, V.M.; Cai,W.;Chettiar,U.K.; Yuan,H.; Sarychev,A.K.; Drachev,V.P.; Kildishev, A.V. "Negative index of refraction in optical metamaterials" *Optics Letters* **2005**, *30*, 3356.

[2] a) Foss Jr., C.A.; Hornyak, G.L.; Stockert, J.A.;Martin, C.R. "Optical properties of composite membranes containing arrays of nanocsopic gold cylinders" *J. Phys. Chem.* **1992,** *96*, 7497 b) van der Zande, B.M.I.; Bo1hmer,M.R.; Fokkink, L.G.J.; Scho1nenberger,C. "Aqueous Gold Sols of Rod-Shaped Particles" *J. Phys. Chem. B* **1997**, *101*, 852.

[3] Pollard, A.P.; Heron, C. "Archaeological Chemistry", Royal Society of Chemistry**. 1996;** Chapter 5.

[4] Faraday, M."Experimental Relations of Gold (and other metals) to Light" *Philos. Trans.* **1857**, *147*, 145.

[5] Schmid, G.; Corain, B., "Nanoparticulated gold: Syntheses, structures, electronics, and reactivities" *European Journal of Inorganic Chemistry* **2003**, *17*, 3081.

[6] Marie-Christine,D.; Didier,A."Gold nanoparticles: assembly, supramolecular chemistry, quantum-size-related properties, and applications toward biology, catalysis, and nanotechnology" *Chemical reviews* **2004,** *104*, 293.

[7] Turkevich, J.; Stevenson, P. C.; Hillier, J. "The nucleation and growth processes in the synthesis of colloidal gold" *Discussions of the Faraday Society* **1951**, *11* 55.

[8] Torigoe,K.; Esumi,K. "Preparation of Colloidal Gold by Photoreduction $AuCl_4^-$-Cationic Surfactant Complexes" *Langmuir* **1992**,*8*, 59.

[9] Esumi,K.; Matsuhisa,K.; Torigoe,K. "Preparation of Rodlike Gold Particles by UV Irradiation Using Cationic Micelles as a Template" *Langmuir* **1995**,11, 3285.

[10] Esumi,K.;Junko, H..;Nariaki, A.; Usui,K.; Torigoe,K. "Preparation of Anisotropic Gold Particles Using a Gemini Surfactant Template" *Journal of Colloid and Interface Science* **1998**, *208*, 578.

[11] Kameo,A.; Suzuki,A.; Torigoe,K.;Esumi,K. "Fiber-like Gold Particles Prepared in Cationic Micelles by UV Irradiation: Effect of Alkyl Chain Length of Cationic Surfactant on Particle Size" *Journal of Colloid and Interface Science* **2001**, *241*, 289.

[12] Kim, F.; Song, J. H.;Yang, P. "Photochemical synthesis of gold nanorods" *J. Am. Chem. Soc*., **2002**,*124,* 14316.

[13] Niidome,Y.;Nishioka,K.; Kawasaki, H.; Yamada, S. "Rapid synthesis of gold nanorods by the combination of chemical reduction and photoirradiation processes; morphological changes depending on the growing processes" *Chem.Commun*. **2003,** 2376.

[14] Yu,Y; Chang,S; Lee,C; and Wang, C. R. C. "Gold Nanorods: Electrochemical Synthesis and Optical Properties" *J. Phys. Chem. B*, **1997**, *101*, 6661.

[15] Jana, N. R.; Gearheart, L; Murphy,C. J."Wet Chemical Synthesis of High Aspect Ratio Cylindrical Gold Nanorods*" J. Phys. Chem. B*, **2001**, *105*, 4065.

[16] Brown, K. R.; Walter, D. G.; Natan, M. "Seeding of Colloidal Au Nanoparticle Solutions. 2. Improved Control of Particle Size and Shape" *J. Chem. Mater*. **2000**, *12*, 306.

[17] Busbee, B.D.; Obare, S.O.; Murphy, C.J. "An improved synthesis of high-aspect-ratio gold nanorods" *Advanced Materials* **2003**, *15*, 414.

[18] Canizal, G.; Ascencio, J. A.; Gardea-Torresday, J.; Yacaman, M. J. "Multiple twinned gold nanorods grown by bio-reduction techniques" *Journal of Nanoparticle Research* **2001**, *3,* 475.

[19] Mieszawska, A. J.; Zamborini, F. P. "Gold Nanorods Grown Directly on Surfaces from Microscale Patterns of Gold Seeds" *Chemistry of Materials* **2005**, *17,* 3415.

[20] Nikoobakht, B; El-Sayed, M. A. "Preparation and Growth Mechanism of Gold Nanorods(NRs) Using Seed-Mediated Growth Method" *Chem.Mater*. **2003**, *15*, 1957.

[21] Bakshi,S.; Kaur, I. "Head-group-induced structural micellar transitions in mixed cationic surfactants with identical hydrophobic tails" *Colloid Polym. Sci*. **2003**, *281*, 10.

[22] Jana, N. R.; Gearheart, L.; Murphy, C. J. "Seeding Growth for Size Control of 5-40 nm Diameter Gold Nanoparticles" *Langmuir* **2001**, *17*, 6782.

[23] Frens, G. "Controlled Nucleation for the Regulation of the Particle Size in Monodisperse Gold Suspensions" *Nature: Phys. Sci*. **1973**, *241*, 20.

[24] Goia, D.V.; Matijevic E. "Preparation of monodispersed metal particles" *New Journal of chemistry* **1998**, *22*, 1203.

[25] Zweifel,D.A.;Wei,A. "Sulfide-Arrested Growth of Gold Nanorods" *Chem. Mater.* **2005,** *17,* 4256.

[26] Gao,J.; Bender,C.M.;Murphy,C.J. "Dependence of the Gold Nanorod Aspect Ratio on the Nature of the Directing Surfactant in Aqueous Solution" *Langmuir* **2003**, *19*, 9065.

[27] Veisz,B.; Kiraly,Z. "Size-Selective Synthesis of Cubooctahedral Palladium Particles Mediated by Metallomicelles" *Langmuir* **2003**, *19*, 4817.

[28] Puddephatt, R.J. "The chemistry of gold" Elsevier:Amsterdam-Oxford-New York, **1978**

[29] Bard,A. J. "Encyclopedia of Electrochemistry of the elements" vol. IV, Marcel Dekker: New York and Basel, **1975**

[30] Velegol, S. B. ; Fleming, B. D.; Biggs,S.; Wanless,E. J.; Tilton, R. D. "Counterion Effects on Hexadecyltrimethylammonium Surfactant Adsorption and Self-Assembly on Silica" *Langmuir* **2000**, *16*, 2548.

[31] Atkin, R;. Craig, V.S.J.; Wanless, E.J. ; Biggs, S., "The influence of chain length and electrolyte on the adsorption kinetics of cationic surfactants at the silica–aqueous solution interface" *Journal of Colloid and Interface Science* **2003,** *266*, 236.

[32] Nikoobakht, B; El-Sayed, M. A. "Evidence for bilayer assembly of cationic surfactants on the surface of gold nanorods" *Langmuir*, **2001**, *17* , 6368.

[33] Gai, P.L.; Harmer, M.A. "Surface Atomic Defect Structures and Growth of Gold Nanorods" *Nano lett.* **2002**, 2, 771.

[34] Bakshi, M. S.; Kaur,I. "Head-group-induced structural micellar transitions in mixed cationic surfactants with identical hydrophobic tails" *Colloid Polym. Sci.* **2003,** *281*, 10.

[35] Ross, S.; Kwartler, C. E.; Bailey, J.H. "Colloidal association and biological activity of some quaternary ammonium salts" *Journal of Colloid Science* **1953**, *8*, 385.

[36] Sau, T.K.;Murphy,C.J. "Seeded High Yield Synthesis of Short Au Nanorods in Aqueous Solution" *Langmuir* **2004**, *20*, 6414.

[37] Chen,S.; Wang,Z. L.; Ballato,J. ;Foulger, S. H.; Carroll,D. L. "Monopod, bipod, tripod, and tetrapod gold nanocrystals" *J. Am. Chem. Soc*. **2003**, *125*, 16186.

[38] Perez,J.; Gonzalez,E.R., "Hydrogen Evolution Reaction on Gold Single-Crystal Electrodes in Acid Solutions" *J.Phys.Chem.B* **1998**, *102*,10931.

Chapter III

Morphology and Growth mechanism of Gold Nanorods

Abstract

Growth mechanism of gold NRs (NRs) was elucidated by studying the crystallography of nanoparticles (NPs).

The seed particles grow in strong kinetics-controlled environment. They are cubo-octahedra with a certain size distribution. Depending on the confinement and the initial size of the seed particle, some of them grow to become NRs which are enclosed mainly by {100} and {110} facets and their axial growth direction is [001] and some grow to become truncated cubic having {100} and {111} facets. Experimental images of gold NRs are shown that corroborate the proposed structure.

3.1. Introduction

In the wet chemical synthesis of NPs, the structures of particles are determined both by the kinetic and thermodynamic factors. In most cases, a mixture of different structures is obtained which represents the statistical thermodynamics of the energies and the effects of kinetics during the growth process[1]. When there is very strong kinetic control of the growth, it results in special types of particle morphologies such as rods, needles, platelets, and dendrites.

This strong kinetic control is found in the synthesis of gold NRs where a weak reducing agent and larger amount of surfactant are used for stabilizing unstable facet.

We reviewed the literature to summarize the key findings in the crystallographies of gold NRs and how the specific structure is related to the growth mechanism. The knowledge of the crystal structure of the particles may assist to deduce the growing mechanism.

Characterization of gold NRs has been done mostly by the image of particle and electron diffraction using transmission electron microscope (TEM).

Large fiber-like gold particles (2μm) obtained by UV irradiation at higher concentration surfactant were found to have {110} faces while large gold particles grown in the absence or low concentration of surfactant generally show {111} facets, which have the lowest surface energy[2]. The preferential growth of the specific plane

is attributed to the adsorption of the surfactant molecules.

Wang et al. studied gold NRs synthesized electrochemically using surfactant micelles as a capping material using high resolution transmission electron microscope (HRTEM)[3] and found that short gold NRs with aspect ratios of 3-7 were single crystals without dislocation, stacking fault or twin enclosed mainly by {100} and {110} facets with a [001] axial growth direction(Figure 3.1).

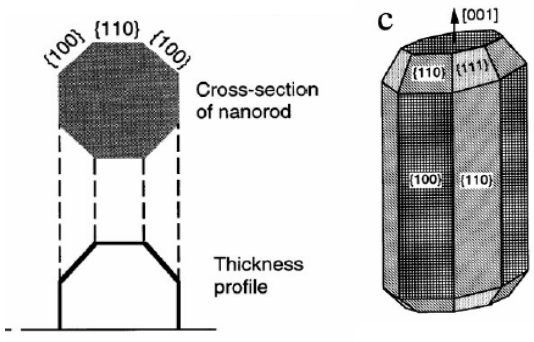

Figure 3.1. The structural model of gold NRs proposed by Wang et al. [3]

They also found that longer gold NRs with aspect ratios 20-35, which are observed occasionally, contained single twinning. Their surfaces were predominantly {111} and {110}, and their axial growth direction was <112>. Spherical particles with mass equivalent to the short rods, was found to be truncated octahedra, icosahedra, or decahedra with {111} and {100} facets and multiple twinning.

Kim et al obtained gold NRs by UV irradiation and found that the

crystallographic facets are the same as the electrochemically synthesized gold NRs, with the growth direction being [001] and the side mostly covered with {001} and {110} facets[4].

A seed-mediated sequential growth process has been taken by many research groups as a synthesis method to obtain high aspect ratio of NRs. In the observation of gold NRs prepared by this method, Johnson et al.[5] suggested that the gold NRs had a penta-twinned structure with five {111} twin boundaries arranged radially to the <110> direction of elongation and ten {111} end faces. The side faces were believed to be either {100} or {110}, or both. Gai et al[6] also suggested that NRs are multiply twinned particles (MTPs) with (110), (111) faces on sides and [100] direction.

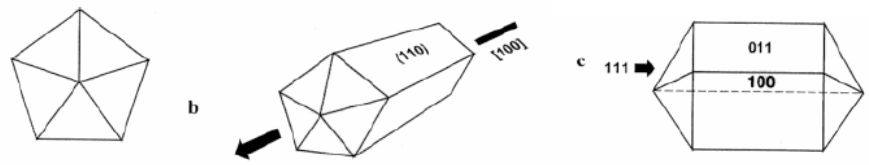

Figure 3.2. The structural model of gold NR proposed by Gai et al.[6]

One can notice that some of the fcc metal NRs have been claimed to be single crystals, while others are composed of multiple crystal units. The apparent discrepancy may originate from the different synthesis methods which result in different kinetics of growth. For example, in seed-mediated sequential method, NRs are synthesized by multiple steps such that usually seed solution is added to the

growth solution and this growth solution becomes seed solution and again added to the new growth solution. It takes several hours to complete the whole process of growth. The final size of NRs which is used in the characterization of crystallography is usually in the range of hundreds nanometers in length. By contrast, electrochemically grown NRs can be obtained in an hour and the size is tens of nanometer.

The presence of the {110} facets is the common observation in the literature. It is a unique feature of gold NRs and is not usually observed in spherical NPs because the {110} facet has higher energy than that of the {111} and {100} facets.

It is necessary to examine the mechanism and link the mechanism to the resulting crystallography of NRs. Several possible growth mechanisms have been recently proposed [6-8].

Zipping mechanism[7] was proposed focusing on the role of CTAB. Gold atoms are added to the end faces while gold-surfactant complexes are added to the side of the rods where CTAB binds as a bilayer to the growing sites assisting NP elongation. This mechanism assumes the pre-existence of rod shaped particles and fails to explain the formation of significant amount of nanosphere.

Gai et al. proposed that multiply twinned particles are made prior to the rod formation, which have twin boundaries[6]. Weaker bonding in twin boundary areas

can provide sites for agglomeration. Leontides et al.[8] reported the synthesis of thread-like gold particles by UV irradiation as the reduction path and proposed that the gold-surfactant pairs are solubilized in the micelles and intially formed particles aggregates directionally by preferential surfactant binding.

These proposed mechanisms have difficulties explaining several aspects of the observations made in the synthesis. For example, they fail to explain the diversity of shapes produced in a single synthesis reaction.

Therefore,we need to approach the mechanism of gold NRs formation not by considering only rod shape but considering all the possibility to form the different structure and to elucidate why the formation of rod shape is preferred.

We prepare gold NRs by the one step seed-mediated method in binary surfactant system and attempt to elucidate the growth mechanmis by examining the crystallographies of gold NRs and sphercal particles.

3.2. The crystallographic model of gold nanorods

Before proceeding to discuss crystallography of gold nanorods, we want to point out some issues in TEM observation.

TEM is the classical way to determine the size and shape of the NPs. But there are a number of drawbacks to the TEM technique. Many materials require

extensive sample preparation to produce a sample thin enough to be electron transparent, and changes in the structure may be caused during this process. Also the field of view is relatively small, raising the possibility that the region analyzed may not be characteristic of the whole sample, which leads to bad statistics[9]. Also, it has the limitation such that it only provides a projected image, and although there is some depth data, this is not cleanly interpretable.

We demonstrated how data can be biased depending on the field of view. Figure 3.3 shows 3 images taken from the same TEM grid in different field of view. The size of NRs was measured from each image was tabulated in Table 3.1 showing a significant differences depending on the field of view and the sample size.

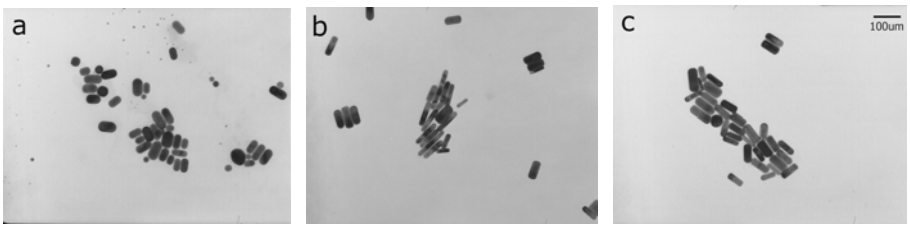

Figure 3.3. The TEM images of gold NRs taken from the different field of view of a specimen, showing different aspect ratios.

It is known that NPs are self assembled especially driven by evaporation of the water. This process is sure to occur in the process of preparing the TEM grid. Therefore, measuring some (200) particles from subjectively selected spots and determining the size of the NRs cannot be the legitimate method. TEM observation has to be accompanied by other methods such as UV-Vis-NIR absorption

spectroscopy, light scattering and size exclusion chromatography

Table 3.1. Particle size analysis of gold NRs using different sampling area and number of sample.

	count (N)	length(nm)	diameter(nm)	aspect ratio
A	100	70.6±12.1	15.4±1.5	4.5±1.0
B	100	85.4±20.1	15.5±1.9	5.5±1.9
C	100	81.5±11.6	15.5±1.3	5.3±1.0
D	300	80.2±15.2	15.6±1.6	5.2±1.3

Figure 3.4 illustrates the collection of different shapes and sizes of NPs produced by the synthesis method we used. For NRs, the shape is spherocylinder for all aspect ratios. The ends of the NRs don't have sharp edges. It rather has a flat end with tapered side**.**

Figure 3.5 shows the electron diffraction from a single rod. From the diffraction contrast, it is clear that gold NRs have the single crystalline structure regardless of the aspect ratio. Electron diffraction pattern supports the facets enclosing the NRs are {110} and the growth direction is [001].

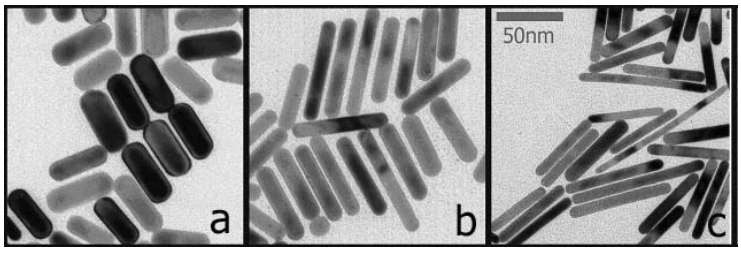

Figure 3.4. The collection of different shape and size of NPs produced by the one step seed mediated synthesis in binary surfactant system. a) aspect ratio of 3, b) aspect ratio of 5, and c) aspect ratio of 7.

a) b)

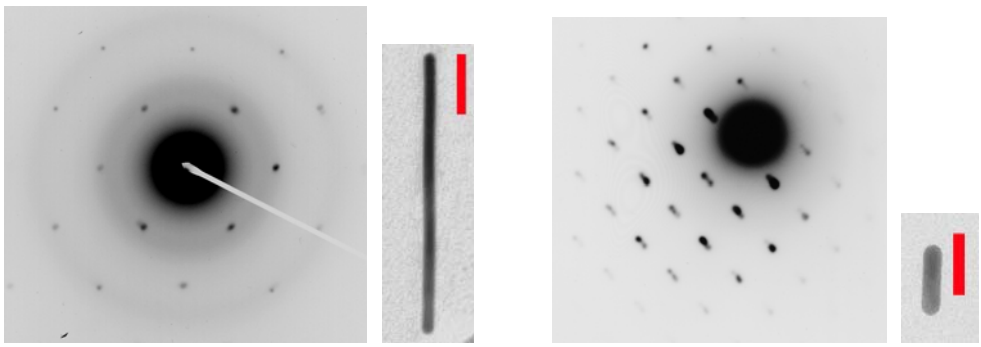

Figure 3.5. The electron diffraction pattern of gold NRs from a single rod. a) L/d= 24 and b) L/d= 4. Scale bar is 50nm.

For isomeric NPs, polygonal shape of particles and cubic particles are found as byproduct depending on the synthesis condition (the ratio of CTAB/BDAC, the concentration of surfactant). The big spherical particles (>50nm) exist in a very small fraction and appear to be MTP (Figure 3.6 a). Figure 3.6 b shows the truncated cubic particle.

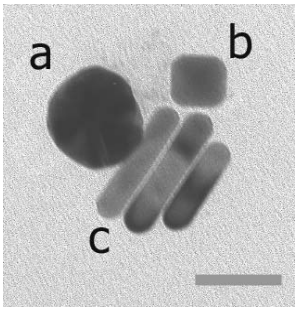

Figure 3.6. TEM image of NRs along with bigger MTP and cubic as byproducts.

Since the majority of NPs we prepared are single crystal, the models based on MTP are not relevant.

TEM observation has the limitation of providing only the projected image of particle. However, we were able to obtain the information of cross section through TEM. We prepared TEM grid with highly concentrated NRs solution to study self assembly of NRs. Upon assembly of the rods into a nematic phase, we found areas of what appears to be defects that are characteristics of nematic fluids. Upon looking at the core of these defects we found what appear to be spheres, however, on tilting it is clear that they are not spheres, but rather rods standing up on their ends.

Thus we were able to visualize the cross section of NRs. We found that the cross section is octagon shape. Figure 3.7 shows octagonal cross section of the NRs packed as a square packing.

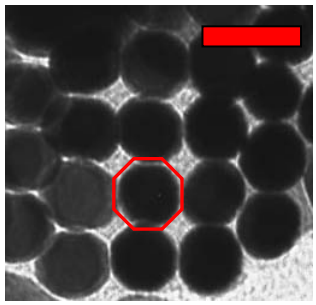

Figure 3.7. Octagonal cross section of the NRs packed as a square packing.

The TEM observation of NRs is consistent with Wang's model[3] where single crystal gold NR is enclosed mainly by {100} and {110} facets and its axial growth direction is [001].

3.3. Growth mechanism

Then the question is which growth mechanism leads to this morphology. Since we choose the seed-mediated synthesis method, the crystalline structure of the seeds at the nucleating stage is critical for guiding the shapes of NPs due to its characteristic unit cell structure. Also, it is important to know the interface between the seed and growing materials, which has not been well resolved yet.

There have been several reports that the size of seed made by $NaBH_4$ reduction is about 4nm[10] , but neither direct TEM observation nor the information about the crystal structure of seed particle is available since the size is too small. Though, it is reported earlier that small single crystal of gold is of roughly wulff construction shape with (111) and (100) facets [1].

Growth rates are controlled by the sticking probability on a given face. Since, for instance a (001) face of an fcc material has a higher sticking probability, being of higher surface free energy than a (111) face, it will grow faster. The kinetic structure will therefore be dominated by slower growing faces such as (111), and might contain no (001) facets.

When the shape of the seed is assumed as a cubo-octahedral particle which has 8 hexagons of (111) surface and 6 square shapes of (100) surfaces, we can expect the same results. Since (111) surface is more stable than (100) surface, growth will take

place mainly in <100> direction. When the growth rate is the same for every <100> direction, then the particle will become truncated cubic which we observed in our synthesis.

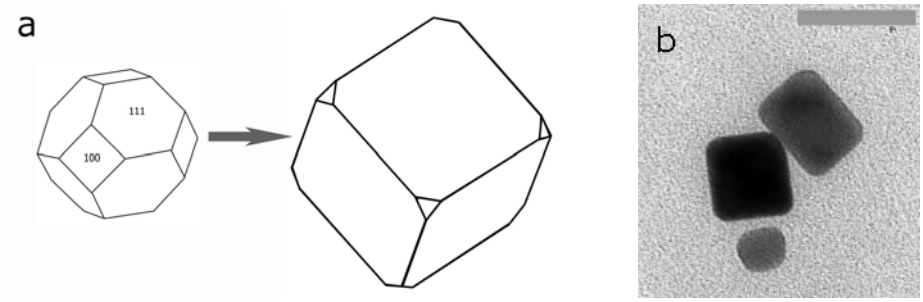

Figure 3.8 a) Possible growth mechanism of gold nanocube. b) Resulting gold cubic particles. Scale bar is 50nm.

However, preferential adsorption of molecules onto one or more of the surface planes can significantly alter the relative stabilities of different planes. Assuming the case when the growth rate is low and the growth rate of each direction is not all the same. While growing to <100>, there is chance to have (110). If this metastable (110) face is stabilized by the surfactant, it will promote the faster growing in that specific direction of <100>, hence rod shaped particle formation can be envisioned.

The relation between the diameter and length of NRs may provide another key to approach the growth mechanism. The general trend in our results shows that longer NRs have smaller diameter. Figure 3.9 shows the different aspect ratios of NRs synthesized in one batch. It is clearly shown that longer NRs have smaller

diameter.

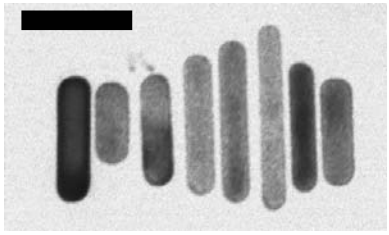

Figure 3.9. TEM image of NRs synthesized in one batch. Scale bar is 50nm.

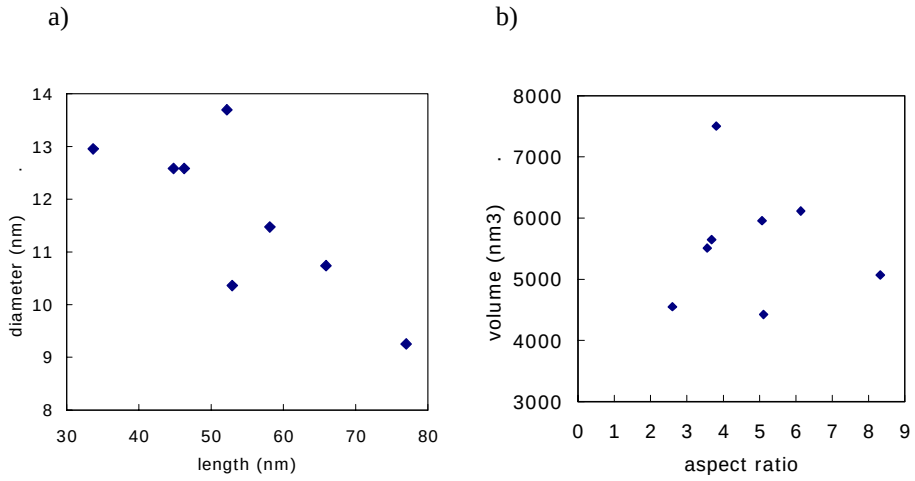

Figure 3.10. a) The relation between diameter and length of NRs. b) The relation between aspect ratio and volume of NRs.

The calculation of volume shows that there is no correlation between the aspect ratio and the volume of NRs. We reasoned that initially smaller seed becomes longer NR and initially larger seed becomes shorter NR in a given period of time. The amount of gold reduced on a given particle is almost the same.

We synthesized the NRs without seed solution. Instead of adding seed solution, a very small amount of $NaBH_4$ solution equivalent to the amount of $NaBH_4$ in the seed solution was added. Figure 3.11 shows the TEM image of NRs we obtained from this synthesis. Comparing the dimension of NRs, we found that the

diameter of NRs obtained from this synthesis is smaller than that of the seeded method for all aspect ratio.

Figure 3.12 shows the relation between the length of NRs and the diameter of NRs. The longer the NRs, usually the thinner the NRs. The NRs from seedless synthesis shows the same trend but the diameter is smaller. For the seedless synthesis, nucleation and growth cannot be separated. As the primary particle forms, it grows to NRs . Therefore the preferential adsorption can be involved from the initial stage of growth to enduce the thinner NRs.

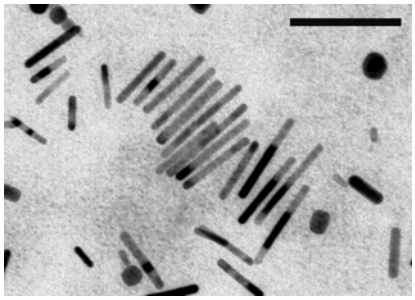

Figure 3.11. TEM image of gold NRs grown without seed solution. Scale bar is 100 nm.

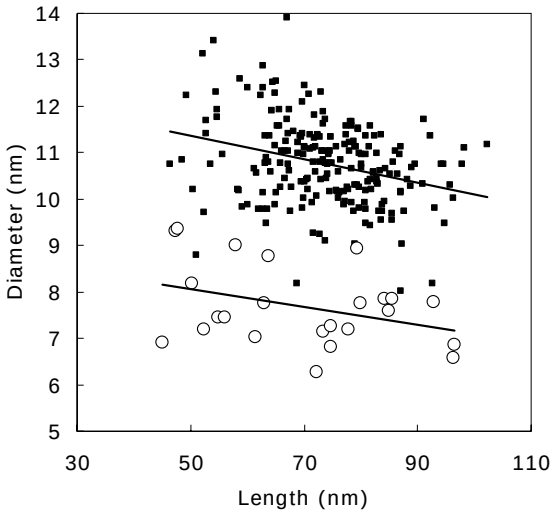

Figure 3.12. The relation between length and diameter of NRs. Open circle represents the NRs prepared without seed and filled square represents the NRs prepared with seed. The diameter of NRs without seed is smaller when the length is similar.

We propose the following as the growth mechanism for gold NRs.

Step I. Formation of gold-surfactant complex

CTA-Br + $HAuCl_4 \rightarrow$CTA-[$AuCl_mBr_{4-m}$] (m=0-4)$\rightarrow$ CTA -[$AuBr_4$]

Au^{+3} is reduced to Au^{+1} by ascorbic acid resulting in CTA -[$AuBr_2$].

Step II. Solubilization of the complex by micelle

Metallomicelles are formed. gold-surfactant complex is protected from spontaneous consumption.

Step III. Formation of primitive NPs

The primitive cubo-octahedral NPs are produced. . CTAB molecules start to be adsorbed on the surface of the particles.

Step IV-1. Growth of NRs and nanocubes

Gold-surfactant complex is transferred from the micelle to the growing site. Gold ion diffused and is reduced by ascorbic acid with the

catalytic effect of seed. At the same time, CTAB molecule is adsorbed on the surface of NP joining the existing layer of CTAB due to hydrophobic interaction between the long carbon chains. The layer of CTAB stabilizes the elongated NPs. As CTAB forms the first layer on the surface of NPs, free molecule of CTAB in the solution starts to be adsorbed to the existing layer of CTAB forming bilayer.

Depending on the efficiency of stabilization of metastable face of (110), the faster growing in that specific direction of <100> results in the formation of NRs. When the growth rate is the same for every <100> then particle will become truncated cubic which we observed in our synthesis.

Step IV-2. Growth of spherical shape NPs

Some of the primitive particles aggregate to become spherical shape of NPs. Since the aggregation is random, the size is not uniform.

What can be explained by this growth mechanism?

- The effect of concentration of surfactants: when the concentration is lower, the size and number of micelle are not enough to solubilize Au-surfactant complex to protect them from spontaneous reduction. As the concentration increases, more complexes are protected and released to the growing site over longer period of time.
- The existence of optimum ratio of mixing BDAC and CTAB: when BDAC and CTAB are mixed at the optimum ratio, the micelle size is maximized for protecting more complex inside the micelle. And the number of free CTAB molecule in the solution is also maximized to facilitate absorption of surfactant on the surface of NPs.

- The formation of NRs as well as byproducts: the shape and size of the NPs are decided by the size of primitive particle to begin with.
- The formation of nanobone: after the growth stops, CTAB molecule continuously is absorbed on the surface of NP to make dense bilayer. When the growth resumes, the reduction is reinitiated only at the ends of NPs resulting branched shape.

3.4. Conclusions

In summary, we describe the growth mechanism of gold NRs elucidated by crystallography of NPs. The particle shape of the seed corresponds to cubo-octahedron. The seeds which grow in strong kinetics controlled environment already have a certain size distribution. Depending on the confinement and the initial size of seed particle, some of them grow to become NRs which are enclosed mainly by {100} and {110} facets and their axial growth direction is [100] and some grow to become truncated cubics having {100} and {111} facets.

References

[1] Marks, L. D. "Experimental studies of small particle structures" *Rep. Prog. Phys.* **1994**, *57*, 603.

[2] Kameo, A.; Suzuki,A.;Torigoe,K.; Esumi,K. "Fiber-like Gold Particles Prepared in Cationic Micelles by UV Irradiation: Effect of Alkyl Chain Length of Cationic Surfactant on Particle Size" *Journal of Colloid and Interface Science* **2001**, *241*, 289.

[3] Wang, Z.L.; Mohamed, M.B.; Link, S.;El-Sayed, M.A. "Crystallographic facets and shapes of gold nanorods of different aspect ratios" *Surface Science* **1999**,*440*,L809.

[4] Kim, F.; Song, J. H.;Yang, P."Photochemical synthesis of gold nanorods" *J. Am. Chem. Soc*. **2002**,*124*, 14316.

[5] Johnson, C.J.; Dujardin, E.; Davis, S.A. ; Murphy, C.J.; Mann, S. "Growth and form of gold nanorods prepared by seed-mediated, surfactant-directed synthesis" *Journal of Materials Chemistry* **2002**, 12, 1765.

[6] Gai, P.L.; Harmer, M.A. "Surface Atomic Defect Structures and Growth of Gold Nanorods" *Nano lett.* **2002**, 2, 771.

[7] Gao,J.; Bender,C.M.;Murphy,C.J. "Dependence of the Gold Nanorod Aspect Ratio on the Nature of the Directing Surfactant in Aqueous Solution" *Langmuir* **2003**, *19*, 9065.

[8] Leontidis,E.;Kleitou,K.;Kyprianidou-Leodidou, T.; Bekiari,V.; Lianos, P. "Gold Colloids from Cationic Surfactant Solutions. 1.Mechanisms That Control Particle Morphology" *Langmuir* **2002**, *18*, 3659.

[9] Schnabel,U; Fischer,C.; Kenndler,E."Characterization of Colloidal Gold Nanoparticles According to Size by Capillary Zone Electrophoresis" *J. Microcolumn Separations*, **1997**, *9*, 529.

[10] Nikoobakht, B; El-Sayed, M. A. "Preparation and Growth Mechanism of Gold Nanorods(NRs) Using Seed-Mediated Growth Method" *Chem..Mater*. **2003**, *15*, 1957.

Chapter IV

Shape and Size Separation of Gold Nanorods

Abstract

The shape separation of gold nanorods from a mixture of rods and spheres is accomplished by centrifugation. We elucidate the hydrodynamic behavior of nanoparticles of various shapes to identify the parameters to achieve efficient separation. We describe the relative sedimentation behavior of colloidal rods and spheres by the ratio of the sedimentation coefficients between rods and spheres where the relative diameter of the particles determines the relative sedimentation of rods and spheres for a given aspect ratio.

4.1. Introduction

Nanoparticle synthesis is characterized by a polydispersity in shape and size. The physical and chemical properties as well as the applications of nanoparticles are controlled and limited by their dimensions and shape[1] .

As significant research efforts have been directed to optimize the synthesis conditions[2], there have been efforts to separate nanoparticles of different sizes and shapes, since most of the synthesis methods result in mixture of particles with different morphologies.

Size selective precipitation has been commonly used for nanospheres dispersed in organic solvents[3,4]. Capillary electrophoresis[5] and column chromatography[6] have been used in the separation of metal nanoparticles.

In gold nanorod(NR) synthesis, the production of spherical particles as byproduct is inevitable. Depending on the different methods, the fraction of byproduct can be 10% to almost 90 %[7,8,9]. The use of separation methods mentioned above is limited because some methods are not applicable and some methods only result in partial separation[10].

Regular centrifugation has been a part of the routine procedure to concentrate nanoparticle solution and to separate excess capping material from the solution. Also under certain conditions, separation of particles with significant mass difference

has been achieved[8] . The advantages of the separation by centrifugation are ease of procedure and applicability to large-scale samples.

One can find the centrifugation parameters such as acceleration and duration mentioned in the scattered reports[7,8,11]. The centrifugation methods can be classified into 2 cases. When the size of NRs is less than 100nm in length, as-made solution is centrifuged at lower rpm (2000 to 6500rpm). Then, the supernatant containing NRs is centrifuged at much higher rpm (>10000rpm) to obtain precipitate at the bottom (case 1)[7,11]. When the size of NRs is much bigger, lower rpm(2000rpm) is used for getting these big particles at the bottom (case 2)[8]. Through the repeated procedure, relatively monodisperse gold NRs can be separated from small size spheres and NRs.

However, we failed to achieve efficient separation repeatedly and reproducibly using those parameters in the literature[7,8,11] because, depending upon cases, small differences in concentrations, particle dimensions and centrifugation parameters drove rods either to sediment out or remain in solution.

Centrifugation in a sucrose gradient, having been used in biological application, was adopted to separate spherical particles from rod-shaped particles[12]. Separation was conducted in a solution of sucrose where the density of the solution increases from the top to the bottom of the centrifuge tube. The particles at the bottom part of the tube are spherical particles and NRs were sorted based on their

mass with increasing aspect ratio from the top to the bottom tube. Faster sedimentation of spherical particles and slower sedimentation of NRs were attributed to the volume effect which affected the buoyancy. Although the experiment was done systematically, the theoretical explanation was not entirely satisfactory.

Jana observed precipitation of NRs from a mixture of rods, spheres and plates with different sizes[13]. This observation was made only when the solution of the mixture was concentrated and the extra CTAB was added. The precipitation of NRs on the bottom of the flask was attributed to the surfactant assisted self assembly of NRs without further theoretical considerations.

Driven by the need and desire to understand these separation phenomena, we set out to identify the physics that drives shape separation in centrifugation. We aim to investigate the role of hydrodynamics in the centrifugation of Brownian rods and spheres, to determine the size, shape and concentration dependence of sedimentation coefficients and velocities, and to establish conditions that optimize shape separation. The analysis was performed in collaboration with Vivek Sharma, and successfully interprets and explains the experimental observations of centrifugation.

4.2. Theory

We consider a simple phenomenological analysis of sedimentation-diffusion equilibrium[14]. The forces exerted on the particles during centrifugation include centrifugal force, $F_c = \omega^2 rm$, buoyant force, $F_b = -\omega^2 rm_o$, Brownian fluctuating force, $F_{f,}$ and viscous drag force, $F_d = -fv$, where ω is the centrifugation speed in rpm, m is the mass of particle, m_o is the mass displaced by the particle, r is the distance from the center to the location of particle, f is the friction or drag coefficient, and v is the sedimentation velocity. The balance of these forces leads to the Langevin equation of particle undergoing Brownian motion under the influence of an external force. In the stationary state, $F_{total} = F_d + F_b + F_c + F_f = 0$ yields the Svedberg coefficient, $S = v/\omega^2 r = (m - m_o)/f$, which expresses sedimentation velocity per unit of applied centrifugal acceleration. Svedberg coefficient is a measure of sedimentation rate and depends upon the ratio of effective mass and friction factor. Next, we need to compute f, which is shape dependent, and compare the sedimentation coefficients of rods to those for spheres. The relative importance of thermal diffusion and flow is judged by a dimensionless group called Peclet number (Pe), which is the ratio of the time a particle takes to diffuse a distance equal to its diameter D to the time it takes to sediment this distance. Pe for typical Brownian nanosphere is $Pe = va/D = (m - m_o)\omega^2 ra/k_B T < 1$, where a is the radius of the

sphere, and D is the thermal diffusivity, implying that the thermal fluctuations are non-negligible. This distinguishes nanoparticle sedimentation theories from the theories applied to macroscopic falling objects while the low Reynolds number implies that the inertial effects are negligible and the Stokes or creeping flow equations apply[15].

Drag on a Stokesian sphere is $6\pi\eta av$, where η is the viscosity of the solution, and a is the radius of the sphere, implying a friction coefficient, $f=6\pi\eta a$ and $S_0^{sph} = 2(\rho - \rho_o)a^2 / 9\eta$, where ρ is the density of the sphere and ρ_0 is the density of the solvent. In fact, the friction coefficients are similar for spherically isotropic objects, hence the description of dynamics of spheres holds equally well for the cubic, icosahedra and octahedral bodies encountered during synthesis of colloidal particles[16]. For anisotropic bodies, both force and torque balances are required, and coupling of translation and rotation needs to be considered. Translational friction coefficient of a falling single rod depends on the orientation of rod, and the friction felt parallel to the rod is ½ that of the transverse falling rods, i.e $\zeta_\perp = 2\zeta_{//}$, and $S_o^{rod} = (\rho - \rho_o)d^2\left[2\ln(L/d) - (\upsilon_\perp + \upsilon_{//})\right]/24\eta_o$ where L is the length of the rod, d is the diameter of the rod, and $\upsilon_\perp$ and $\upsilon_{//}$ are the correction factors of the rod perpendicular or parallel to the rods orientation, respectively. The actual values of $\upsilon_\perp$ and $\upsilon_{//}$ for cylindrical rods are equal to -0.84 and 0.21, respectively[17].

Thus in calculating drag for the rods, the orientation of the rods plays as big a role as the dimensions of the rod itself.

Relative sedimentation behavior of colloidal rods and spheres can be described by the ratio of the sedimentation coefficients between rods and spheres.

$$s_o^{rod} / s_o^{sph} = v_o^{rod} / v_o^{sph} = \beta_o = 6(d/2a)^2 [2 \ln L/d - (\upsilon_{\perp} + \upsilon_{//})]$$

This ratio for single rod and single sphere allows us to see that, for this case, the central role in separation is played by the square of the ratio of the diameters of the rod and sphere. For a given L/d, whether the rods or spheres sediment faster is mainly controlled by the relative diameters of the particles, and since the aspect ratio dependence enters through the log term, the effect is much less dramatic than the effect of the diameters.

We plot the ratio of the sedimentation coefficient between the rod and the sphere (β_0) as a function of the ratio of the diameter of rod and sphere for different aspect ratios of the rods (Figure 4.1). We fix the diameter of sphere as 20nm and increase the diameter of rod from 5 nm to 20 nm to obtain the ratio ranging from 0.5 to 1. Depending on the predetermined aspect ratio of rod, the length of rod is calculated by multiplying aspect ratio and the diameter of rod.

When the diameter difference between sphere and rod is small, β_0 largely depends on the aspect ratio and it is obvious that NRs with higher aspect ratio

sediment faster than spheres. In case that the diameter of sphere is larger than that of NR, β_0 becomes much smaller than the previous case indicating higher possibility of getting faster sedimentation of spheres.

The experimental parameters shown in the literature could be represented by the marked regimes in the plot. When lower rpm was used to separate NRs by taking supernatant as a result of the faster sedimentation of nanospheres, the aspect ratio of NRs is less than 5 and the ratio between the diameter of rod and sphere is less than 1[7,9,11] . This condition can be mapped in regime I.

When the aspect ratio of NRs is much larger (>15) and the diameter of NRs is comparable with that of spherical particles, lower rpm is used for getting these big particles at the bottom[8] because centrifugation results in the faster sedimentation of NRs than spherical particles. This condition can be mapped in regime II.

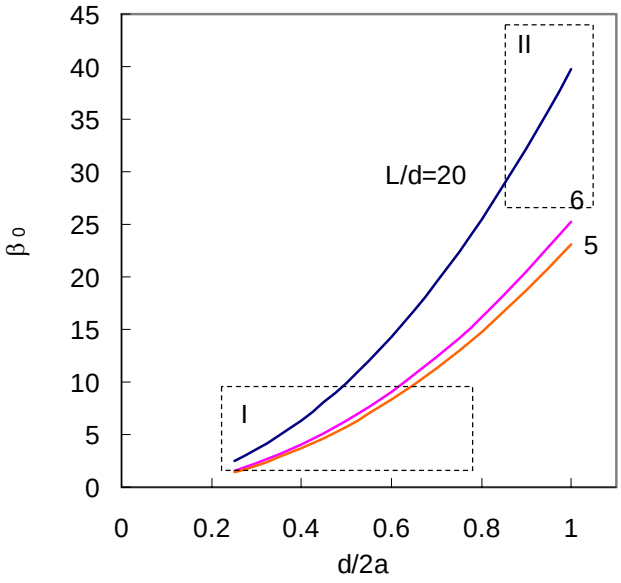

Figure 4.1**.** The ratio of the sedimentation coefficients between rod and sphere as a function of the ratio of diameters between them. The higher the ratio is, the higher the chance for rod sediment faster.

Hence, the presented analysis successfully interprets and explains the experimental observations of centrifugation.

In this chapter, we validate this analysis by our own results. We further investigate the parameters affecting the efficient separation by centrifugation.

4.3. Experimental

Gold NRs with different aspect ratios were synthesized according to procedures described in chapter 2.

4.3.1. Centrifugation of as-made solution

As-made gold NR solution was centrifuged at 5600 G for 20 to 40 min (Jouan

centrifuge MR23i). After the centrifugation, the tube was visibly inspected.

The concentrated dark solution at the bottom (inside) of the tube was taken using syringe. The supernatant was carefully removed. Solid-like deposit on the side wall was dissolved by adding distilled water.

The yield of obtaining NRs was calculated based on the intensity of the LSP and the volume of NR solution obtained.

$$Yield\ of\ the\ separation = \frac{A_p \times V_p}{A_m \times V_m}$$

where A_m is the absorbance at longitudinal surface plasmon peak of the mother solution, A_p is the absorbance at longitudinal surface plasmon peak of the purified solution, V_m is the volume of the mother solution and V_p is the volume of the purified solution.

4.3.2. Precipitation of NRs in gravitational field.

As-made NRs solution (or the solution of interest) was kept in an Erlenmeyer flask at 20°C. After 24hrs, the supernatant solution was taken and distilled water was added to the flask to dissolve the sedimentation.

UV-vis spectra were acquired with a Cary 5G UV-visible-near IR spectrophotometer. The morphology and the mean size of NPs were examined by TEM (JEOL100 at 100 KV). For each sample, the size of more than 500 particles in the TEM images were measured to obtain the average size and the size distribution.

4.4. Results and Discussion

4.4.1. Separation of nanorods from spherical particles.

Figure 4.2 shows the TEM images taken from the mother solution showing the mixture of rods and spherical particles. The average diameter of the spherical particles is 16.59 nm while the average diameter of NRs is 8.06nm. The average length of NR is 58.54 nm. Hence, the aspect ratio is 7.3. The number fraction of spherical particles is less than 10% (counting 700 particles) which is confirmed by the UV-Vis-NIR spectroscopy where the intensity of transverse surface plasmon peak (TSP) is low (Figure 4.3).

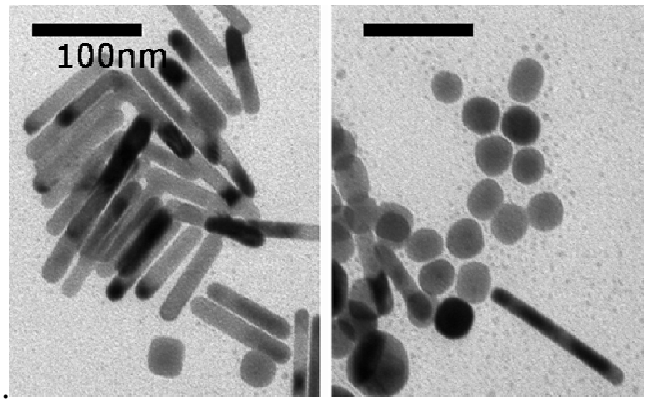

Figure 4.2. TEM image of the nanoparticles in the mother(as-made) solution, showing coexistence of the nanorods and nanospheres. L/d of gold NRs is 7.3.

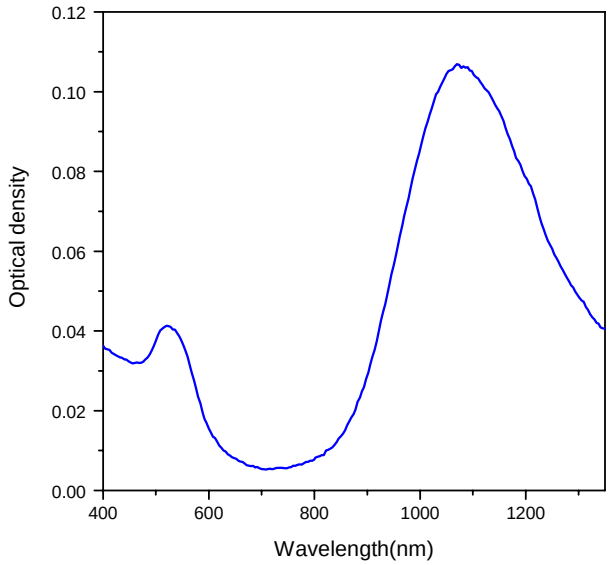

Figure 4.3. UV-Vis –NIR spectrum of the mother solution. L/d of the gold NRs is 7.3.

Figure 4.4 schematically shows the centrifuge tube after the centrifugation. A fixed angle rotor was used in this experiment. In a fixed angle rotor, since the tube is inclined, the materials are forced against the side of the centrifuge tube, and then slide down the wall of the tube. Therefore deposition on the bottom is what settles down faster. The deposition on the wall is what is later settled down. The color of the solutions taken from the bottom and the side wall of the centrifuge tube is distinctively different, which indicates that the particles deposited in different sites have different optical property due to the different size and shape.

a) b)

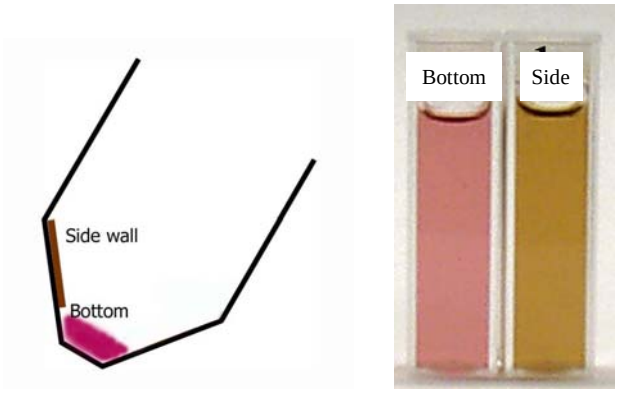

Figure 4.4. a) Schematic drawing of a centrifuge tube after the centrifugation and the color of resulting solutions. b) the color of the solution taken from two different locations shown in (a).

The UV-Vis-NIR spectrum (Figure 4.5) of the solution of the NPs from the side wall shows intense longitudinal surface plasmon peak (LSP), red shifted from the mother solution, and very weak TSP, indicating that it contains mostly NRs and the aspect ratio is larger than that of the mother solution. The spectrum of the solution of the bottom shows broad TSP with high intensity indicating that it contains mostly spherical particles and some NRs. The LSP of this solution is blue shifted from the mother solution, indicating that the aspect ratio of NRs is smaller than that of the mother solution.

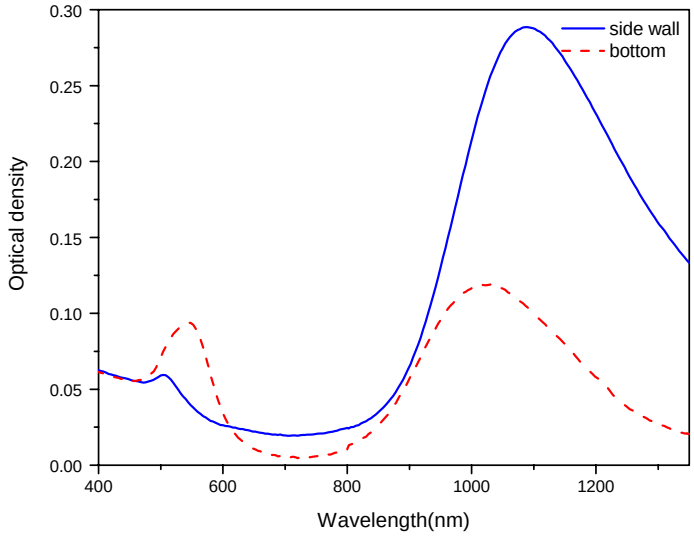

Figure 4.5. UV–Vis-NIR spectra of the solutions of the deposits on the side wall of the tube and at the bottom.

The size of the particles in these two solutions was measured by TEM (counting 500 particles from each case). TEM images (Figure 4.6) show that indeed the separation of NRs was successfully done by centrifugation. The bottom solution contains lots of spherical particles, while the solution from the side wall contains mostly NRs. In the NRs solution we prepared, the diameter of spherical particle is almost twice larger than that of NRs, resulting the smaller ratio of sedimentation between rods and sphere (average diameter of sphere is 16.6 nm). Therefore, the spherical particles are sedimented faster than the rods. We compared the dimension of NRs before separation and after separation (Table 4.1). Separated NRs from the side wall have longer length and smaller diameter thus higher aspect ratio than those in the mother solution. Shorter NRs were found in the bottom solution.

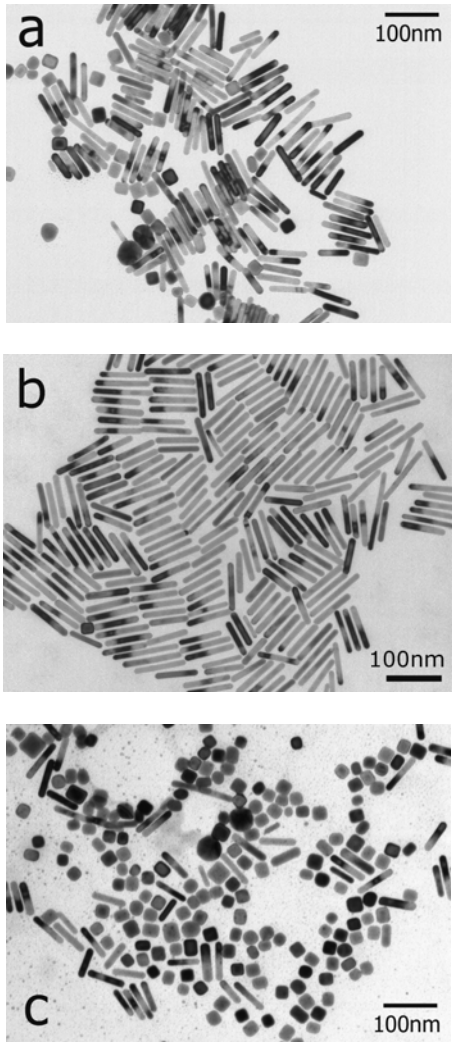

Figure 4.6. TEM images of gold nanoparticles: a) mother solution, b) after centrifugation, NRs deposited on the side wall of the tube, and c) after centrifugation, sedimented at the bottom, nanocubes, spheres and NRs with larger diameter.

Table 4.1. The size of NRs before and after the separation (unit:nm).

	L	d	L/d
Mother	58.54	8.06	7.30
Separated	65.73	7.87	8.35

Through a single centrifugation, the yield of separation was 20 to 60 percent depending on the property of as-made solution such as the aspect ratio of NRs, the

fraction of nanosphere and the diameter difference between NRs and nanospheres. The yield can be increased up to 70 to 80 percent by repeated centrifugation of the supernatant solution containing NPs which remain after the previous centrifugation. But more than 3 times of centrifugation results in the irreversible precipitation of NRs due to the loss of stabilizer on the surface of the particles resulting from the abrasion of the particles along the wall of the centrifuge tube[18] .

4.4.2. Separation of different aspect ratios.

The NR solution separated from spherical particles by the centrifugation above was further centrifuged. The centrifuge was stopped every 10 minute and the deposit at the bottom was taken.

Figure 4.7 shows the UV-Vis-NIR spectra of the centrifuged sample as a function of time. By the red-shift of LSP and blue-shift of TSP, it is apparent that the aspect ratio of the NRs obtained at different time becomes larger as a function of time indicating longer NRs sediment later then the shorter NRs. Also the shape of TSP changes as a function of time: the solution obtained earlier has a broad shoulder and it is suppressed towards the later stage.

In our synthesis, generally longer NRs have smaller diameter (Figure 4.8). Our result shows that relatively shorter NRs having larger diameter sedimented faster which agrees with the theoretical explanation that the diameter is the key factor for

the sedimentation of NRs.

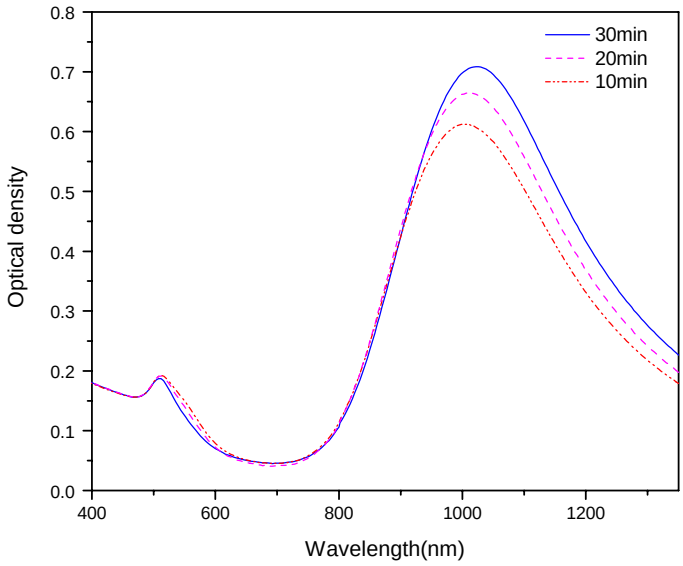

Figure 4.7. The UV-Vis-NIR spectra of the centrifuged samples as a function of time.

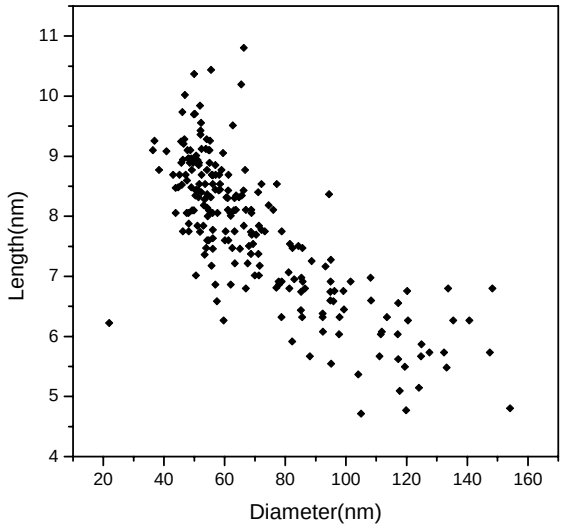

Figure 4.8. The plot of relationship between diameter and length of the NRs.

4.4.3. Effect of the surfactant concentration

Centrifugation has been routinely done to remove excess stabilizer for the

preparation of TEM grids. During many trials, we have found that there is a thin layer of dark deposition spread on the side wall of the centrifuge tube. We rinsed the wall with distilled water and obtained pure NR solution. This is observed only when as-made solution is centrifuged. When we ran 2nd round of centrifugation to increase the yield of separation or to remove more surfactant, and hence distilled water is added to the concentrated solution, this film was not observed. As it was pointed in chapter 2, we used higher concentration of surfactant to obtain NRs with higher aspect ratio and lower byproduct. The concentration of surfactant is almost double the concentration used in most literature. We deduced from this unique observation that the concentration of surfactant may affect the parameters of the centrifugation.

We set out an experiment where we divided as-made solution into different tubes and added different amount of CTAB. We prepared 4 tubes which contain 40 ml of as-made solution. 0.3, 0.9 and 1.2 g of CTAB were added to each tube. They were centrifuged at 5600 G for 30min. After the centrifugation, concentrated bottom solutions were removed by a syringe and the UV-Vis-NIR spectra were taken without dilution. The supernatants were poured out and 5ml of distilled water was added to each tube to rinse the deposit on the side wall.

Figure 4.9 shows the UV-Vis-NIR spectra of the bottom solutions and the solutions from the depositions taken from 4 different tubes. As CTAB concentration

was increased, the intensity of bottom solution was decreased while the intensity from the deposition on the side wall was increased. Decrease in the intensity of the bottom solution indicates the slower sedimentation of spherical NPs.

a)

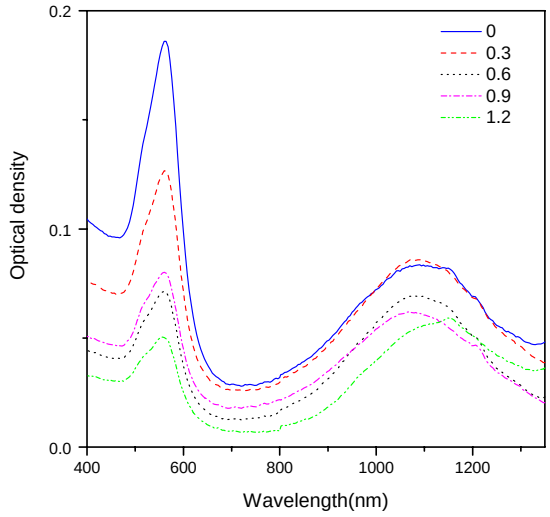

b)

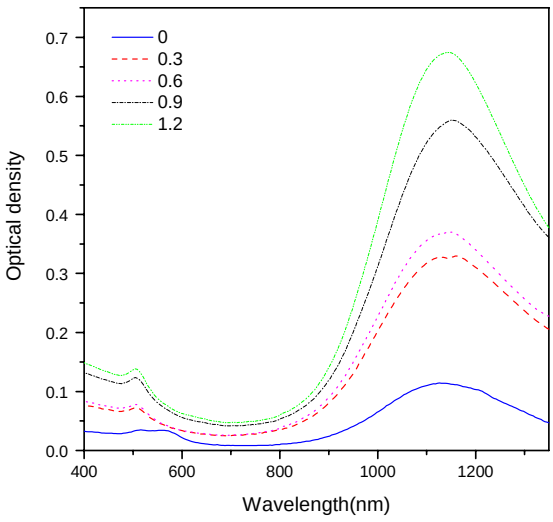

Figure 4.9. UV–Vis-NIR spectra of the separated solutions. a) Deposit on the bottom and b) deposit on the side wall as a function of the amount of extra CTAB added(g/50ml).

The yield of obtaining NRs from different conditions was shown in Figure 4.10. When extra CTAB was added, the yield of separation was increased from 36 to 74% as shown from the spectra.

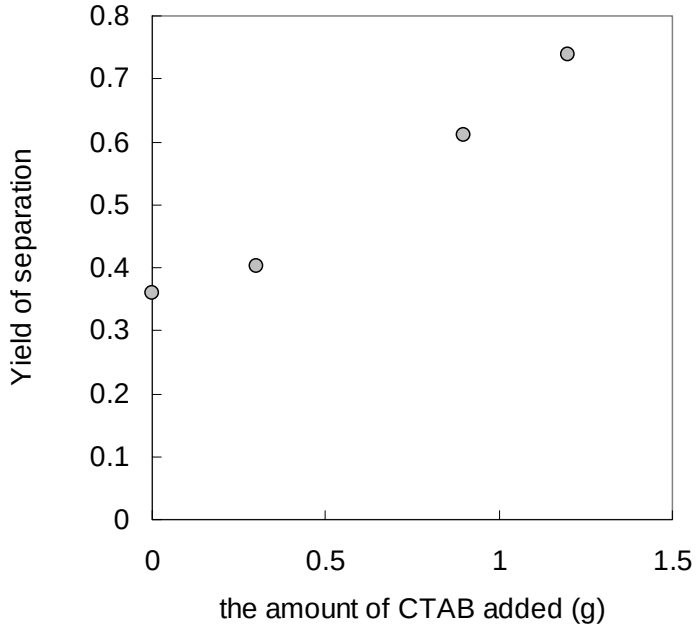

Figure 4.10. The yield of obtaining NRs as a function of amount of CTAB contained in the solution

Therefore the addition of surfactant prevents the sedimentation of nanosphere and promotes the deposition of NRs on the side wall of the centrifuge tubes.

We need to understand why nanospheres do not sediment fast with increased surfactant concentration and how the efficient deposition of NRs on the side wall is promoted. First, the viscosity of the solution changes upon adding surfactant and affects the sedimentation velocity of the particles[19]. But this can only partially explain the slower sedimentation of nanosphere. We still need to explain why rods

sediment as before and even more efficiently and stick to the wall of the tube.

To answer this question, we considered colloidal interaction. Colloidal particles are usually thermodynamically unstable[20]. Aggregation is prevented by the presence of either electric double layers or by steric stabilization. When the repulsions provided by theses energy barriers become smaller than attractions, the particles will aggregate. The aggregation strongly depends on the strength and character of the interactions. By increasing CTAB concentration, the ionic strength of the solution is increased, which results in the compression of electrical double layer promoting the flocculation of particles. The effect of colloidal interactions on the colloidal dispersion is expected to be more pronounced for rods than for sphere since both the specific surface area and the rotational volume per particle volume is much larger for rods than for spheres[21]. The flocculated particles will eventually settle into sediment. Due to the large interaction volume ($\sim L^3$), rods may form space-filling networks at very low particle concentrations. Therefore, NRs form a larger flocculation and sediment, while the sedimentation of spherical particle is slowed down due to the higher viscosity of the solution.

Once the flocculation of NRs reaches to the side of the tube, the friction between the surface of the tube and the flocculation results in the strong deposition of NRs on the surface of the tube preventing NRs sliding down towards the bottom.

4.4.4. Separation by flocculation of rods in gravitational field

Jana[13] reported surfactant assisted ordering of NRs in a concentrated dispersion which results in the phase separation of NRs from the spheres. It is observed that NRs precipitated at the bottom of the flask while spheres stayed in the supernatant. This observation was attributed to the higher concentration of particles and addition of extra surfactant which assists the formation of liquid crystal of NRs. But the mechanism of promoting the liquid crystalline phase of NRs by surfactant as well as the specific concentration of NRs at which LC phase starts to form were not mentioned.

We tried to use the same experimental parameters to reproduce the result of Jana's. However we couldn't observe any separation.

It is worth to notice that the size of NRs which Jana used was larger since they were made by sequential growth method[8]. It was mentioned that the width was 12nm and the aspect ratio was 20, hence the length of NRs was 240nm.

We reasoned that the size of NRs might be the key parameter for this separation. When we used the NRs of larger size (average length 80 nm and average diameter 11 nm) which were synthesized by reinitiating reduction of as-made NRs solution (Chapter 2), we also observed the similar phenomena without concentrating the solution and adding extra surfactant.

When the as-made solution was observed after 24hrs, a thin layer of dark color was formed at the bottom of flask, which was so stable that it didn't flow when the supernatant was poured out. Distilled water was added and the deposition was redispersed.

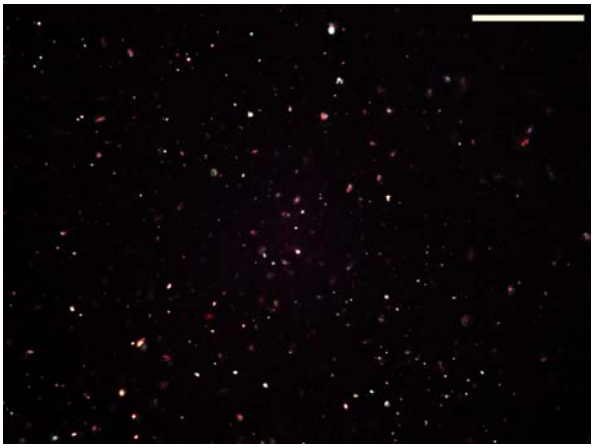

Figure 4.11. Gold NRs flocculation observed under the microscope with crossed polarizers. The scale bar is 100μm.

Figure 4.11 shows a cross polarized microscopy image of the solution in which the precipitation was redispersed. We observed gold NRs flocculation in micron size showed birefringence. The size of theses domains is about 1 μm in diameter. Since the gold NRs form flocculation, we sonicated the solution for 1hr to ensure the deflocculation of gold NRs and took the UV-Vis-NIR spectrum of the solution.

Figure 4.12 shows the UV-Vis-NIR spectra of solution before and after separation. The solution from the precipitate has very small transverse peak and most of the shoulder was removed indicating that it contained mostly longer NRs.

This result cannot be explained by the Jana's explanation since the concentration of gold NRs in the solution is extremely low.

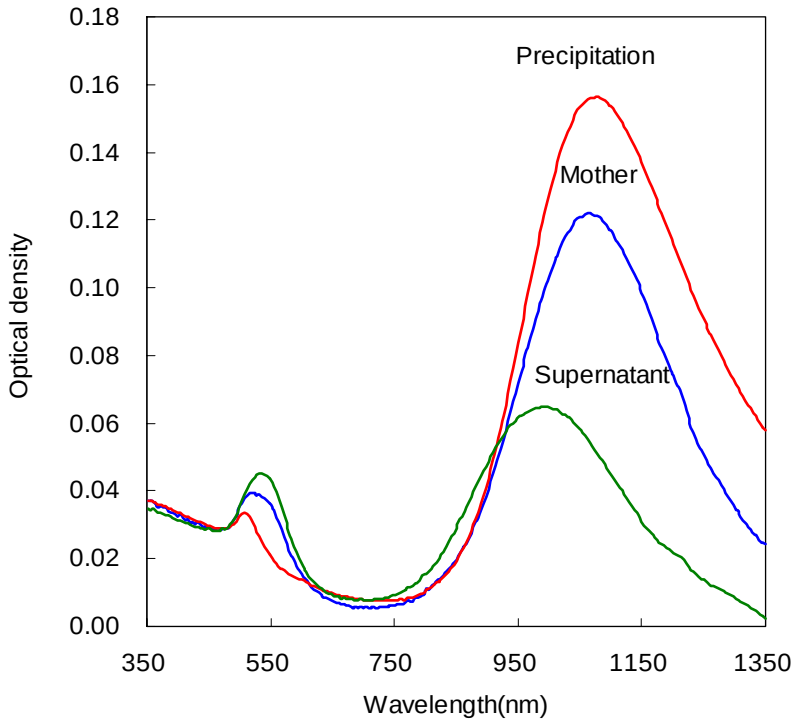

Figure 4.12. UV–Vis-NIR spectrum of separated solutions in gravitational field.

Since the stationary-state sedimentation velocity is proportional to the square of the radius of the particle, theses flocculations sediment approximately 10000 times faster than individual nanoparticles[14]. Therefore we believe that NRs of large aspect ratio form flocculation which has ordered structure and eventually sediment in relatively short time. However, the mechanism of forming flocculation needs to be studied.

In the general literature for centrifuge[22], the swinging bucket rotor is recommended if the purpose of centrifugation is to separate molecules or organelles on the basis of their movements through a viscous field. In the case of fixed angle rotor, the sediment is forced against the side of the centrifuge tube, and then slides down the wall of the tube which leads to abrasion of the particles along the wall of the centrifuge tube. We observed the irreversible aggregation of gold NRs from the repeated centrifugation in our own experiment and in the literature. Even though the type of rotor was rarely mentioned in the literature, since the rpm is usually higher than the maximum rpm to be obtained by swing-bucket rotor, we assumed that they all used a fixed angle rotor which causes such a problem.

4.5. Conclusions

In conclusion, we elucidate the hydrodynamic behavior of nanoparticles of various shapes to identify the parameters to achieve efficient separation. For a given L/d, whether the rods or spheres sediment faster is mainly controlled by the relative diameters of the particles. By centrifugation, we succeeded in separating NRs from spherical nanoparticles and to separate different aspect ratio of NRs. The purity of the NRs is more than 99% (number fraction) and the yield of separation through a

round of centrifugation can be increased up to 78% by increasing CTAB concentration which affects the colloidal interaction.

Centrifugation can be a choice of separation method when the size and shape of the mixed particle result in sufficiently different sedimentation coefficient between different particles.

References

[1] (a) Burda,C.; Chen,X.; Narayanan, R.; El-Sayed, M. A., "Chemistry and properties of nanocrystals of different shapes" *Chemical Reviews* **2005**, *105*, 1025 (b) El-Sayed, M.A., "Some Interesting Properties of Metals Confined in Time and Nanometer Space of Different Shapes" *Acc.Chem. Res*. **2001**, *34*, 257 (c) Schmid, G.; Corain, B. "Nanoparticulated Gold: Syntheses, Structures, Electronics, and Reactivities" *European Journal of Inorganic Chemistry* **2003**, *17*, 3081 (d) Daniel, M.; Astruc, D. "Gold Nanoparticles: Assembly, Supramolecular Chemistry,Quantum-Size-Related Properties, and Applications toward Biology, Catalysis,and Nanotechnology" *Chemical Reviews* **2004**, *104*, 293.

[2] (a) Yin,Y.; Alivisatos,A.P. "Colloidal nanocrystal synthesis and the organic–inorganic interface" *Nature* **2005**, *437*, 664 (b) Lisiecki I. "Size, Shape, and Structural Control of Metallic Nanocrystals" *J. Phys. Chem. B* **2005**, *109*, 12231.

[3] Murray, C. B.; Norris, D. J.; Bawendi, M. G. "Synthesis and characterization of nearly monodisperse CdE (E = sulfur, selenium, tellurium) semiconductor nanocrystallites" *J. Am. Chem. Soc*. **1993**, *115*, 8706.

[4] Whetten, R. L.; Khoury, J. T.; Alvarez, M. M.; Murthy, S; Vezmar, I.; Wang, Z. L.; Stephens, P.W.; Cleveland, C. L.; Luedtke, W. D.; Landman,U. "Nanocrystal gold molecules" *Adv. Mater*. **1996**, *8*, 428.

[5] Liua,F.; Koa,F.; Huang,P.,Wub, C.; Chuc, T. "Studying the size/shape separation and optical properties of silver nanoparticles by capillary electrophoresis" *Journal of Chromatography A*, **2005**,*1062*, 139.

[6] Wei, G-T; Liu, F-K; Wang, C. R. Chris. "Shape separation of nanometer cold particles by size-exclusion chromotography" *Analytical Chemistry* **1999**, *71*, 2085.

[7] Yu,Y; Chang,S; Lee,C; and Wang, C. R. C. "Gold Nanorods: Electrochemical Synthesis and Optical Properties" *J. Phys. Chem. B*, **1997**, *101*, 6661.

[8] Jana,N. R; Gearheart, L,; Murphy,C. J. "Wet Chemical Synthesis of High Aspect Ratio Cylindrical Gold Nanorods" *J. Phys. Chem. B*, **2001**, *105*, 4065.

[9] Nikoobakht, B; El-Sayed, M. A. "Preparation and Growth Mechanism of Gold Nanorods(NRs) Using Seed-Mediated Growth Method" *Chem.Mater*. **2003**, *15*, 1957.

[10] Pérez-Juste,J.; Pastoriza-Santos ,I.; Liz-Marzán ,L.M.; Mulvaney, P. "Gold nanorods: Synthesis, characterization and applications" *Coordination Chemistry Reviews* **2005**, *249*, 1870.

[11] Kim, F.; Song, J. H.;Yang, P.,"Photochemical synthesis of gold nanorods" *J. Am. Chem. Soc.*, **2002**,*124*, 14316.

[12] Nikoobakht,B. "Synthesis, characterization and self-assembly of gold nanorods and surface-enhanced Raman studies" Ph.D thesis **2002** Georgia Institute of Technology.

[13] Jana, N. R. "Nanorod shape separation using surfactant assisted self assembly" *Chem. Comm*. **2003**,1950.

[14] Hiemenz, P.C.; Rajagopalan, R. "Pinciples of Colloid and Surface Chemistry" 3rd ed., Marcel Dekker **1997.**

[15] Ramaswamy, S. "Issues in the statistical mechanics of steady sedimentation", *Adv. Phys*. **2001**,*50*, 297.

[16] Happel, J.; Brenner, H., "*Low Reynold Number Hydrodynamics"*, 2nd ed. Noordhoff International Publishing, Leyden **1973.**

[17] de la Torre, J.G.; V. A. Bloomfield,V.A. "Hydrodynamic properties of complex, rigid, biological macromolecules-theory and applications" *Q. Rev. Biophys*. **1981**,*14*, 81.

[18] Mikkelsen, S.R.; Cortón E., "Bioanalytical chemistry" John Wiley & Sons, **2004**.

[19] $v = \frac{2}{9}\frac{R_s^2(\rho_2 - \rho_1)g}{\eta}$ When η increased, v decreased.

[20] Everett, D.H. "Definitions, Terminology and Symbols in Colloid and Surface Chemistry - Part I, Appendix to Manual of Symbol and Terminology for Physicochemical Quantities and Units" *Pure Appl. Chem*., **1972,** *31*, 579.

[21] Wierenga, A.M.; Philipse A.P., “Low-sheer viscosity of isotropic dispersions of (Brownian) rods and fibres; a review of theory and experiments” *Colloids and Surfaces A: Physicochemical and Engineering Aspects* **1998**,*137*, 355.

[22] Wilson, K.; Walker,J. “Principles and Techniques of Practical Biochemistry” Chapter 5 Cambridge University Press, New York, 1999.

Chapter V

The Optical Properties of Gold Nanorods

Abstract

The current intense interest in metal nanoparticles for their applications in optical sensors and biological imaging is mainly based on their optical properties. In this study, the optical absorption of gold nanorods (NRs) was investigated. The theoretical calculation and experimental results were compared and the color of gold NRs was systematically identified for a wide range of aspect ratios. We also investigated the effect of medium refractive index on the absorbance of gold NRs, which would lead us to the proper choice of solvents for better application of gold NRs.

5.1. Introduction

Although bustling studies on gold nanoparticles have led to dramatically increasing number of publications, especially in the context of emerging nanoscience and nanotechnology, colloidal gold has been known for centuries as a colorant to make ruby glass and for coloring ceramics. The brilliant color is due to the presence of the metallic gold in colloidal form, although this fact was not clearly known until Michael Faraday' lecture on the "Experimental Relations of Gold (and other metals) to Light"[1].

A good understanding of the optical properties of gold nanoparticles is important for several reasons. The optical properties are directly correlated to size and shape of the particles. Hence, the formation of NPs in solution can be easily monitored using UV–Vis–NIR spectroscopy. Also, optical properties may be very sensitive to the surface processes such as adsorption, precipitation and electron transfer. The fact that the spectral characteristics of gold nanoparticles are quite sensitive to their surroundings enables them to be used as sensors. Gold nanoparticles have been used in recent years as markers for optical detection of biospecific intermolecular interactions[2].

The optical properties of noble metal particles originate from surface plasmons. These phenomena occur when electromagnetic field interacts with

conduction band electrons and induces the coherent oscillation of the free electrons. As a result, a strong absorption band appears in some region of the electromagnetic spectrum depending on the size of the particle[3]. This plasmon absorption is a small particle effect. They are absent in the individual atoms as well as in the bulk. Mie first explained this phenomenon theoretically by solving Maxwell's equations for a radiation field interacting with a spherical metal particle under the appropriate boundary conditions[4].

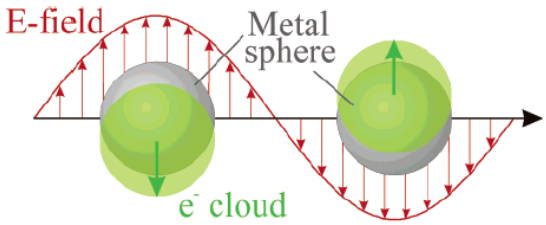

Scheme 5.1. Schematic of plasmon oscillation for a metal sphere[5].

For gold NRs, the plasmon absorption splits into two bands corresponding to the oscillation of the free electrons along and perpendicular to the long axis of the rods. The transverse mode (transverse surface plasmon peak: TSP) shows a resonance at about 520 nm, while the resonance of the longitudinal mode (longitudinal surface plasmon peak: LSP) strongly depends on the aspect ratio of NRs[6] . As the aspect ratio is increased, the longitudinal peak is red-shifted.

To account for the optical properties of NRs, it has been common to treat them

as ellipsoids, which allows the Gans formula (extension of Mie theory) to be applied. A geometrical factor P_j was introduced to calculate the absorbance of light by ellipsoids. Gans' formula[7] for randomly oriented elongated ellipsoids in the dipole approximation is

$$\frac{\gamma}{N_p V} = \frac{2\pi\varepsilon_\alpha^{3/2}}{3\lambda}\sum_{j=A}^{C}\frac{\left(\frac{1}{P_j^2}\right)\varepsilon^2}{\left[\varepsilon_1+\left(\frac{1-P_j}{P_j}\right)\varepsilon_\alpha\right]^2+\varepsilon_2^2}$$

where N_p represents the number concentration of particles, V the single particle volume, λ the wavelength of light in vacuum, ε_α the dielectric constant of the surrounding medium, and ε_1 and ε_2 are the real (n^2 - k^2) and imaginary ($2nk$) parts of the complex refractive index of the particles. The geometrical factors P_j for elongated ellipsoids along the A and B/C axes are respectively given by

$$P_A = \frac{1-e^2}{e^2}\left[\frac{1}{2e}\ln\left(\frac{1+e}{1-e}\right)-1\right]$$

$$P_B = P_C = (1-P_A)/2$$

$$e = \left(\frac{L^2-d^2}{L^2}\right)^{1/2}$$

Figure 5.1 shows the absorbance spectra calculated using the above expressions. The optical parameters for bulk gold are taken from the literature[8]. The refractive index of the medium was assumed to be constant and equal to 1.333 for water. The maximum of the longitudinal absorbance band shifts to longer

wavelengths with increasing aspect ratio. There is a small shift of the transverse resonance maximum to shorter wavelengths with increasing aspect ratio.

Electron microscopy reveals that most NRs are more like cylinders or spherocapped cylinders than ellipsoids. However, an analytical solution for such shapes does not exist.

a) b)

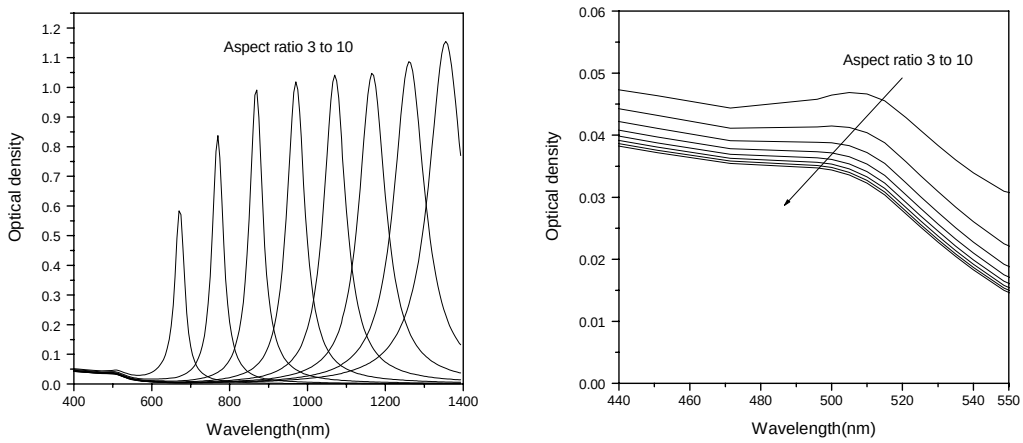

Figure 5.1. Absorbance spectra calculated with the expressions of Gans for elongated ellipsoids using the bulk optical data for gold. a) The numbers on the spectral curves indicate the aspect ratio (L/d). b) Enlargement of the shaded area of a) showing slight blue shift of TSP on increasing aspect ratio.

The discrete dipole approximation (DDA) method is a numerical method first introduced by Purcell and Pennypacker[9] in which the object studied is represented as a cubic lattice of N polarizable point dipoles localized at r_i, i = 1, 2, ... , N, each one characterized by a polarizability α_i. There is no restriction on the localization of cubic lattice sites so that the DDA represents a particle of arbitrary shape and composition.

Recently, Schatz and co-workers showed that DDA is suited for optical calculations of metallic systems with different geometries and environments through the extensive studies on the extinction spectrum and the local electric field distribution in metal particles[5].

Brioude et al.[10] used DDA method to simulate the absorption efficiency of gold NRs where they took into account the real shape of gold NRs. A dominant surface plasma band corresponding to the longitudinal resonance is observed. Its maximum position shifts to the red as the aspect ratio increases. These data are in good agreement with previous theoretical calculations based on classical electrostatic predictions which assume that gold NRs behave as ellipsoidal particles[6]. From the experimental point of view, good agreement with the published data for gold NRs is obtained.

The color of colloidal gold depends on both the size and shape of the particles, as well as the refractive index of the surrounding medium[11]. Understanding the color change of gold NRs surrounded by different medium is quite important. So far, gold NRs have been made in aqueous solution. In the mean time, surface modification of gold NRs for further application often involves using a mixture of organic solvents due to the limited solubility of the reactant in water. Since, most characterization is

done by UV-Vis-NIR spectrum and TEM, the color change of NRs solely by the change of medium has to be studied before advancing to modification of NRs.

A number of groups have reported the absorption spectra of gold spheres prepared in solvents other than water and they were compared with theoretical calculations[12]. For gold NRs, theoretical prediction of their optical properties of gold NRs upon changing medium was made by several groups and compared with the experimental results[13,14,15]. They found that there is a linear relationship between LSP and dielectric constant of medium. But so far these studies were limited in the narrow range of aspect ratios. Also the process to transfer gold NRs to organic solvent is non-trivial.

The purpose of this section is to have comprehensive knowledge of the optical properties of gold NRs. We compared the optical properties of gold NRs from the theoretical calculation and experimental results for a wide range of aspect ratio of gold NRs and systematically identified the color of gold NRs as a function of aspect ratio. We also investigated the effect of medium refractive index on the color of gold NRs and converted the spectral data to conform with the language of color science[16].

5.2. Experimental

Gold NRs with different aspect ratios were synthesized according to

procedures described in chapter 2.

The changes in the absorption spectrum of solution of NRs were determined at different solvents/water ratios using glycerol, dimethylsulfoxide (DMSO), dimethylformamid (DMF) and acetonitrile. Water was purified by ion exchange. The sample was immersed in a thermostat bath at 25°C and the absorption spectrum of the sample was measured when the sample solution was in equilibrium with the thermostat temperature. UV-Vis-NIR spectra were acquired with a Cary 5G spectrophotometer. Morphology and mean size of NPs were examined by TEM (JEOL100 at 100 KV).

To simulate the color of gold NRs from the calculated absorption spectra and experimental spectra, CIE XYZ tristimulus values were calculated[16]. The absorbance (A) was converted to transmittance (T) according to the following equation.

$$A = log_{10} \frac{1}{T}$$

CIE XYZ tristimulus values were calculated by the integration of the transmittance values $T(\lambda)$, the relative spectral energy distributions of the illuminant $E(\lambda)$, and the standard observer functions $x(\lambda)$, $y(\lambda)$, and $z(\lambda)$. We use the spectral distribution power function of daylight D_{65}. The integration is approximated by summation, thus:

$$X = \frac{1}{k}\int T(\lambda)\, E(\lambda)\, x(\lambda)$$

$$Y = \frac{1}{k}\int T(\lambda)\, E(\lambda)\, y(\lambda)$$

$$Z = \frac{1}{k}\int T(\lambda)\, E(\lambda)\, z(\lambda)$$

where $k = \int E(\lambda)\, y(\lambda)$ and λ = wavelength.

The amounts of red, green, and blue needed to form any particular color are called the tristimulus values and are denoted X, Y, and Z, respectively. A color is then specified by its trichromatic coefficients, defined as

$$x = X / (X + Y + Z)$$

$$y = Y / (X + Y + Z)$$

$$z = Z / (X + Y + Z)$$

$$x + y + z = 1.$$

The color was identified by positioning x and y values in the CIE chromaticity diagram.

5.3. Results and Discussion

5.3.1. Color of gold nanorods in aqueous solution.

The relation between aspect ratio and LSP is plotted according to Gans' calculation[6] and DDA simulation[5] and compared with experimental results. In both

theoretical data, the dielectric constant of 1.77 was used which corresponds to the value for water where the NRs are dissolved.

Calculation by Gans' theory and simulation by DDA are plotted in Figure 5.2 showing the similar trend where LSP lineary increases with increasing aspect ratio. There is a small discrepancy in the LSP between two predictions which is within 20nm originating from the initial assumption of different shape of NRs (ellipsoid for Gan's calculation and spherocyliner for DDA). Experimental results are overlaid showing good agreement with the predicted values. DDA simulation has better agreement than Gans' calculation. From these results, it can be said that the use of dielectric constant of water is reasonable to predict the optical properties of gold NRs.

There is a discussion about the effect of capping material on the optical properties of NRs in a way that CTAB and the capping structure might be involved in determining the dielectric constant of medium[15]. Since NRs are stabilized by surfactant, we cannot exclude the effect of surfactant. To probe the effect of capping materials on the optical properties of gold NRs, the surfactant in the gold NR solution was removed as much as possible by centrifugation. The concentrated solution was diluted and different amount of CTAB was added which will affect the structure of CTAB on the surface of gold NRs. We found that there is no dependence of the concentration of CTAB on the optical properties of gold NRs

within the concentration range studied. Therefore the capping material has no significant role in optical properties of gold NRs while the refractive index of shell is important in core shell structure of nanomaterial[17].

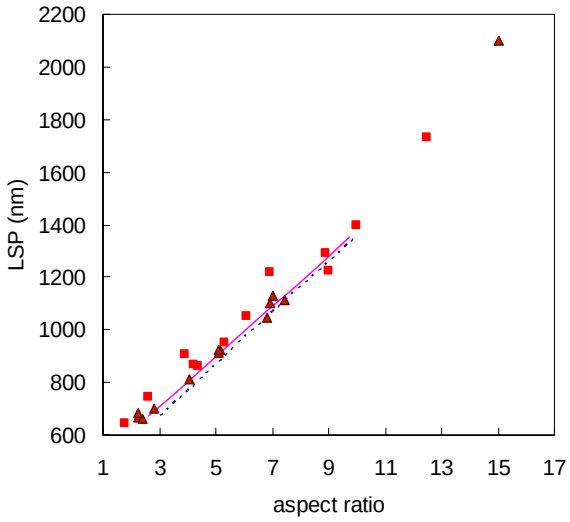

Figure 5.2. Longitudinal surface plasmon peak versus the aspect ratio of gold NRs. Simulation results using the DDA method and the corresponding fit (solid line) and Gans' calculation (dotted line). Experimental data from the work of van der Zande et al[18](square). Experimental data from our study (triangle).

It is often mentioned in the literature that the optical properties of gold NRs are tunable as a function of NP size and shape[19]. But the color has not been defined systemically as a function of aspect ratio.

One has to consider the fact that the TSP is not sensitive to the change of aspect ratio and only the LSP is sensitive to the aspect ratio. This visible light region consists of a spectrum of wavelengths, which range from approximately 700 nm to 400 nm. Therefore once the LSP goes beyond 700nm, basically the color of gold NRs

solution has to be the same. From the simulation and our experimental result, LSP of 700 nm corresponds to the NRs of aspect ratio around 3.

Therefore the color change could be only observed for relatively short range of aspect ratios. We simulated the color of the gold NRs using theoretical absorbance data. As predicted, the color does not change significantly when L/d is greater than 4 (Figure 5.3).

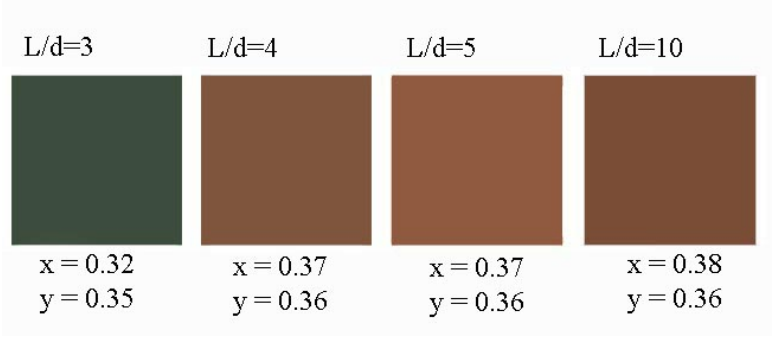

Figure 5.3. The simulated color of gold NR solution of different aspect ratios and their trichromatic coefficients.

Figure 5.4 shows the UV-Vis-NIR spectrum of gold NR solution experimentally prepared. Each solution contains mostly NRs as it can be seen from the small TSP in the spectrum. We obtained these pure NR solutions by optimizing synthesis condition and separating byproduct from the rods by centrifugation (for details, see chapter 2 and 4). The transverse peak matches with theoretical prediction where TSP shifts to shorter wavelength as increasing aspect ratio.

a)

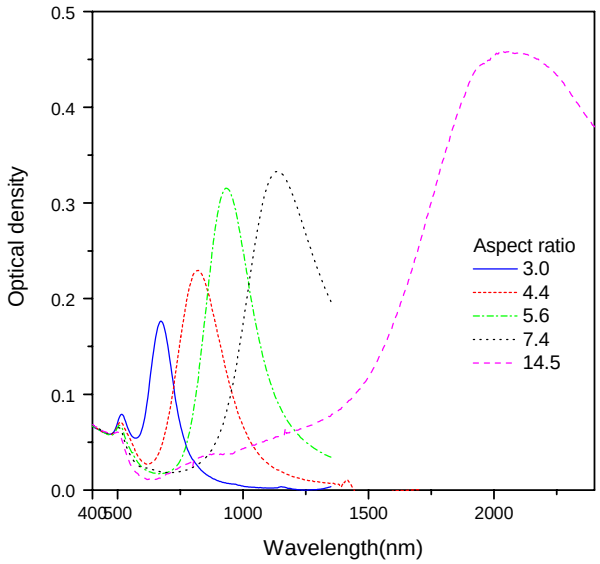

b)

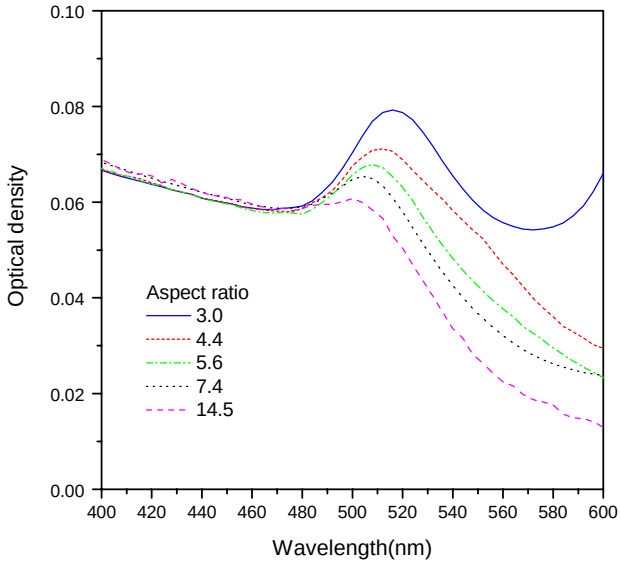

Figure 5.4. a) UV-Vis-NIR spectra of gold NR solutions having different aspect ratios and b) transverse peak in detail.

Figure 5.5 shows the photograph of the gold NR solution and the color patches simulated using theoretical absorbance data equivalent to the aspect ratio of

gold NRs. The color of solution is basically the same beyond the aspect ratio around 4. Also the color of the gold NR solution we made is identical to the simulated color (Figure 5.5 b).

Therefore in a visible region, the dramatic color change can not be achieved only by changing aspect ratio. But the tunability of optical properties of gold NRs as a function of the aspect ratio provides potentials to use gold NRs as an optical filter in near infrared region.

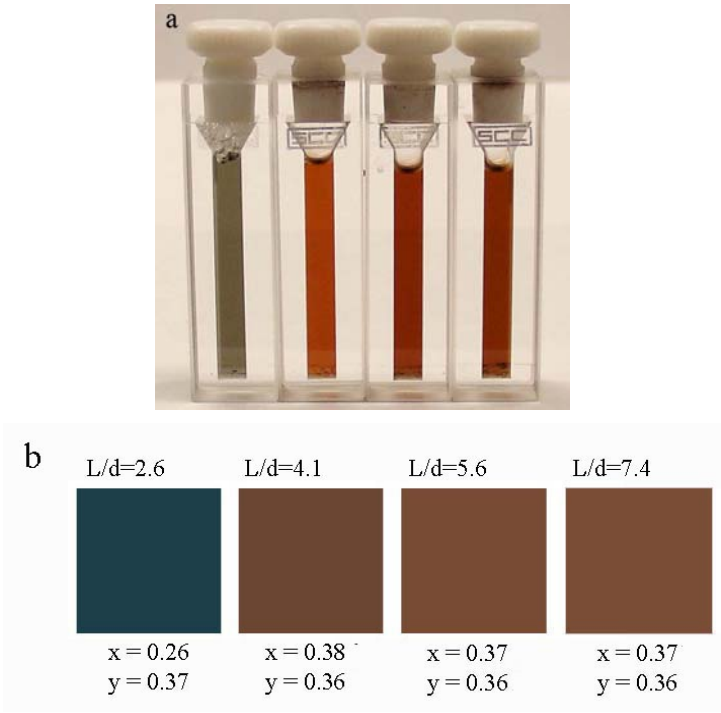

Figure 5.5. a) Photograph of 4 solutions of colloidal gold prepared in water. Aspect ratios are 2.6, 4.1, 5.6, 7.4 (from the left), respectively. b) The simulated color of gold NR solution of different aspect ratios.

We found that the color in a visible region is rather sensitive to the amount of spherical particles included as byproduct since surface plasmon peak of sphere positions between 500 to 550nm.

Figure 5.6 shows the simulated color of gold NR (aspect ratio is 5) solution having different amount spheres (surface plasmon peak at 520nm) as byproduct. The color changes from purple to brown as the amount of byproduct decreases.

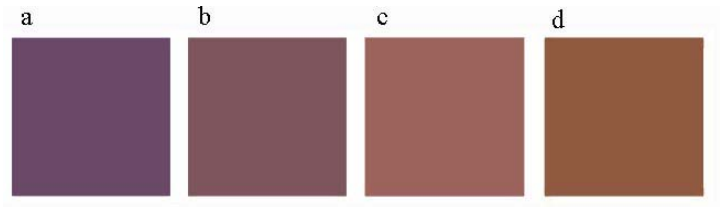

Figure 5.6. The color of gold NR solution of having different amount of spheres as byproduct. a) 50%, b) 30%, c) 10%, and d) 0%.

5.3.2. Effect of refractive index of medium

We simulated dependence of absorbance of gold NR solution on changing refractive index of medium. The LSP increases linearly as the refractive index of medium increases (Figure 5.7). And the effect of medium is pronounced for longer NRs as is shown from the slop of the plot.

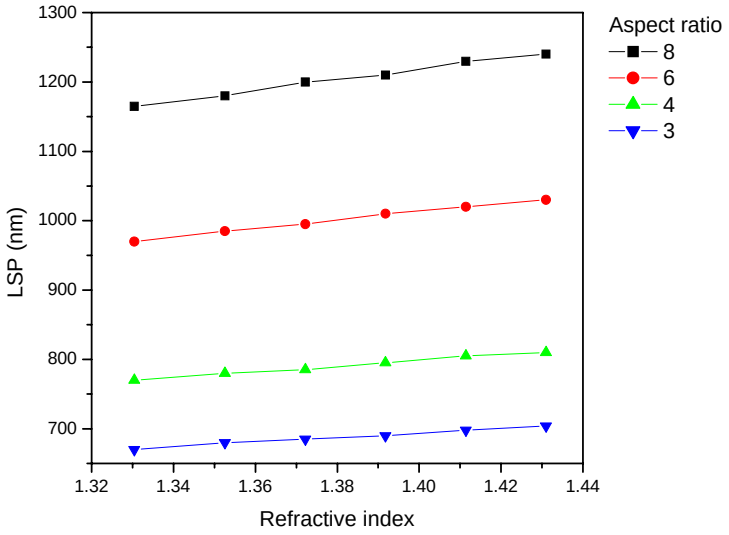

Figure 5.7. Calculated LSP as a function of refractive index of medium.

To validate the predicted LSP and the experimental value, we conduct the study on the changing refractive index of medium by changing the volume fraction of water and glycerol. We choose glycerol because it does not cause precipitation, and there is no need to exchange the capping material to transfer gold NRs to different medium.

Figure 5.8 shows the experimental data for the change of LSP upon adding glycerol to water. As we expected, LSP red-shifts as the medium refractive index increases.

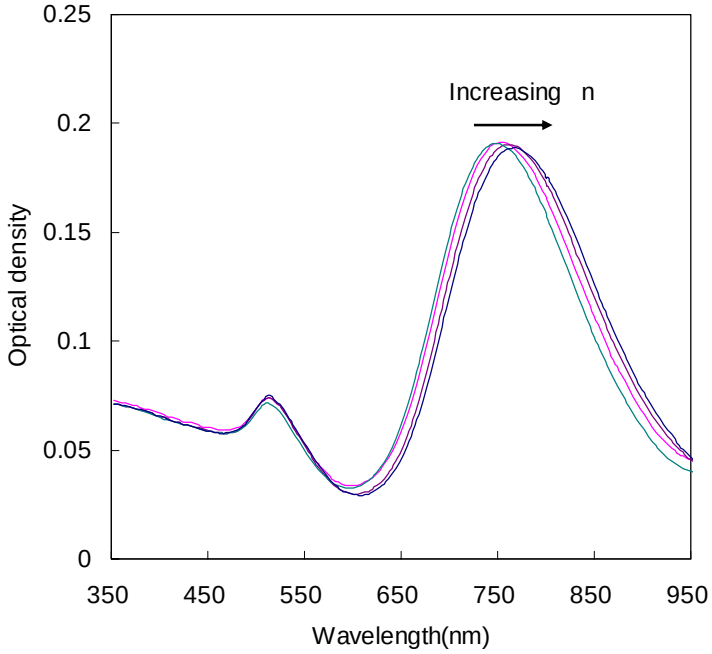

Figure 5.8. Absorption spectra of gold NRs with aspect ratio L/d = 3.5 in various glycerol/ water ratios. From left, water, 20, 40 and 50 % (v/v) of aqueous glycerol solutions.

Using the refractive index of the mixture (shown in Table 5.1) in the Gans' equation we calculated the absorbance of NR solutions, and compared the calculations to the experimental values obtained (Figure 5.9). The experimental results show good agreement with the calculated values. The effect of medium is indeed pronounced for longer NRs.

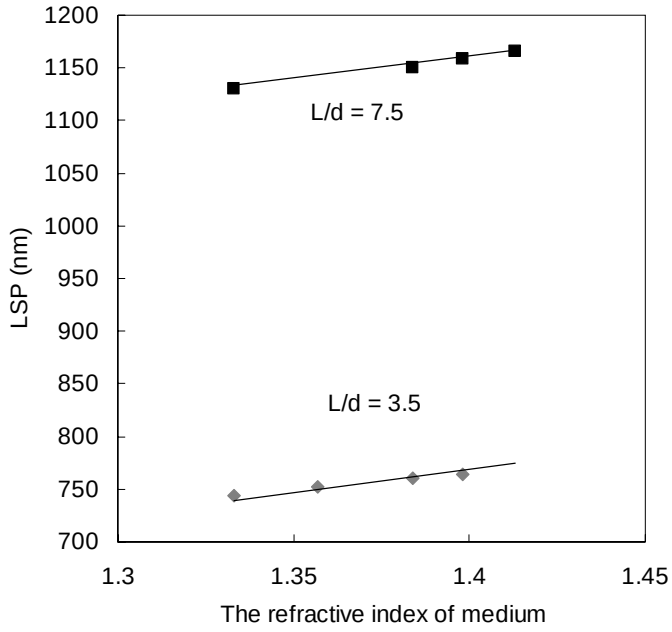

Figure 5.9. Experimental and calculated results of LSP of gold NRs as a function of refractive index of medium (water/glycerol mixture). Filled dots represent the experimental data and straight line is calculated data.

Table 5.1. The refractive index of water/glycerol mixture.[20]

Volume fraction	Refractive index
0% glycerol	1.46
10% glycerol	1.33
30% glycerol	1.34
50% glycerol	1.37
70% glycerol	1.40
90% glycerol	1.43

There is a great deal of multidisciplinary research in recent years on the assembling NPs using linkers. Using organic solvent is inevitable since most of the linker molecules are water insoluble. It is often the cases that the aqueous gold NR solution is mixed with organic solvent. Depending on the mixing ratio, gold NRs may aggregate and precipitate. Therefore, it is important to find the optimum mixing

ratio for the reaction and to know the optical properties of gold NRs in the solvent mixture.

DMSO is among the popular solvents of choice. We conducted the experiments where refractive index of medium changes by changing the volume fraction of water and DMSO. Gold NR suspension is stable in the water/DMSO mixture and the LSP increases with increasing the amount of DMSO up to of 40% of volume fraction of DMSO. Above 40% DMSO, gold NRs start to aggregate and precipitate out. Figure 5.10 shows the theoretical calculation and experimental results for two different aspect ratios of NRs.

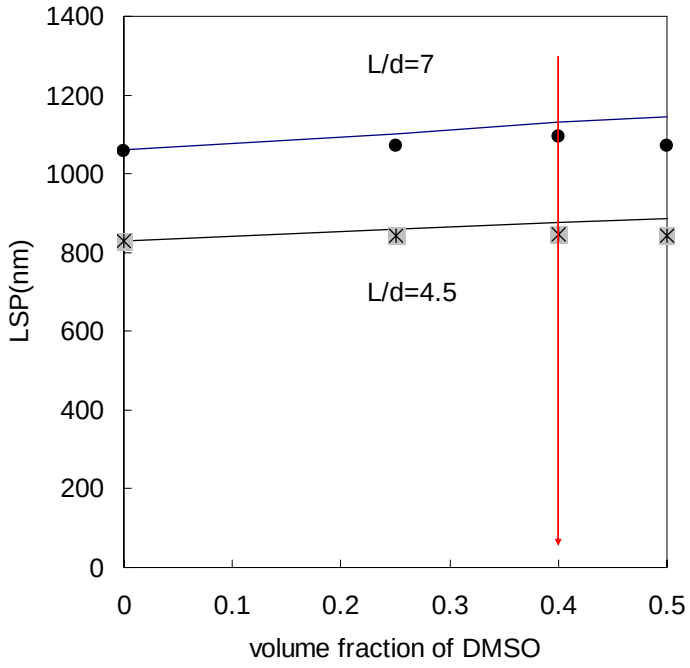

Figure 5.10. Experimental and calculated results of LSP of gold NRs as a function of volume fraction of DMSO in water. Filled dots represent the experimental data and straight line represents the calculated data.

In both cases, there is an increasing deviation between theoretical LSP and experimental LSP as the fraction of DMSO increases. Finally LSP starts to decreases, which indicates the aggregation of NRs. In the case of mixing ratio of 1 to 1, NRs precipitate in several hours.

DMF shows results that are similar to DMSO. Since DMF has a higher refractive index than that of water, as the fraction of DMF increases, the LSP increases. When the fraction of DMF is increased beyond 50%, NRs start to aggregate and precipitate.

Acetonitrile is among the solvents used for preparing self assembly of gold NRs[21]. It is reported that the spectral properties of gold NRs were unaffected upon increasing the composition of acetonitrile (acetonitrile: water = 4:1) and the rods were quite stable for several hours. Acetonitrile could be a good choice of solvent since it has similar refractive index (n=1.3441) as water. When acetonitrile was added in minor fraction to gold NR solution, there is indeed no change in absorbance peaks. But as the fraction of acetonitrile increases, LSP red shifted in a large amount with decreasing intensity indicating the aggregation of NRs. Figure 5.11 shows the UV spectrum of gold NRs in aqueous solution and solvent mixture (acetonitrile: water = 4:1 by volume. This ratio is used in the literature). We found that the gold NRs in this solvent mixture precipitate out the next day.

The mixing ratio may be chosen based on the solubility of the reactants in the solvent mixture. For example, α,ω-alkanedithiols which are used to make gold NRs "link" is only soluble in the mixture of acetonitrile and water when the fraction of organic solvent is higher. But one needs to check the stability of gold NRs before proceeding to further experiment.

Therefore it is essential to find the optimum ratio of mixing at which NRs can be dispersed in stable condition and to know the changing optical properties due to the solvent mixture.

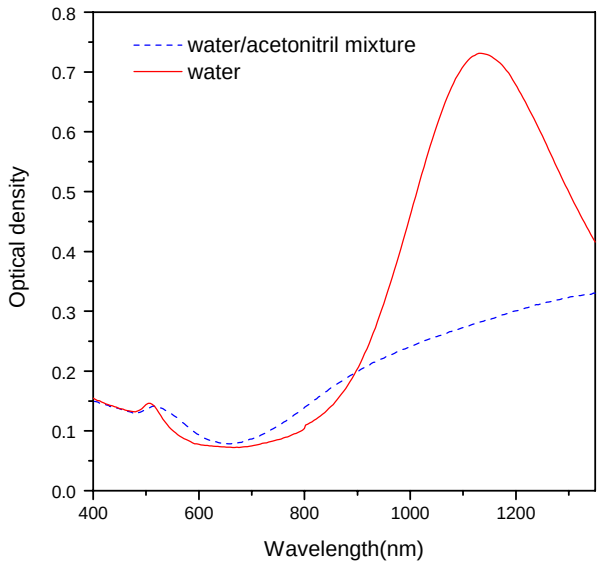

Figure 5.11. Uv-Vis-NIR spectra of gold NRs in water and water acetonitrile mixture (water: acetonitrile= 1:4).

5.4. Conclusions

In summary, we found that both Gans' theory and DDA simulation provide a good representation of the experimental results for absorbance of gold NRs. The color of gold NR aqueous solutions matches well with the simulated color which is generated using theoretical absorbance of equivalent aspect ratio. The medium refractive index affects the absorbance of gold NRs. There is a linear relationship between LSP and refractive index. . The effect of the medium is greater for longer NRs.

Our results suggest that the knowledge of the refractive index of a known solvent and absorbance of gold NRs provide an easy method to determine the aspect ratio of the NRs. Also, our results will be useful as the foundation for the potential optical applications of gold NRs.

References

[1] Faraday, M., "Experimental Relations of Gold (and other metals) to Light" *Philos. Trans.* **1857**, *147*, 145.

[2]. a) Huang, X; El-Sayed, I. H.; Qian, W; El-Sayed, M. A."Cancer Cell Imaging and Photothermal Therapy in the Near-Infrared Region by Using Gold Nanorods" *J. Am. Chem. Soc.* **2006**, *128*, 2115, b)Englebienne P.; Van Hoonacker, A; Verhas, M. "Surface plasmon resonance: principles, methods and applications in biomedical sciences" *Spectroscopy-an international journal*, **2003**, *17*, 255.

[3] Kreibig ,U; Vollmer,M. "Optical Properties of Metal Clusters" Springer, **1995.**

[4] Mie,G. "Contributions to the Optics of Turbid Media, Especially Colloidal Metal Solutions" *Ann. Physik* **1908**, *25*, 377.

[5] Kelly, K. L.; Coronado, E.; Zhao, L. L.; Schatz, G. C. "The optical properties of metal nanoparticles: The influence of size, shape, and dielectric environment" *J. Phys.Chem. B.* **2003**, *107*, 668.

[6] Link, S; El-Sayed M.A. "Spectral properties and relaxation dynamics of surface plasmon electronic oscillations in gold and silver nanodots and nanorods" *J. Phys. Chem B* **1999,** *103*, 8410.

[7] a) Gans,R. "The Form of Ultramicroscopic Gold Particles" *Ann. Physik* **1912**, *37*, 881 b) Gans,R. "Form of ultramicroscopic particles of silver" *Ann. Physik* **1915**, 47, 270.

[8] Johnson, P. B.**;** Christy, R. W. **"**Optical Constants of the Noble Metals**"** *Phys. Rev. B*, **1972**, *6*, 4370.

[9] Purcell, E. M.; Pennypacker, C. R. "Scattering and absorption of light by nonspherical dielectric grains" *Astrophys. J.* **1973**, *186*, 705.

[10] Brioude, A.; Jiang,X. C.; Pileni, M. P. "Optical Properties of Gold Nanorods: DDA Simulations Supported by Experiments" *J. Phys. Chem. B* **2005**, *109*, 13138.

[11] Khlebtsov, N.G.; Trachuk,L. A.;. Mel'nikov, A. G. "The Effect of the Size, Shape, and Structure of Metal Nanoparticles on the Dependence of Their Optical Properties on the Refractive Index of a Disperse Medium" *Optics and Spectroscopy*, **2005**,*98*, 77.

[12] Underwood, S.; Mulvaney, P. "Effect of the Solution Refractive Index on the Color of Gold Colloids" *Langmuir* **1994,** *10*, 3427.

[13] Link,S.; Mohamed, M. B.; El-Sayed M. A. "Simulation of the Optical absorption Spectra of Gold Nanorods as a Function of Their Aspect Ratio and the Effect of the Medium Dielectric Constant" *J. Phys. Chem. B* **1999**, *103*, 3073.

[14] Yang, J.; Wu, J.; Wu, Y.; Wang, J.; Chen, C. "Organic solvent dependence of plasma resonance of gold nanorods : a simple relationship" *Chemical Physics Letters* **2005,** *416*, 215.

[15] Al-Sherbini, A. "Thermal instability of gold nanorods in micellar solution of water/glycerol mixtures" *Colloids and Surfaces A: Physicochem. Eng. Aspects* **2004**, *246*, 61.

[16] Nassau, K. "Color for Science, Art and Technology" Elsevier Science & Technology Books **1998**

[17] Pérez-Juste,J.; Pastoriza-Santos ,I.; Liz-Marzán ,L.M.; Mulvaney, P. "Gold nanorods: Synthesis, characterization and applications" *Coordination Chemistry Reviews* **2005**, *249*, 1870

[18] van der Zande, B.M.I.; Böhmer, M.R.; Fokkink,L.G.J.; Schönenberger, C. "Colloidal Dispersions of Gold Rods: Synthesis and Optical Properties" *Langmuir* **2000,** *16*, 451.

[19] Murphy,C.J.; Sau,T.K.; Gole, A.M.; Orendorff, C.J; Gao,J.; Gou,L.; Hunyadi, S.E.; Li,T. "Anisotropic Metal Nanoparticles: Synthesis, Assembly, and Optical Applications" *J. Phys. Chem. B* **2005**, *109*, 13857.

[20] Borst, J.; Hink, M. A.; Hoek, A.; Visser, A. J. W. G. "Effects of refractive index and viscosity on fluorescence and anisotropy decays of enhanced cyan and yellow fluorescent proteins" *Journal of Fluorescence* **2005**, *15*, 153.

[21] Joseph, S. T. S.; Ipe, B. I.; Pramod, P.;Thomas, K.G. “Gold Nanorods to Nanochains: Mechanistic Investigations on Their Longitudinal Assembly Using α-ϖ-Alkanedithiols and Interplasmon Coupling” *J. Phys. Chem. B* **2006**, *110*, 150.

Chapter VI

Optical Properties of PVA/Gold Nanorods nanocomposites

Abstract

Gold nanorods (NRs) with well defined aspect ratio were introduced into a poly (vinyl alcohol) (PVA) matrix by means of solution-casting techniques. The resulting nanocomposites film was drawn to induce the uniaxial alignment of gold NRs. The absorption spectra of the drawn nanocomposites in the UV-Vis-NIR wavelength region were found to depend strongly on the polarization direction of the incident light. The observed optical anisotropy originates from uniaxially oriented gold NRs. It is shown that the polymer-inorganic nanocomposites can be employed as color polarizing filters. Films of different colors were prepared by changing aspect ratio and mixing rod and spheres, which also show the sensitive color change upon the changing polarization angle. By using higher aspect ratio of NRs (L/d=6.3 and above), the polarizing filters in the NIR region was achieved.

6.1. Introduction

Because the plasmon resonance peaks of gold nanorods (NRs) arise from the anisotropy of NRs, the optical property of a single NR is greatly influenced by the polarization of incident light[1]. When the incident light is polarized parallel to the main axis of the particle, the spectrum displays only the longitudinal resonance. In the case of light polarized perpendicular to the main axis of the rod-shaped particles, the spectrum displays only the transverse resonance. The UV-vis spectrum of gold NRs solution shows the optical response of randomly distributed gold NRs to the unpolarized incident light. Therefore if NRs have the orientational order by alignment process and the direction of polarization of incident light is controlled, the magnitude of both the longitudinal and transverse resonance will be sensitive to the angle between the orientation of NRs and the polarization of incident light and show the optical dichroism in a certain wavelength region.

Obtaining the alignment by stretching the film has the potential for many applications since there is increasing interest to make polymer nanomaterial composite where the optical properties of nanoparticles can be utilized to make some smart applications in the fields of sensing, optics, or electronics[2]. Immobilization of NRs on the surfaces or their incorporation into bulk materials is essential and the optical properties of nanocomposites with the same nanoparticles are subject to

change depending on the polymer matrix.

Al-Rawashdel et al. prepared polyethylene/gold rods nanocomposites and found that the composite films exhibit linear dichroic properties which result from a net orientation of the rods[3] . The plasmon resonance absorption maxima occur at the longest wavelengths when the incident electric field is polarized along the direction of particle orientation, and are blue-shifted as the polarization angle is perpendicular to the orientation direction. These results were confirmed to be in qualitative accord with Rayleigh scattering theory and T-matrix scattering calculations[4].

Dirix et al. utilized these properties and showed that the polymer-inorganic nanocomposites can be employed as color polarizing filters[5]. They incorporated alkanethiol coated spherical gold particles into a polyethylene matrix. Upon uniaxial drawing, spherical shapes of individual nanoparticles form aggregation of different aspect ratio. The absorption spectra of the drawn nanocomposites in the visible region were found to depend strongly on the polarization direction of incident light (demonstrated in Figure 6.1).

a) b)

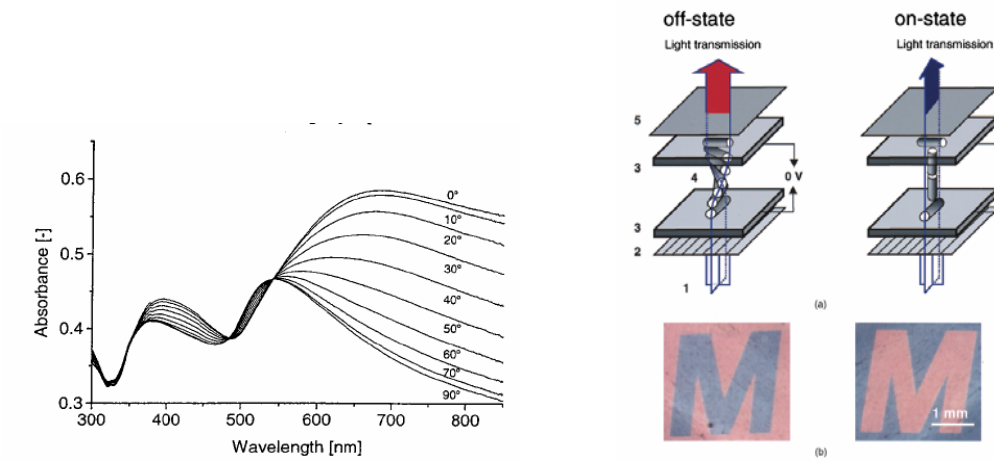

Figure 6.1. a) UV-Vis spectra of drawn nanocomposites comprising of high-density polyethylene and gold, taken in linearly polarized light at different angles between the polarization direction of the incident light and the drawing direction. b) Twisted-nematic liquid crystal displays (LCD) equipped with a drawn polyethylene-silver nanocomposite. The "M" represents the on state, the drawing direction is in the picture above parallel and below perpendicularly oriented to the polarizer[6].

The choice of polymer is important because the inorganic particles typically aggregate in polymer solution owing to their high surface energies which results in excessive light scattering by the composite material.

Poly (vinyl alcohol) (PVA) offers a suitable matrix for the fabrication of composites of gold NRs. Synthetic procedures giving NRs in high yield are based on aqueous solution. Since PVA is water soluble, the nanocomposites can be made by mixing of the individual components in a polymer solution. When the composite films are stretched, the gold NRs tend to align in a preferred direction. The alignment is driven by the mechanical force conveyed through the polymer film.

Van der Zande et al., prepared thin film of gold NRs dispersed in PVA[7]. Although they used PVA, they took somewhat complicated procedure. The gold NRs were first transferred from water to ethylene glycol and PVA was added to the gold NRs/ethylene glycol solution. The solution was heated to 195°C and casted on a glass plate. The resulting film was post processed to insure the quality of film. The orientation was obtained by stretching film at 120°C. They found that the rods are completely oriented when the film is stretched 4-6 times its original length. The polarization absorbance spectra showed polarization dependence. A similar procedure was adopted by other research groups where nanocomposites are made by mixing gold NRs aqueous solution directly to PVA aqueous solution. Murphy et al.[8] casted solution on a Petri dish and cured for 18h at 80°C. Then the film was stretched at 60°C by hand and cooled to room temperature. Pérez-Juste et al.[9] used the similar approach to prepare PVA gold NRs composite, but they didn't specify the post processes. They briefly mentioned that the NRs were aligned by warming and stretching (by hand) the composite film. They also mentioned that care should be taken to avoid overheating, since this can lead to modification of the optical properties due to thermal reshaping of the rod.

Although several groups show dichroic properties of aligned gold NRs, the tunablity of peak position was not demonstrated extensively.

The aim of this study is to investigate the optical properties of anisotropic gold particles embedded in PVA films as a function of the net orientation of the rods and polarization angle. By changing aspect ratio of gold NRs and mixing with spherical particle, we will probe the potentials to use these nanocomposites as color polarizing filters. Also, by using higher aspect ratio of NRs, we will probe the possibility that the optical dichroism can be shifted from the visible to the near IR.

6.2. Experimental

Gold NRs with different aspect ratios were synthesized according to procedures described in chapter 2.

For the preparation of PVA/gold NRs nanocomposites, typically, 10 w % PVA aqueous solution was prepared by dissolving PVA (Mw: 95000, 98-99% Hydrolyzed, Aldrich) in 50 ml of water. The solution was stirred at 50°C for 12 hrs. Concentrated gold NRs solution was mixed with the PVA solution and poured to Petri dish which is covered for 24 hrs for the formation of uniform thickness of film (the final concentration of gold NRs in the film is about 6×10^{-4} wt % . Then the cover was removed and water was evaporated. After the water evaporation, the polymer film was carefully peeled from the substrate. The film thickness was approximately 50μm.

The film was cut to the size of 1cm × 2cm and mounted on drawing equipment specially manufactured. The drawing was done on the hot plate at 60°C by moving the knob on the equipment. The oriented nanocomposites were analyzed in linearly polarized light at different angles between the polarization direction of the light and the drawing direction of the nanocomposites.

Absorption spectra were acquired using a CARY 5G UV-vis near-IR spectrophotometer and UV-vis spectra of composite films were measured with SEE-1000 microspectrophotometer.

Confocal Scanning Laser Microscopy (CSLM) measurements were performed in the reflection mode with a Leica TCS NT confocal microscope equipped with a krypton/argon gas laser and an oil immersion lens.

6.3. Results and discussions

6.3.1. Optical properties of gold NRs in PVA

Figure 6.2 shows the absorbance spectra of randomly oriented gold rods in water and in PVA films. The films were transparent indicating the colloidal gold rods were well dispersed in PVA.

a) L/d=4.3

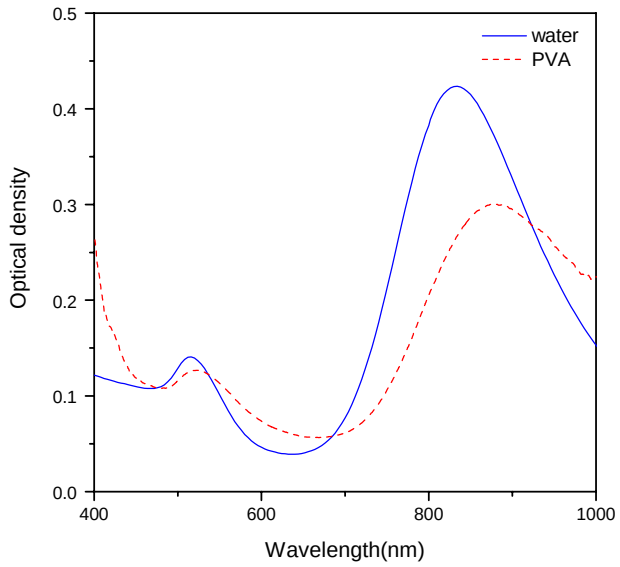

b) L/d=6.3

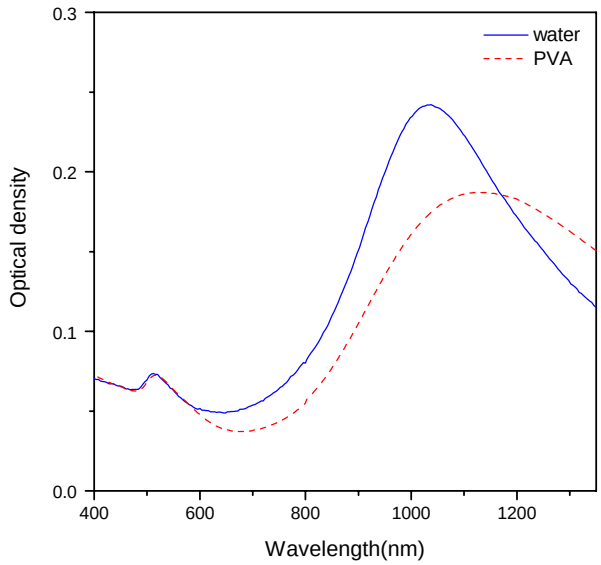

Figure 6.2. The absorbance spectra of randomly oriented gold rod dispersions. a) aspect ratio 4.3 , b) aspect ratio 6.3. The blue line is the absorbance spectra of aqueous gold NR solution. The red line is the absorbance spectra of gold NRs in PVA film.

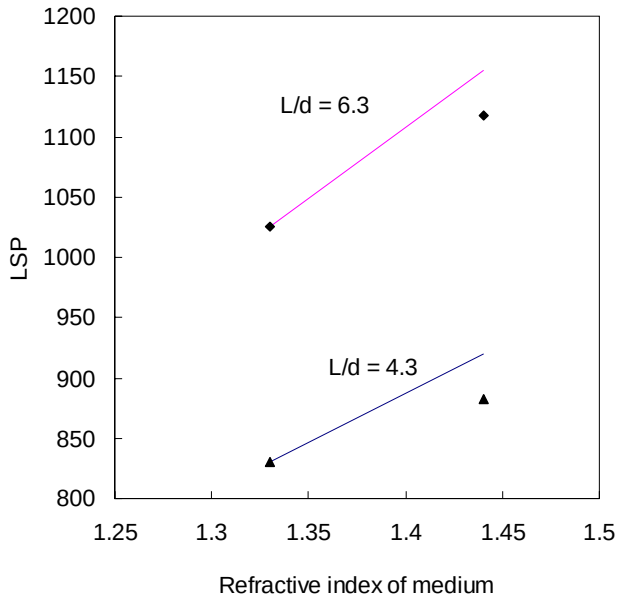

Figure 6.3. Longitudinal surface plasmon peak (nm) versus refractive index of the medium. Straight line is obtained from the calculation of Gans theory. Diamonds and triangles are the experimental data.

The spectra of the PVA films were similar to those of the aqueous solution. The LSP shifted to longer wavelengths due to the change in refractive index of the medium. This shift can be theoretically predicted by calculating the peak positions using the expressions of Gans. The optical parameters for bulk gold are taken from the reference[10]. The refractive index of the medium was assumed to be constant and equals 1.521 for PVA[11] and 1.333 for water. Figure 6.3 shows the change of LSP as a function of refractive index for two different aspect ratios of gold NRs.

The experiment data show fewer shifts than the calculation for both cases. The shift is greater for longer NRs ($\Delta_{L/d=4.3}$=53nm, $\Delta_{L/d=6.3}$=92nm). This deviation

might be attributed to the difference in the refractive index between the PVA film we made and the one in the literature. We also infer that the process of stretching probably lead to a less dense host medium for the gold NRs.

6.3.2. Polarization dependent color filters

As mentioned in the introduction, polymer-gold NRs nanocomposites have the potential for the color filters showing an absorption spectrum that depends on the polarization direction of incident light, which allows for the generation of multiple colors in a single electro-optical element.

We used gold NRs of well-defined aspect ratio so that the color is predictable and reproducible. Figure 6.4 shows the experimental set-up for the polarization studies.

Figure 6.5 shows the polarizated spectra of the films containing gold NRs with L/d= 2.8. The spectra demonstrate that for polarization parallel to the draw direction, the transverse absorbance maximum completely disappears when the film is stretched 3 times, whereas the longitudinal resonance is still present. The intensity of longitudinal resonance slightly decreases as draw ratio increases because of the decrease in film thickness. Using perpendicular polarized light, the longitudinal absorbance peak completely disappears when the film is stretched 4 times, whereas

the transverse resonance is still present. Since we obtained the complete disappearance of longitudinal peak of transverse peak at the draw ratio above 4, we use this ratio for the rest of the experiment.

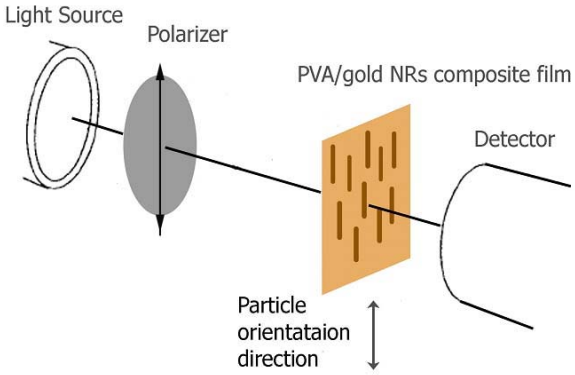

Figure 6.4. The experimental set-up of the polarization spectroscopy studies. At a polarization angle θ=0°, the electric field of the light is polarized parallel to the stretch direction, whereas, at a polarization angle θ=90°, the electric field of the light is polarized perpendicular to the stretch direction.

a) b)

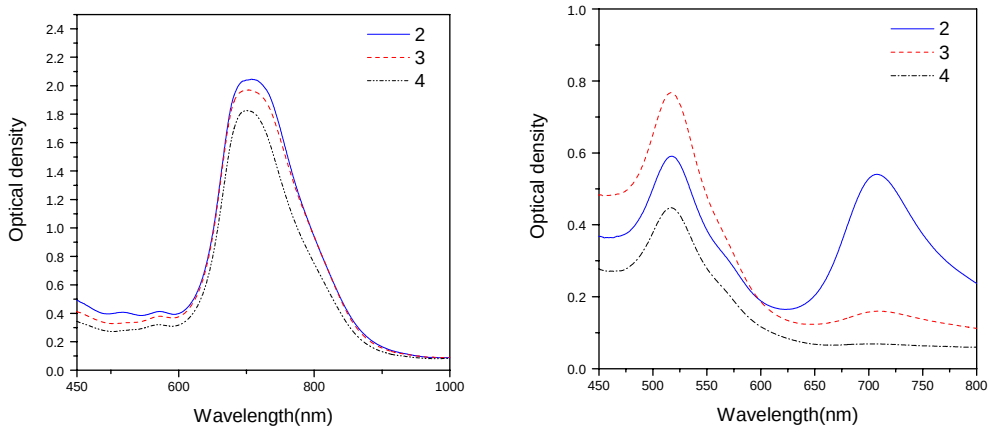

Figure 6.5. The polarization spectra of the gold NRs with L/d=2.8 dispersed in PVA for various elongation numbers with respect to the original film. Indicated on the spectral curves. a) θ=0°, b) θ=90°.

The alignment of gold NRs was also confirmed by confocal microscopy. Figure 6.6 compares the alignment of gold NRs obtained by stretching. The random distribution of single rods is observed in the unstretched film (a). When stretched, a strong preferential orientation in the stretch direction is present.

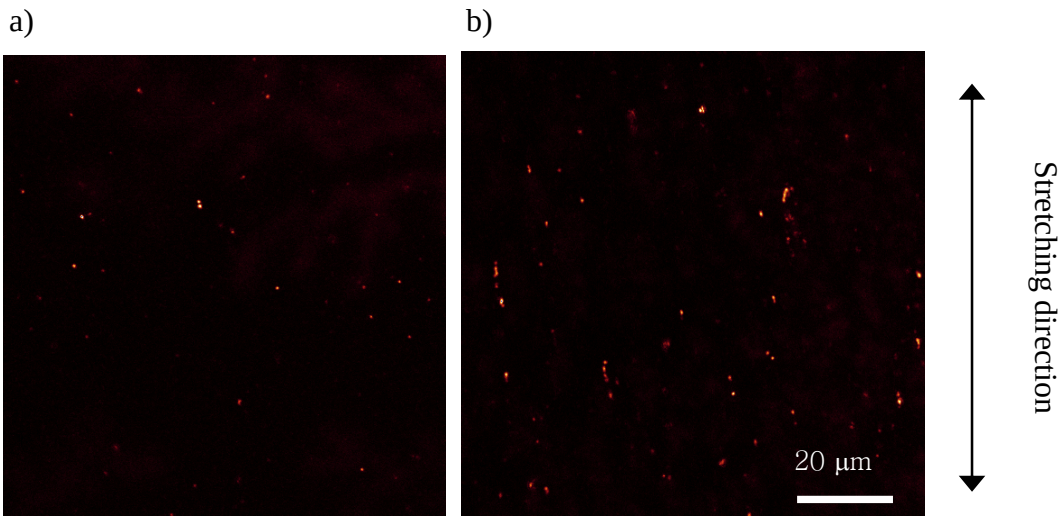

Figure 6.6. CSLM micrographs of the PVA film containing gold rods with L/d = 7 demonstrating alignment with stretching (a) the unstretched film and (b) stretched film.

Figure 6.7 shows the absorption spectrum at various intermediate polarization angles. As the angle changes from 0° to 90°, intensity of longitudinal plasmon starts to decrease and that of transverse starts to increase. LSP appears at the longest wavelengths when the angle is 0°and is blue-shifted as the polarization angle changes to 90°. These results are in general accord with the calculation and the experimental results of other groups[2]. Changes from blue to red were observed by switching the polarizer from the parallel to the perpendicular polarization direction, respectively.

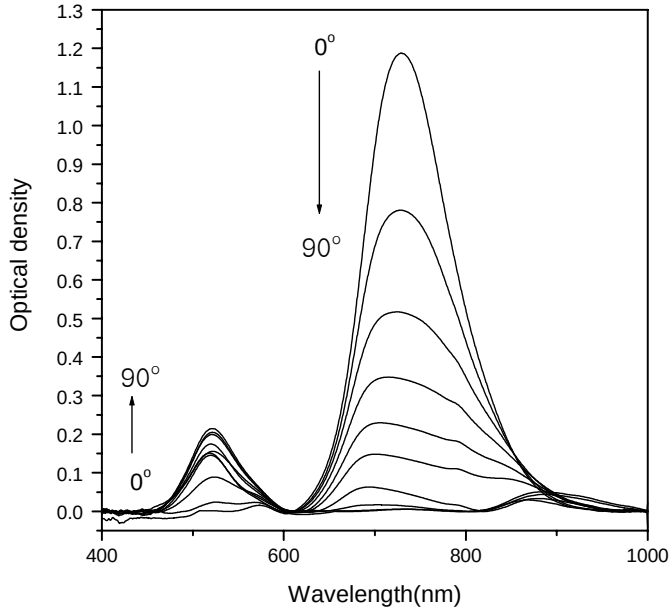

Figure 6.7. UV-vis-NIR spectra of PVA/gold NRs nanocomposites for varying polarization angles. L/d of gold NRs is 2.8.

Figure 6.8. Optical micrographs of drawn PVA-gold nanocomposites with ca 4 wt % gold NRs and draw ratio 4. Aspect ratio of NR is 2.8. a) unpolarized, b) polarization direction parallel to the drawing direction and c) polarization direction perpendicular to the drawing direction. Scale bar is 50μm.

We obtained transmittance spectra at different polarizer angle (Figure 6.9). Based on the spectra, extinction ratio was calculated.

$$\text{Extinction ratio} = 10\log_{10}(T_{\perp}/T_{//})\,[\text{dB}]$$

where $T_{\perp}$ and $T_{//}$ are the transmittance perpendicular and parallel to the stretching

direction, respectively. Maximum extinction ratio was 18 dB at λ=LSP which is considered to be fairly good, compared to those previously reported in the literature[12]. The thickness of the film is 50μm and it has good flexibility.

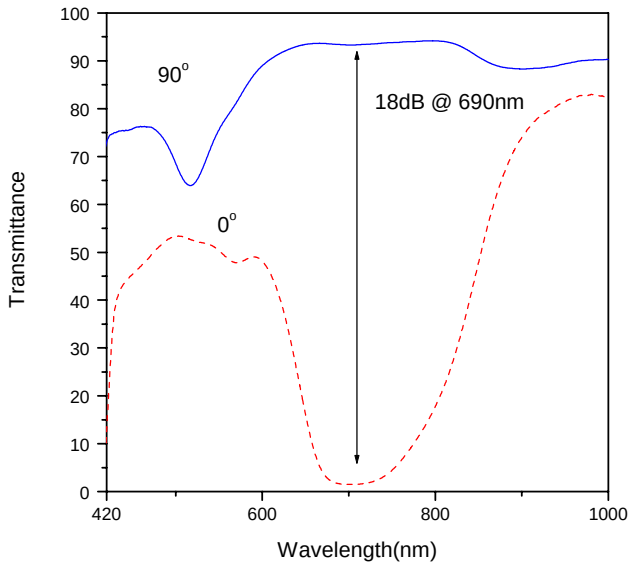

Figure 6.9. Transmittance spectra of PVA/gold NRs nanocomposites for varying polarization angles. L/d of gold NRs is 2.8.

To obtain films with vivid colors in the visible region, shorter NRs with L/d=2.5 were mixed with larger nanosphere (d=30nm) and used to prepare the nanocomposites film. The UV-Vis spectra of drawn nanocomposites in linearly polarized light are shown in Figure 6.10. When the angle is 0°, we observed not only the LSP but also the peak from the sphere which was not affected by the stretching of the film. When the angle is 90°, broad peak at around 540nm was observed which was attributed to the TSP of NRs and nanospheres. The LSP was

not completely gone in this case, since the aspect ratio is lower.

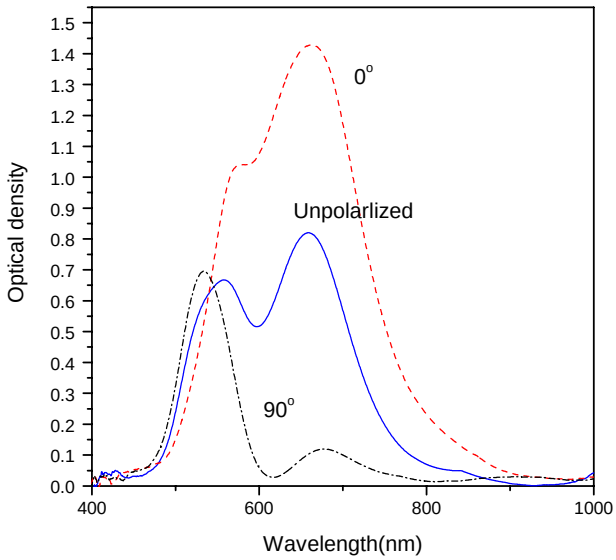

Figure 6.10. UV-Vis-NIR spectra of PVA/gold NPs nanocomposites for varying polarization angles. Gold NPs consist of NR of L/d= 2.5 and nanosphere of diamerter=30nm.

Figure 6.11. Optical micrographs of drawn PVA-gold nanocomposites with ca 4 wt % gold NPs mixture and draw ratio 4. a) unpolarized, b) polarization direction parallel to the drawing direction and c) polarization direction perpendicular to the drawing direction. Scale bar is 50μm.

Figure 6.11 shows the color of the film under the different polarizer angles. Polarization angle dependence of color is apparent.

When the aspect of NRs is sufficiently large, the LSP shifts to the near-IR region. This means that the wavelength region displaying optical dichroism can be

shifted from the visible to the near-IR. This enables the fabrication of thin-film optical filter that responds to the wavelengths in the near IR region. We probe this possibility by preparing the film with longer aspect ratio of NRs.

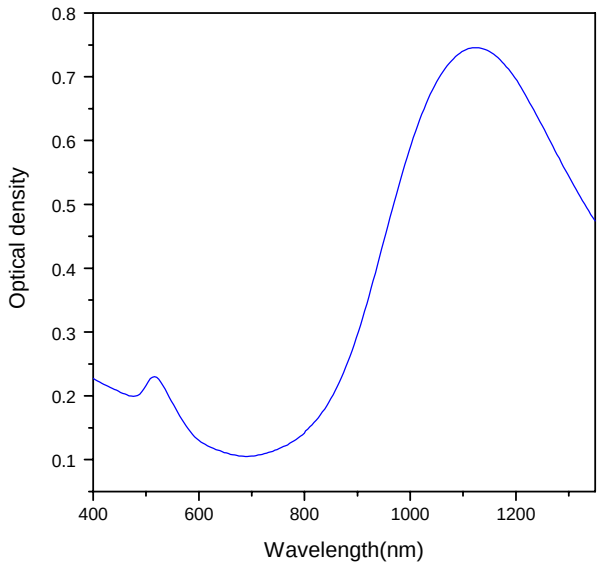

Figure 6.12. UV-Vis-NIR spectrum of PVA/gold NRs nanocomposites film. The aspect ratio of NRs is 6.3.

Figure 6.12 shows the UV-vis-NIR spectrum of the nanocomposites film prepared by using the NRs of aspect ratio 6.3. In the visible region, only the transverse peak contributes to the color of the film. When the film is stretched, the UV-vis-NIR spectra show the polarization dependence (Figure 6.13). The spectra were split to 2 wavelength regions because of the use of different polarizers. When the angle is 0, transverse peak is completely disappears as expected. The LSP was appeared at longer wavelength. When the angle is 90°, the longitudinal peak is

suppressed and only transverse peak was observed.

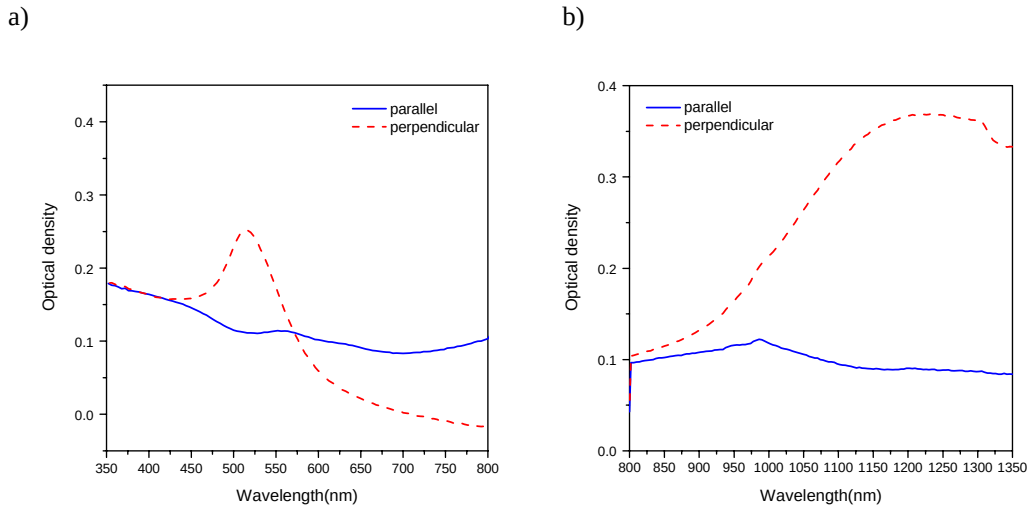

Figure 6.13. The polarization spectra of the gold NRs with L/d=6.3 dispersed in PVA. a) Visible region and b) near IR region.

Figure 6.14 shows the color of the films. Since there is no characteristic peak in the visible region when the angle is 0, the film looks transparent. (Figure 6.14,b).

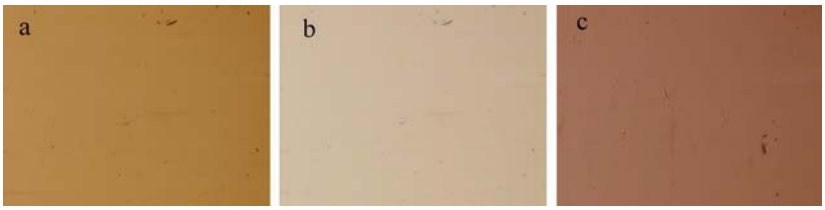

Figure 6.14. Optical micrographs of drawn PVA-gold nanocomposites with ca 4 wt % gold NRs and draw ratio 4. Aspect ratio of NR is 6.3. a) unpolarized, b) polarization direction parallel to the drawing direction and c) polarization direction perpendicular to the drawing direction. Scale bar is 50μm.

6.4. Conclusions

We prepared gold NRs /PVA nanocomposites film and obtained the alignment of gold NRs in the PVA film d by simple stretching film method. The possibility of using this film as polarization dependant color filters was demonstrated. The polarization–dependent optical response of the NRs was measured and we confirmed that good agreement was found with the theoretical prediction and previous studies. By using higher aspect ratio of NRs, we observed strong optical dichroism in the near – IR region which can be utilized to make optical device in near-IR region. We believe that gold NRs provide an alternative to conventional, organic polarizers because of their tunable peak positions and higher photo stability.

References

[1] Van der Zande, B.M.I ; Koper, Ger J. M.; Lekkerkerker, Henk N. W. "Alignment of Rod-Shaped Gold Particles by Electric Fields" *J. Phys. Chem. B* **1999**, *103,* 5754.

[2] Carotenuto, G.; Her, Y,; Matijevic, E. "Preparation and Characterization of Nanocomposite Thin Films for Optical Devices" *Industrial & Engineering Chemistry Research* **1996**, *35*, 2929.

[3] Al-Rawashdeh, N.A.F. ;Foss, Jr., C.A. "UV/visible and infrared spectra of polyethylene/nanoscopic gold rod composite films: Effects of gold particle size, shape and orientation" *Nanostructured materials* **1997,** *9,* 383.

[4] Al-Rawashdeh, N.A.F.; Sandrock,M.L; Seugling, C.J,;Foss, Jr., C.A. "Visible Region Polarization Spectroscopic Studies of Template-Synthesized Gold Nanoparticles Oriented in Polyethylene" *J. Phys. Chem. B* **1998**, *102*, 361.

[5] Dirix, Y.;Darribere, C. Heffels, W.; Bastiaansen, C.; Caseri, W.; Smith, P., "Optically anisotropic polyethylene-gold nanocomposites" *Applied Optics* **1999**, *38,* 6581.

[6] Caseri,W. "Nanocomposites of polymers and metals or semiconductors: Historical background and optical properties" *Macromol. Rapid Commun.* **2000**,*21,* 705.

[7] van der Zande,B.M.I.; Pages,L.; Hikmet, R.A.M.;van Blaaderen, A. "Optical Properties of Aligned Rod-Shaped Gold Particles Dispersed in Poly(vinyl alcohol) Films" *J. Phys. Chem. B* **1999**, *103,* 5761.

[8] Murphy, C.J.; Orendorff C.L. "Alignment of gold nanorods in polymer composites and on polymer surfaces" *Adv. Mater.* **2005**, *17*,2173.

[9] Pérez-Juste, J.; Rodríguez-González, B.; Mulvaney, P.; Liz-Marzán, L. M. "Optical Control and Patterning of Gold-Nanorod-Poly(vinyl alcohol) Nanocomposite Films" *Adv. Func. Mater.* **2005**,*15*, 1065.

[10] Johnson P. B**.;** Christy, R. W. **"**Optical Constants of the Noble Metals**"** *Phys. Rev. B,* **1972,** *6,* 4370.

[11]Cheremisinoff, N. “Handbook of Engineering Polymeric Materials” Marcel Dekker New York **1997**

[12] Matsuda, S.;Yasuda,Y.;Ando,S. “Fabrication of Polyimide-Blend Thin Films Containing Uniformly Oriented Silver Nanorods and Their Use as Flexible , Linear Polarizers” *Adv.Mater*.**2005**, *17*,2221.

Chapter VII

Pattern Formation of Gold Nanorods by Drying-Mediated Self Assembly

Abstract

In this chapter, we investigate the microscopic patterns formed by evaporation of gold NR suspensions in water. The drying of thin films of gold NR solution creates structured patterns such as ribbon, ring and cellular network, depending on the concentration (surface coverage) and evaporation rate. We probe the mechanism to form such a pattern and analyze the structure to provide fundamental knowledge to design statistically patterned arrays of nanoparticles and fabricate spontaneously organized nanoscale devices.

7.1. Introduction

One of the growing interest in nanoparticles (NPs) research is to use NPs as building blocks for constructing optoelectronic, electronic and magnetic devices[1]. To achieve this goal, individual NP has to be organized into a specific structure. Among various methods of making nanostructures, self assembly is considered to be one of the few practical strategies because it is simple, versatile, and cost-efficient[2]. And in some occasions, one can take advantage of spontaneous development of patterns of NPs as a convinient path for sophisticated products.

In the self assembly process, it is important to understand the various interactions between NPs, substrates, and solvents, which lead to the patterns formed. There are several competing interactions/forces between particles that control the self assmebly behavior, such as Brownian motion, electrostatic attraction and repulsion, van der Waals attraction, steric repulsion, and capillary force, etc[3]. Since most of the self assembly is accomplished by evaporating thin film of solution on a substrate, drying kinetics, substrate roughness, solvent wetting/dewetting, hydrodynamic effects and self–diffusion of the NPs on a substrate also play important roles in governing the morphologies of self aseembly leading to unusual nonequilibrium structures[4].

Evaporation of solvent affects particle/particle interaction, since the relatively weak attraction between NPs, which are efficiently screened in dilute solution, becomes noticeable as the solvent evaporates, initiating assembly of slowly evolving structures[5].

It is observed that for sufficiently monodisperse systems, hard colloidal spheres self assemble into a wide range of highly orderd phases due to entropic effects[6]. The driving force of this self assemly is repulsive interactions between colloidal spheres. At high volume fractions, the extra packing entropy due to local motions about lattice sites compensates for the loss of configurational entropy arising from long-range ordering. The factors affecting the mechanism are the concentration of the particles, softness of the interparticle potential, the existence of slight interparticle attractions and particle polydispersity.

Ohara et al. observed a solution of sufficiently polydisperse gold nanocrystals self assembled showing size-segregation during solvent evaporation, suggesting that the size-dependent attraction between the nanocrystals is sufficient to induce size segregation[7] since entropic effect is suppressed due to the polydispersity.

Ge et al. suggested that self assembly is the result of aggreration from a phase separation between a dense nanocrystal liquid and dilute nanocrystal vapour (phase

condensation model) that is triggered by the increase of interaction between NPs when a good solvent is replaced by a poor solvent (air)[8]. They showed a variety of structured aggregate spatial patterns as a function of surface coverage from the drying of thin nanocrystal solution film.

Rabani et al. further extended phase condensation model to present a model of NP self assembly which included the dynamics of the evaporationg solvent[5]. The simulations account for all observed spatial and temporal petterns including network structure. They categorized two distinct mechanisms of ordering, corresponding to the homogeneous and heterogeneous limits of evaporation dynamics. In the case of homogeneous evaporation, evaporation is spatially homogeneous while the boundaries of nanoparticle domains remain fluxional throughout the growth dynamics. Depending upon coverage and the evaporation condition, different patterns were observed (Figure 7.1).

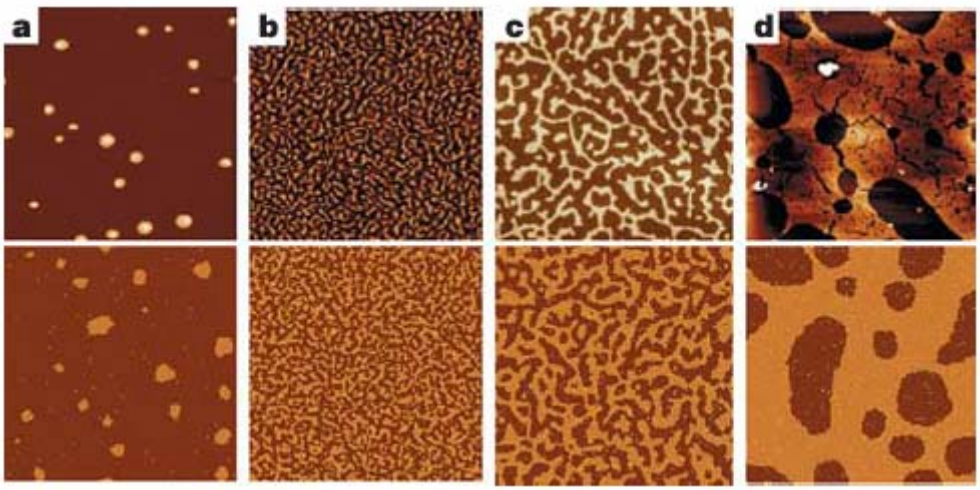

Figure 7.1. Self-assembled morphologies resulting from homogeneous evaporation and wetting of nanoparticle domains. The upper panels show the experimental results. The lower panels show results of model simulations for coverages of 5% (a), 30% (b), 40% (c) and 60% (d). The upper panels show corresponding experimentally observed morphologies for CdSe nanocrystals at similar coverages. From reference 5.

In the case of heterogeneous evaporation (evaporation is instead strongly heterogeneous in space), the dynamics of self assembly can be dramatically different. Phase change occurs not by long-wavelength fluctuations, but by nucleation and growth of vapor bubbles leading to network-like morphologies (Figure 7.2). These heterogeneous structures are highly versatile and used both in nature and industry. The connectivity of the phases is one of the key factors controlling the transport functions and the mechanical properties of the phase separated structures[9].

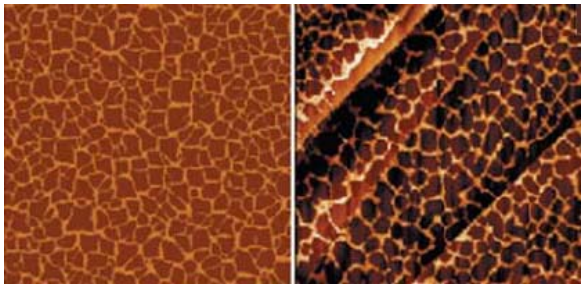

Figure 7.2. Self-assembled morphologies resulting from inhomogeneous evaporation in simulations (left) and in experiments (right). From reference 5.

Ohara et al. further observed annular ring-like arrays when dilute solutions of nearly monodisperse metal NPs were evaporated on a solid substrate[10]. Each annular ring is argued to arise from the pinning of the rim of an opening hole.

a) b)

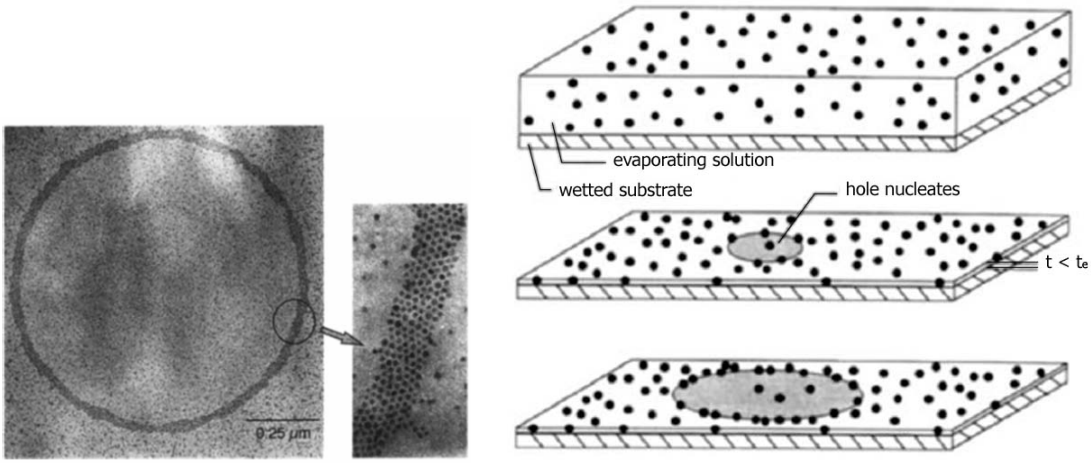

Figure 7.3. a) A ring-like array formed from the dilute solution of nanocrystals. b) Side-view schematic showing a scenario for evaporation of solvent from nanoparticle solution on wetted substrate (top), and its thinning to thickness $t_{hole} < t_e$ where t_{hole} is the thickness of the film and t_e is the critical thickness at which point a hole nucleates (middle). The hole then opens, collecting particles in its growing perimeter (bottom), which becomes an annular ring upon pinning of its contact line. From reference 10.

Capillary-forces-induced self assembly is another way to make a large scale configuration[11]. Capillary forces are interactions between particles mediated by fluid interfaces[12]. As the thickness of the water layer becomes equal to the particle diameter, a nucleus of 2D crystal suddenly forms. The particles surrounding the nucleus begin to move towards the ordered phase to join the ordered array. The quality of assembly is determined by the factors such as the rate of water evaporation, the ionic strength, the surfactant concentration and the particle size and shape distributions.

For the self assembly of anisotropic shape of NPs such as nanorod (NR), nanowire, and nanodisk, the situation becomes even more complex, because they can form liquid crystalline phases. Although a great deal of work has been published on the self assebmly of spherical NPs, to date the assembly behavior of anisotropic particles is largely unexplored.

This chapter will focus primarily on observations of self assembly of gold NRs and will probe the mechanism for the formation of different patterns.

7.2. Experimental

We obtained gold NRs of spherocylinderical shape with controlled aspect ratio and with a little byproduct (20% by number fraction) by using seed-mediated method

with binary surfactant solution according to the procedures described in chapter 2. We successfully separated NRs from spherical NPs employing a single round of centrifugation (described in chapter 4). And excess surfactant was removed by additional centrifugation. Thus the final sample contains NRs with low polydispersity (less than 15%) .

For each aspect ratio of gold NRs, the concentration is varied by adding distilled water to the mother solution. The concentration of gold NRs to form the monolayer on the grid by deposition of 1μl solution is roughly 1×10^{-13} mole/liter (for the NRs with aspect ratio of 6). We fix the concentration of the mother solution at 2×10^{-12} mole/liter so that the observation is not limited by the thick multi layer of the self assembly.

All TEM samples were prepared by depositing 1μl of the solution of specific concentration on TEM grids. Since we used carbon coated copper grid, the deposited solution did not spread and remained stable, hence, the complete evaporation took almost 1hr (condition I). Evaporation was slowed down by placing platform of the grid in the water bath at room temperature and covering it with a glass. The water provided a water vapor atmosphere to allow for slow drying (6-12 h) of the solutions on the grid (condition II). We set the initial film thickness by removing the excess solution with filter paper 3 minutes after deposition. In this case, the complete

evaporation took less than 10 minutes. The nature of the self assembly of NPs was examined by TEM (JEOL100 at 100 KV).

7.3. Results and discussion

7.3.1. Interparticle forces among NRs.

Before we proceed to discuss the self assembly, we need to understand the interactions among gold NRs in solution. The interaction between colloidal particles consists of both electrostatic repulsive forces due to the overlap of electrical double layers and of attractive van der Waals forces. As-made gold NR in water is stable up to considerably long time (several months) because it is covered by the bilayer of surfactant. The governing interparticle force in this case is electrostatic repulsion due to the electrical double layer and steric hindrance. According to our experimental observation, upon repeated centrifugation (usually 3 times), gold NRs aggregate and it is impossible to redisperse them. In this case, the governing interparticle force can be considered to be van der Waals attraction. Therefore, the concentration of surfactant remaining in the solution is critical because the stability of colloidal suspensions depends on the balance between these two forces. We prepared the mother solution for self assembly by centrifuging as-made solution twice. The final concentration of

surfactant is about 1×10^{-3} M. This sample was stable for several months. Thus the colloid-colloid interactions can be approximated by the sum of hard-core, electrostatic (soft) repulsions and van der Waals attraction. And the dominant interaction is determined by the distance between the particles.

7.3.2. Heterogeneity and polydispersity of the sample

As-made solution is essentially a mixture of rods and spherical particles. We observed two different phenomena when as-made solution is evaporated on a TEM grid. When the evaporation is relatively slow (condition II), we observe shape-selective assembly where NRs and spherical particles assemble separately showing micro phase separation on the TEM grid.

a) b)

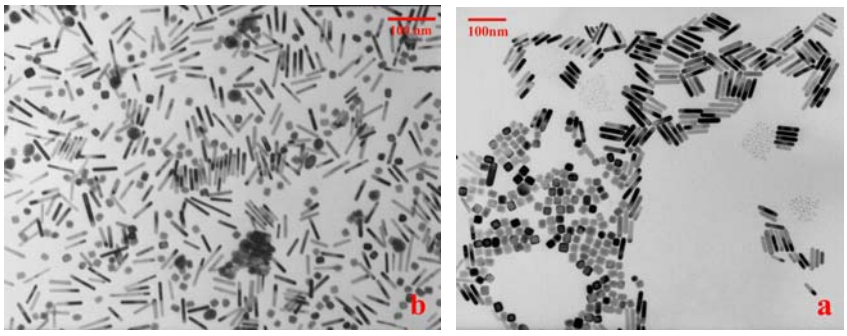

Figure 7.4. TEM image of self assembly of as-made solution. (a) Fast evaporation (condition I) and (b) slow evaporation (condition II). The coverage of the particles in both images is about 20%.

Figure 7.4 (b) shows the shape dependent phase separation. This is driven by

depletion interactions which can be explained in terms of purely repulsive interactions, between particles with different shape. This phenomenon is extensively studied theoretically and has also been confirmed by simulations. The corresponding "depletion potential" is given by[13]

$$W(h) = -\frac{2}{3} k_B T \phi_r \frac{L}{D} \frac{R}{D} (1 - \frac{h}{L})^3$$

where $k_B T$ is the thermal energy, ϕ_r is the volume fraction of the rod, R is the radius of the sphere. L is the length of the rod, D is the diameter of the rod, and h is the distance between the surfaces of the two particles. We observe this separation for NRs of relatively high aspect ratio, since high L/D is one of the favorable conditions.

When the evaporation is rather fast, we do not observe this micro phase separation. We think that in this case, the phase separation could not be achieved because the particles lose their mobility since the evaporation is completed in a short time.

Figure 7.5 is another example showing micro phase separation of 3 different shapes of NPs (nanorods, nanospheres and nanocubes).

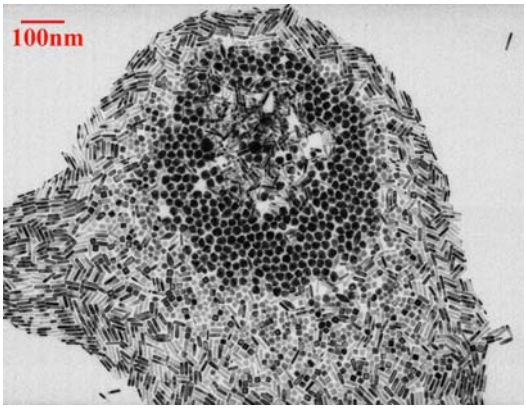

Figure 7.5. TEM image of self assembly of as-made solution showing micro phase separation of 3 different shapes of nanoparticles.

The polydispersity within the same species is also an important parameter affecting the quality of self assembly. NPs with higher polydispersity do not show any regular assembly under any circumstance because polydispersity usually prevents long range ordering[14]. Even on the same TEM grid, local polydispersity does determine the character of self assembly.

There are several reports regarding self assembly of gold NRs[15], focused on the local self assembly in a small domain. It has been proposed that the concentration and pH of the solution determine the properties of self assembly[15,c]. Using TEM, we can observe most of the characteristic patterns both from homogeneous evaporation and heterogeneous evaporation at every level of coverage ratio within a single sample prepared on a TEM grid.

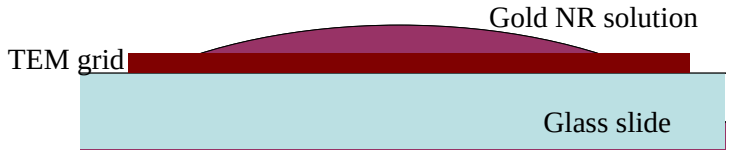

Scheme 7.1. The schematic showing the preparation of TEM samples.

We prepared the sample for TEM observation by deposition of 1μl gold NR solution on a TEM grid. The radius of the drop is smaller (1.4 mm) than that of the grid (3mm). This condition enables us to observe the coffee ring phenomena confined on a TEM grid. The colloidal particles migrate to the edge where the contact line of the drop gets pinned, and the evaporating fluid at the edge is replenished by a strong capillary driven flow that carries nearly all the solute to the edge. The solute becomes concentrated into a fraction of the perimeter during evaporation (We will discuss this phenomena in detail in chapter 8). As a result, on the same TEM grid, the concentration of the solute (gold NPs) increases towards the edge of the grid. Therefore we can observe the concentration dependant pattern formation on the same TEM grid. Also evaporation rate is higher towards the edge providing different evaporation rates on the same grid. Because the local environment such as roughness of the surface and thickness of solution film formed on the grid could not be controlled

even on the same TEM grid, we observe the characteristic patterns both from homogeneous and heterogeneous evaporation.

We discuss the patterns formed by gold NRs depending on the local coverage of gold NRs rather than the concentration since it is impossible to determine the local concentration of the solute. Also, the self assembly observed on a TEM grid is mostly monolayer, therefore it can be considered as two dimensional. The following results were obtained by slow evaporation (condition II).

7.3.3. Patterns formed by homogeneous evaporation

Figure 7.6 shows the patterns taken from the center area of a single TEM grid. The aspect ratio of NRs is 5. At very low coverage (less than 5%) ribbon-like aggregates of nanoparticles dominate the self assembly (Figure 7.6 a). As the coverage increases (Figure 7.6 b), disk-like aggregates of NPs dominate the self-assembly. At higher coverage, NR domains become multilayer anisotropic shape (Figure 7.6 c) and finally become connected cluster, when the particle coverage is higher, around 20-30% (Figure 7.6 d).

Our results are qualitatively consistent with the dynamics of NP assembly in the limit of spatially homogeneous evaporation where the interparticle attractive force,

phase separation kinetics and critical coverage can be revealed from aggregation spatial patterns. We observe these patterns from the NR suspension of aspect ratio 3 to 6. Since the evaporation rate in the center of the drop is considered to be slower than at the edge of the drop, and the thickness of the solution film is relatively stable through out the evaporation, self assembly at the center of the drop results in the characteristic patterns formed in homogeneous evaporation.

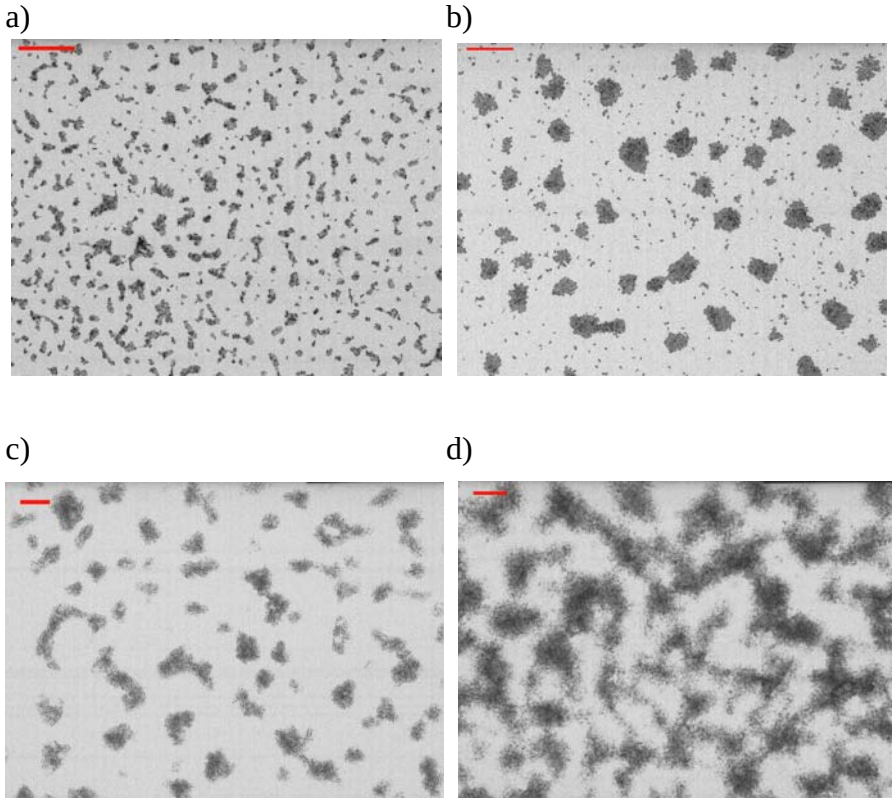

Figure 7.6. The TEM images showing different patterns formed at different coverage ratio of a) 4%, b) 10%, c) 15% and d) 40%. The aspect ratio is 5 and the scale bar is 1μm.

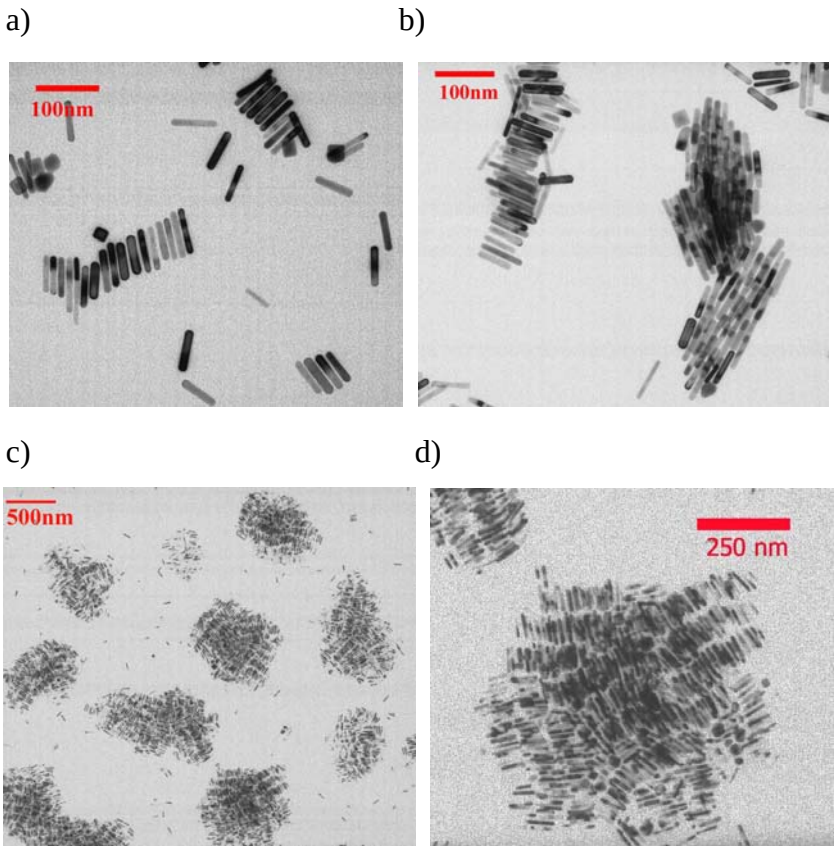

Figure 7.7. TEM images of self assembly of gold NRs showing transition from ribbon-like structure to disk-like smectic domain. a) The individual domain of ribbon-like structure, b) small domain of nematic-like structure, c) domains of smectic-like structure and d) an enlarged image of c showing an individual domain of smectic-like structure.

We also found that as the size of domain (aggregate) increases, the assembly shows the phase transition. We mentioned previously that at low coverage, side by side assembly of gold NRs is dominant. Figure 7.7 a) shows the individual domain of ribbon-like structure. As the size of domain (also the number of particles in the domain) increases, multi layer of ribbon structure is observed as well as monolayer and

ribbons transform into small domain of nematic like structure shown in Figure 7.7 b) and finally into smectic-like structure as shown in Figure 7.7 c).

The ribbon-like structure is simply due to the anisotropy of NRs. Bates et al. studied two dimensional hard rod fluids consisting of spherocylinders confined to lie in a plane by means of Monte Carlo simulations[16]. They predicted that due to the anisotropy of NRs, chains of particles aligning side-by-side form ribbon-like structure. For long rods, a 2D nematic phase and smectic phases are observed at higher density. Our experimental observation is in good agreement with their simulation showing that the transition to nematic like structure and smectic like structure occurs in the domain of aggregation.

In the same region, we often observed a considerably large area covered by monolaryer of NPs, sometimes forming interesting features (Figure 7.8).

a)

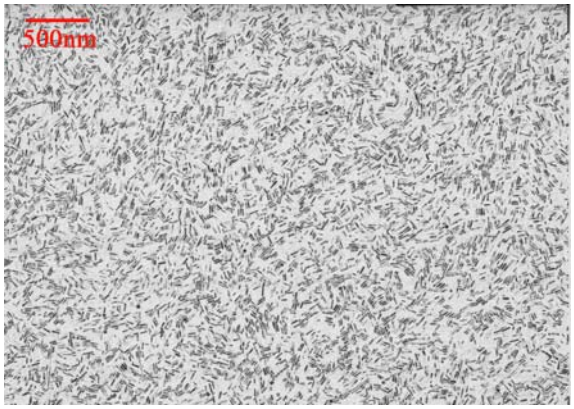

b)

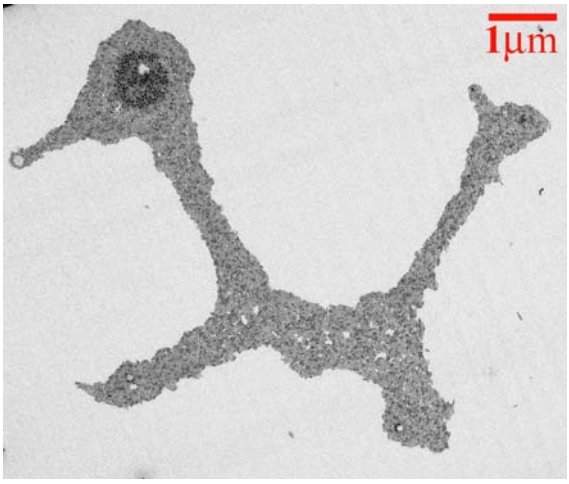

Figure 7.8. a) TEM images of self assembly of gold NRs showing a large area covered by monolayer of gold NRs. b) One of the interesting features formed by the monolayer of gold NRs. The “eye area” is the microphase-separated nanospheres surrounded by NRs.

7.3.4. Patterns formed by heterogeneous evaporation

One of the interesting patterns we observed from evaporation of gold NR suspension on the TEM grid were the ring pattern. This sturcture was observed when

the coverage is 10 to 20% and at the intermediate area between the center and the edge of the drop.

a)

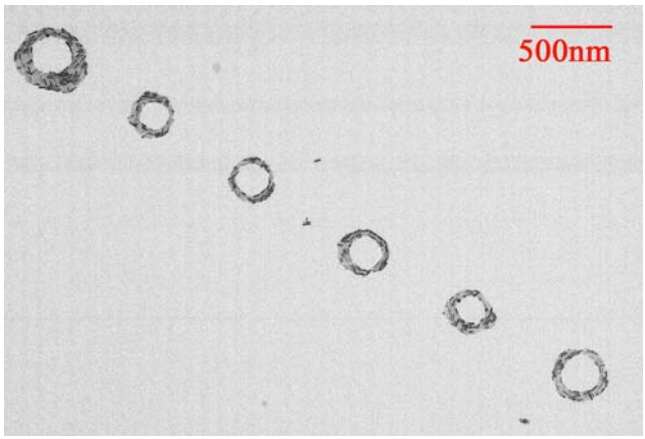

b)

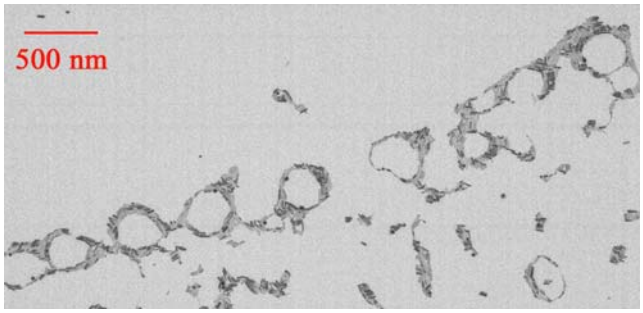

Figure 7.9. Ring-like array observed when the coverage is 10 to 20%. a) aspect ratio 4, b) aspect ratio 6.

The ring patterns formed by various aspect ratio of gold NRs (aspect ratio 4 to 7). The shape of the ring is close to a perfect circle and the diameter of the ring ranged from 200nm to 1μm and not related to the aspect ratio of gold NRs. The neighboring rings are alingned forming a line which could be a part of the circumference. Their size is almost same and the distance between each ring is also very regular.

The ring patterns result from the pinning of the contact lines of nucleating holes in the thin liquid film. The hole opens, pushing most particles out along its advancing rim,which becomes a ring. Depending on the local concentration of particles, the width of the outer rim varies. The reason for the set of ring forming a line is related to the concentration gradient formed in the evaporating drop. After the contact line gets pinned, colloidal particles migrate to edge. This causes dynamic concentration gradient of solutes along the radius of the drop. As the water evaporates, the film gets thinner. Below its critical thickness (t_e), it becomes unstable resulting in the nucleation and growth of holes. Since the condition such as the concentration of solute as well and the thickness of the solution film is radially similar, holes are formed along a macroscopic ring which can be recognized as a line in nanoscale observation.

We measured the volume of the particle within a ring-like array and found that it decreases toward outer rim which indicates that lighter particle is pushed farther than heavier particle (Figure 7.10). This result supports the mechnism that the ring originates from the hole instability.

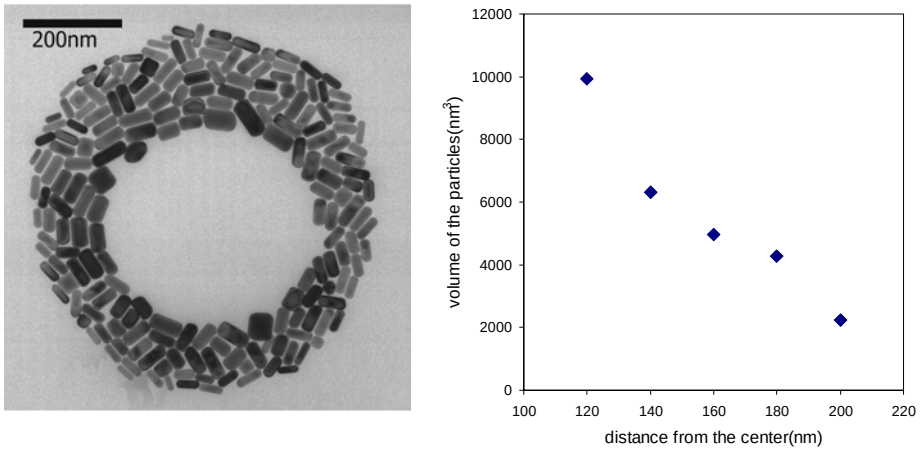

Figure 7.10. The volume of the particle within a ring-like structure decreases toward outer rim which indicates that lighter particle is pushed further than heavier particle.

We also observed circular domains which do not have the hole in the center (Figure 7.11). This structure is similar to the structure formed by percolation of the neighboring holes[17]. When the rims of holes are not pinned, neighboring holes percolate to form a "drop" at their interstices, pushing particles together (middle), resulting in close-packed circular aggregation.

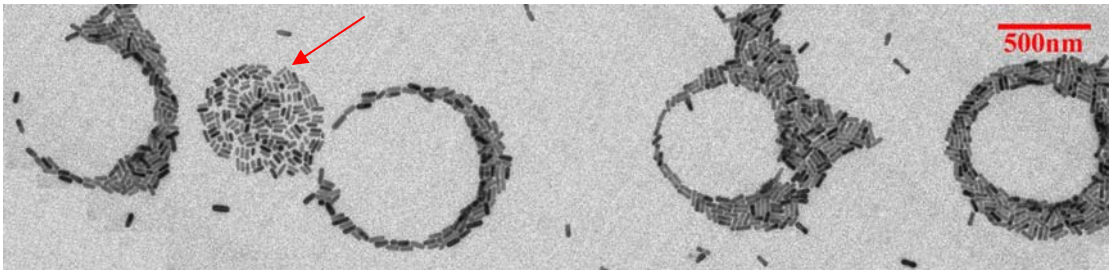

Figure 7.11. The circular domain formed between the ring-like array structures.

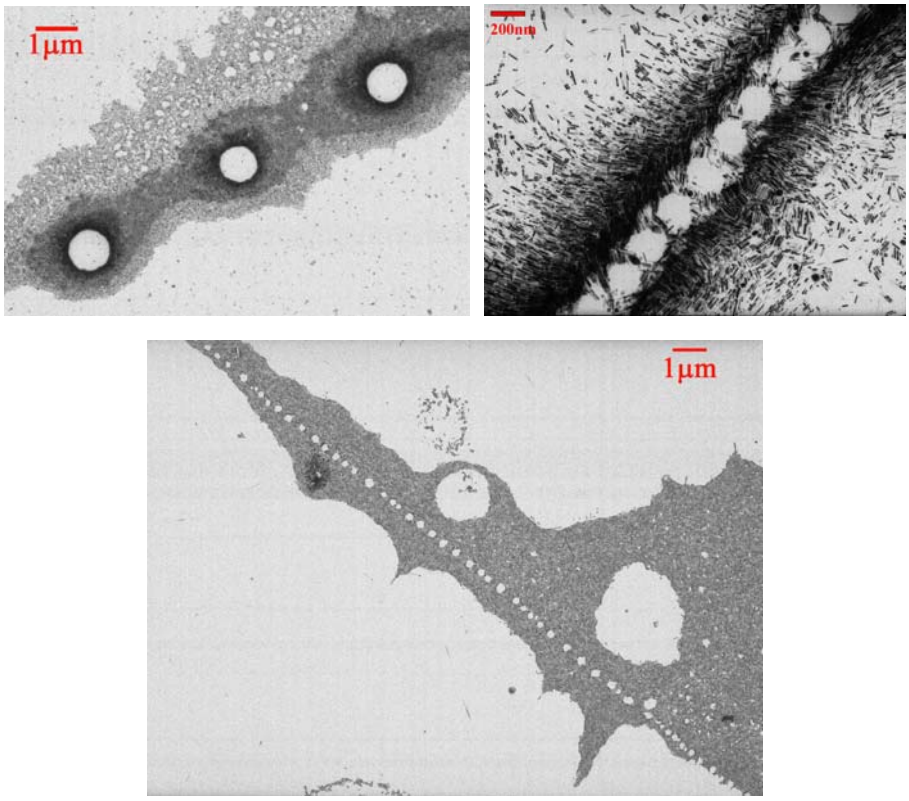

Figure 7.12. TEM images of self assembly of gold NRs showing the formation of the ring-like structure in different patterns.

Figure 7.12 shows the interesting ring array inside the uniform monolayer of self assembly. Figure 7.13 shows another interesting ring array having the monolayer of self assembly as a background. This is the superposition of the two opposite sides (top and bottom) of the TEM grid (both sides of the TEM grid are visualized without distinguishing one from the other). Since the solution smears out to the bottom side of the grid during the deposition, similar phenomena occur on both sides. One side shows the uniformly formed monolayer of NRs while the other side shows the ring-

array structure. We assume that the different local environment is responsible for these different structures.

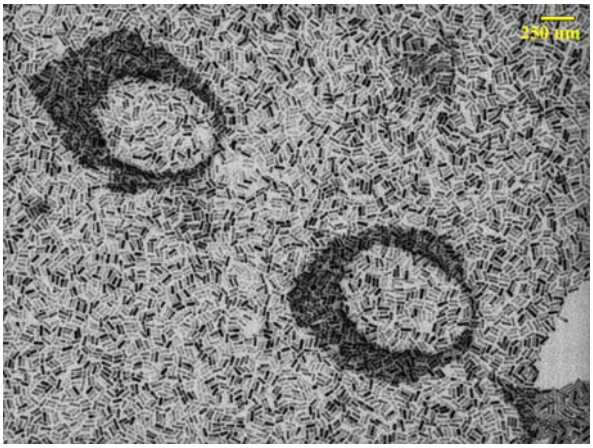

Figure 7.13. TEM image of ring array having the monolayer of self assembly as a background.

As the coverage increases, ring arrays become cellular networks. Figure 7.14 shows the coexistance of ring-like array and the intermediate state between ring-like array and network structure.

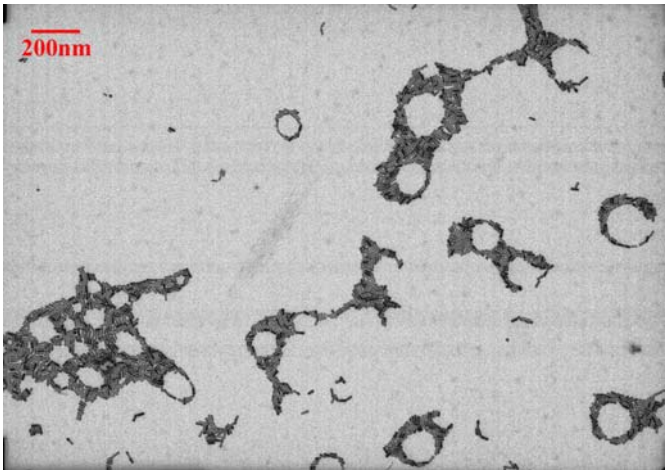

Figure 7.14. TEM image showing the transition from ring-like array to cellular network structure.

The celluar network structures are often observed when the coverage reaches about 30 to 50%. Figure 7.14 shows the transition from ring-like array to cellular network structure.

a)

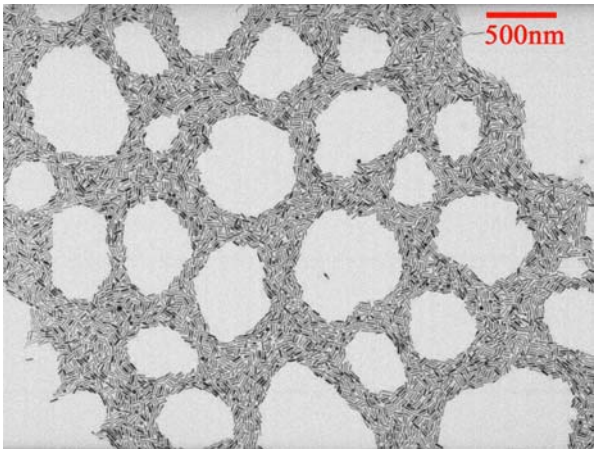

b)

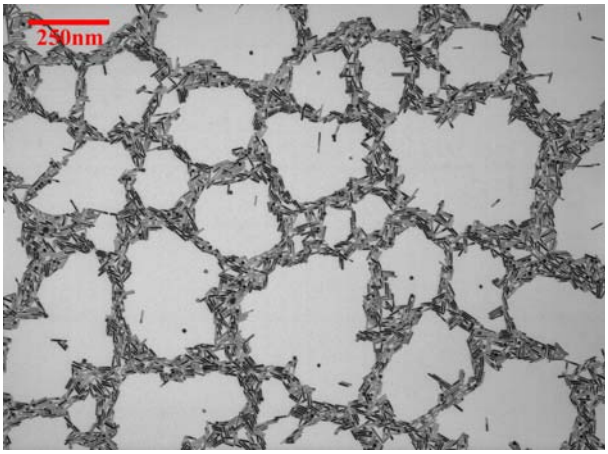

Figure 7.15. The cellular network structures formed by gold NRs with different aspect ratios: a) aspect ratio of 4 and b) aspect ratio of 6.

Figure 7.15 shows the network structure formed with different aspect ratios. The edge of inside cell is better defined for the shorter NRs. The size of the hole ranges

from 100 to 700nm in diameter and is not related to the aspect ratio of NRs. We believe that the difference in the size of the hole originates from the locally different environment such as local film thinkness fluctuation, surface roughness and small temperature differences.

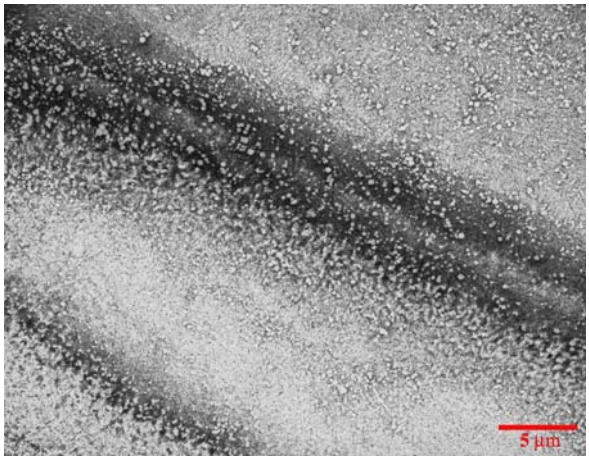

Figure 7.16. Cellular network structure formed in a large area.

The network structure is very useful because it gives the connectivity of the phase at the expense of small amount of materials. We observed that gold NRs can form this network structure over a considerably large area (Figure 7.18) showing the potential applications as in fabricating electronic devices.

7.3.5. Self assembly formed at the edge of the evaporating drop

Figure 7.17 shows a large area of the assembled NRs on the dried edge of the drop. The outer edge consists of monolayer of NRs in which NRs assembly does not

show specific ordered phase. The NRs at the interface of air-solution seem to lie parallel to the interface. Moving inside from the edge, the second region shows more ordered structure where longer chains of NRs are densely packed forming multilayer. Further away from this region, domains of smectic-like assembly of NRs are formed less densely.

The anisotropy of NR is the reason for forming this assembly. As the particles transfer towards the edge by the convective flow, the local concentration reaches high enough for phase transition from isotropic to nematic and smectic. The domains of smectic LC phase joins to the edge and the strong lateral capillary force align them into dense ordered structure

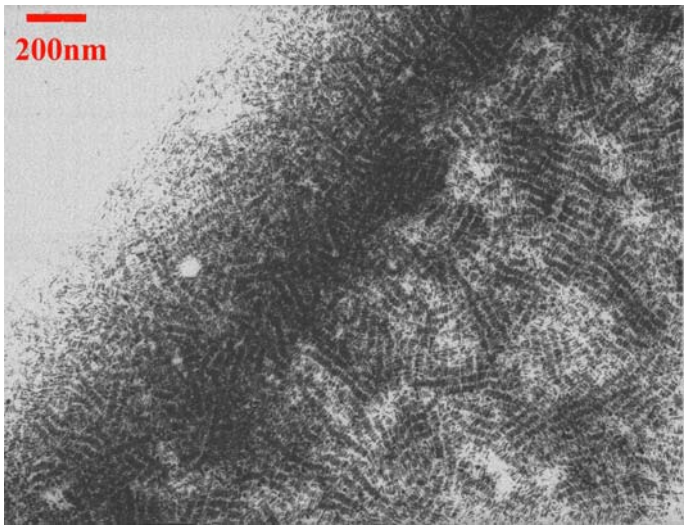

Figure 7.17. The self assembly of gold NRs formed at the edge of the evaporating drop.

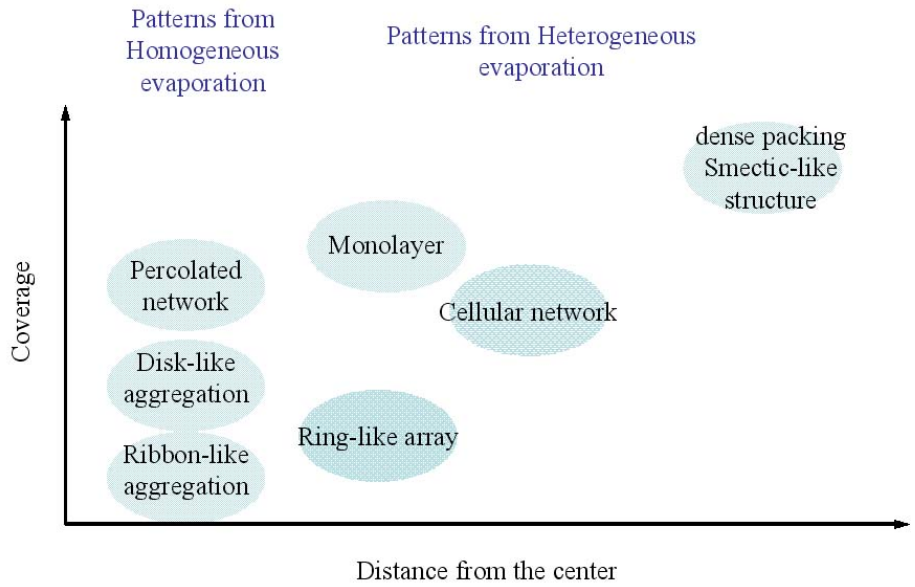

Figure 7.18. Different patterns of self assembly formed by evaporating gold NR solution.

The various patterns are mapped as a function of distance from the center of the drop and the coverage (Figure 7.18). We observe the patterns similar to those from homogeneous evaporation in the center of the drop and various patterns similar to those from heterogeneous evaporation towards the edge of the drop. These observations show that the concentration of NRs, the evaporation rate, the mobility of the particles and the thickness of the solution film are the key factors to determine the properties of self assembly.

7.3.6. Effect of molecular linkage on the self assembly of gold NRs

In nanomaterial research, there is interest in the bulk fabrication of supramolecular nanostructures where individual NPs are arranged in a controlled fashion. Optimally, the NPs can be naturally assembled into the final structure through particle-particle interaction as we aforementioned. Supramolecular assembly of NPs can be achieved by controlled association through complementary recognition of NP surface functionality. In the case of gold NRs, end-to-end assembly has been demonstrated using molecular linkage such as α-ω-alkanedithiols[18], cysteines[19] and biotin-streptavidine connectors[20]. The dense adsorption of surfactant on the side of NR is responsible for this end- to-end assembly.

We also achieved longitudinal assembly through cooperative intermolecular hydrogen bonding by using molecules such as azo dye rotaxane. By changing the concentration of azo dye rotaxane, we were able to control the number of particles linked together (Figure 7.19).

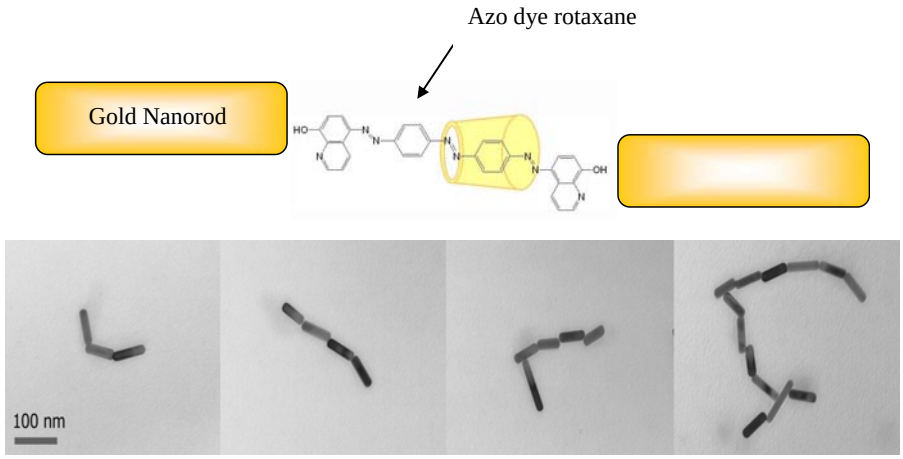

Figure 7.19. TEM images of gold NRs in the presence of azo dye rotaxane showing end-to-end linkage mediated by azo dye rotaxane. The aspect ratio of the gold NRs is 4.5. The concentrations of dye rotaxane increases from a to d. a) 2.0×10^{-6}M, b) 4.08×10^{-6}M, c) 4.9×10^{-5}M and d) 7.35×10^{-5}M.

7.4. Conclusions

A variety of patterns were formed by evaporating solutions of NRs deposited on TEM grids. The patterns can be explained by drying-mediated self asssembly where the coverage ratio and evaporation condition are among the dominant factors that determine the characteristics of the pattern. Depending on the location in the drop, the concentration of the gold NR and the evaporation rate are different, thus self assembly shows the chasracteristic patterns from both homogeneous evaporation and heterogeneous evaporation. The quantitative analysis of the specific mechanism of self assembly needs to be studeid further to design statistically patterned arrays of

nanoparticles and to fabricate spontaneously organized nanoscale device. We believe that by understanding the mechanism of the self assembly and by achieving the controlled evaporation environment, we will be able to use the self assembly as a vasatile nonlithographic technique having potential for large scale fabrication of the next generation of inexpensive electronic devices.

References

[1] El-Sayed, M.A. "Some Interesting Properties of Metals Confined in Time and Nanometer Space of Different Shapes" *Acc.Chem. Res.* **2001**, *34*, 257.

[2] Whitesides, G. M.; Grzybowski, B. "Self-Assembly at All Scales" *Science,***2002**, *295*, 2418.

[3] Hiemenz, P.C.; Rajagopalan, R. "Principles of Colloid and Surface Chemistry" 3rd ed., **1997,** Marcel Dekker, Chapter 10 and 11.

[4] Tang,J.; Ge, G.; Brus, L.E. "Gas-Liquid-Solid Phase Transition Model for Two-Dimensional Nanocrystal Self-Assembly on Graphite" *J. Phys. Chem. B* **2002**, *106*, 5653.

[5] Rabani, E.; Reichman D.R.; Geissler, P.L.; Brus L.E. "Drying-mediated self-assembly of nanoparticles" *Nature* **2003,** *426*, 271.

[6] a) Pusey, P. N.; van Megan,W. "Phase behavior of concentrated suspensions of nearly hard colloidal spheres" Nature **1986,** *320*, 340 b) van Megan,W; Underwood S. M. "Glass transition in colloidal hard spheres: Mode-coupling theory analysis" *Phys. Rev. Lett.* **1993,** *70*, 2766 c) Lin,K.; Crocker,J.C., Prasad,V.; Schofield,A.; Weitz, D. A.; Lubensky, T. C.; Yodh, A. G. "Entropically Driven Colloidal Crystallization on Patterned Surfaces" *Phys. Rev. Lett.* **2000** *85*,1770.

[7] Ohara,P.C.; Leff, D.V.; Heath,J.R.; Gelbart,W.M. "Crystallization of Opals from Polydisperse Nanoparticles" *Phys. Rev. Lett* . **1995**,75, 3466.

[8] a) Ge, G.; Brus, L. E. "Evidence for spinodal phase in two-dimensional nanocrystal self-assembly" *J. Phys.Chem. B* **2000**,*104*, 9573 b) Tang,J.; Ge, G.;Brus,L.E. "Gas-Liquid-Solid Phase Transition Model for Two-Dimensional Nanocrystal Self-Assembly on Graphite" *J. Phys. Chem. B* **2002**, *106*, 5653.

[9] Iwashita,Y.; Tanaka, H. "Self-organization in phase separation of a lyotropic liquid crystal into cellular, network and droplet morphologies" *Nature materials* **2006**, *5*, 147.

[10] Ohara, P.C.; Heath,J.R.; Gelbart,W.M. "Self-Assembly of Submicrometer Rings of Particles from Solutions of Nanoparticles" *Angew. Chem. Int. Ed. Engl.* **1991**, *36*,1077.

[11] Nikoobakht, B; El-Sayed, M. A. "Self Assembly of Gold Nanorods" *J.Phys.Chem. B.* **2000**, 104, 8635.

[12] Kralchevsky, P.A.;Denkov,N.D. "Capillary forces and structuring in layers of colloid particles" *Current Opinion in Colloid and Interface Science* **2001**, *6* , 383.

[13] Koenderink,G.H.; Vliegenthart, G. A.; Kluijtmans, S. G. J. M.; van Blaaderen, A.;Philipse, A. P.; Lekkerkerker, H. N. W. "Depletion-Induced Crystallization in Colloidal Rod-Sphere Mixtures" *Langmuir* **1999,** *15*, 4693.

[14] Gabriel1, J.P.; Davidson, P. "Mineral Liquid Crystals from Self-Assembly of Anisotropic Nanosystems" *Top. Curr. Chem.* **200**3, *226*, 119.

[15] a) Jana,N.R. "Shape Effect in Nanoparticle Self-Assembly" *Angew. Chem. Int. Ed*. **2004**, *43*, 1536 b) Sau,T.K.; Murphy,C.J. "Self-Assembly Patterns Formed upon Solvent Evaporation of Aqueous Cetyltrimethylammonium Bromide-Coated Gold Nanoparticles of Various Shapes" *Langmuir* **2005**, *21*, 2923 c) Orendorff,C.J.; Hankins, P.L.; Murphy,C.J. "pH-Triggered Assembly of Gold Nanorods" *Langmuir* **2005**, *21*, 2022.

[16] Bates, M.A.; Frenkel,D. "Phase behavior of two-dimensional hard rod fluids" *J. Chem. Phys.* **2000,** *112*, 10034.

[17] Ohara,P.C.; Gelbart,W.M. "Interplay between Hole Instability and Nanoparticle Array Formation in Ultrathin Liquid Films" *Langmuir* **1998,** *14*, 3418.

[18] Joseph,S.T.S.; Ipe,B.I.; Pramod, P.;K. George Thomas,K.G. "Gold Nanorods to Nanochains: Mechanistic Investigations on Their Longitudinal Assembly Using αϖ-Alkanedithiols and Interplasmon Coupling" *J. Phys. Chem. B* **2006**, *110*, 150.

[19] Sudeep, P. K.; Joseph, S. T. S.; Thomas, K. G. "Selective Detection of Cysteine and Glutathione Using Gold Nanorods**"** *J. Am. Chem. Soc.***2005**, *127*, 6516.

[20] Caswell, K. K.; Wilson, J. N.; Bunz, U. H. F.; Murphy, C. J. **"**Preferential End-to-End Assembly of Gold Nanorods by Biotin-Streptavidin Connectors**"** *J. Am. Chem. Soc.* **2003**, *125*, 13914.

Chapter VIII

Lyotropic Liquid Crystalline Phases of Colloidal Gold Nanorods Observed in Evaporating Drop

Abstract

We accomplished the experimental observations of lyotropic liquid crystalline (LC) phases of colloidal gold nanorods (NRs) by achieving the phase transition volume fraction through convective flow resulting from solvent evaporation. Characteristics of LC were confirmed by birefringence and fluidity of the LC domain and complemented by the self assembly observed by TEM. LC phase was observed for nanorods with aspect ratios ranging from 4 to 14. By changing the aspect ratio, concentration , and evaporation rate, we observed various patterns formed by the self assembly of gold NRs. When the dilute solution is evaporated fast, the contact line experiences a series of pinning-depinning events, and the gold NRs accumulate where the contact line is pinned resulting in the formation of multiple rings.

8.1. Introduction

Liquid crystalline (LC) phases exhibit properties of liquid and solid crystals. The various LC phases can be characterized by the type of ordering that is present. The nematic phase is one of the most common LC phases showing long-range orientational order and no positional order. In the smectic phase, the molecules are arranged in layers showing positional order in addition to orientational order. Liquid crystals can also be classified into thermotropic and lyotropic LCs. Thermotropic LCs go through a phase transition into the LC phase as temperature is changed, whereas lyotropic LCs exhibit phase transitions as a function of concentration. Scheme 8.1 schematically shows the phase transition of lyotropic liquid crystals due to the change in the concentration.

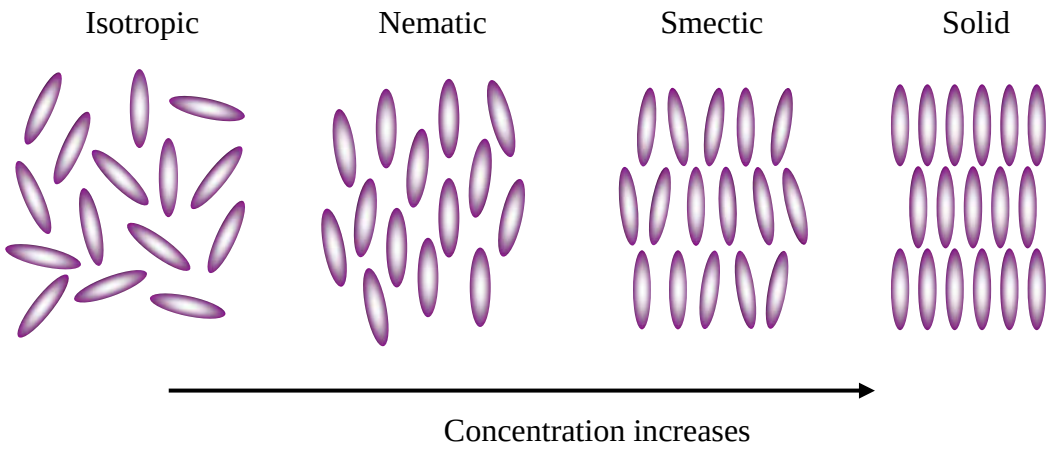

Scheme 8.1. Various liquid crystalline phases as a function of concentration of the solute.

8.1.1. The LC phase of colloidal suspension

The liquid crystalline properties of rod-like colloidal suspensions were first observed and understood by Zocher in 1925.[1] He observed the unusual behavior of colloidal aqueous suspensions of vanadium pentoxide, V_2O_5. Later, in 1938, Langmuir reported the phase separation of suspensions of bentonite clay platelets showing an isotropic (I) phase in equilibrium with a nematic (N) liquid crystalline phase[2]. Bawden et al. also found the nematic ordering of suspensions of Tobacco Mosaic Virus (TMV), a rod-like virus[3]. Since then, several other suspensions of rods have been found to exhibit the I-N phase transition including boehmite (γ-AlOOH)[4], goethite (α-FeOOH)[5], and rod-like virus particles (fd virus)[6].

Onsager recognized that systems of long rods may undergo an isotropic-nematic phase transition without attractive interactions between the particles and proposed a "hard rod model" to describe the nematic ordering of suspensions of rod-like particles such as the Tobacco Mosaic Virus (TMV) in 1949[7]. This model considers the volume excluded from the center-of-mass of one idealized cylinder as it approaches another. When the rods become more or less aligned, a loss of orientation entropy is compensated by a decrease in excluded volume. Thus in some cases greater positional order will be entropically favorable. This theory predicts that a solution of rod-shaped objects will undergo a phase transition, at sufficient

concentration, into a nematic phase. The critical concentration for a isotropic-nematic first-order transition at which phase separation appears is inversely proportional to the aspect ratio of the rods.

Since Onsager theory is quantitatively valid only for rigid rods with aspect ratio larger than 100, modified theories have been developed to account for the behavior of short rods and rods with polydispersity and electrostatic interactions, which have been successfully applied to various colloidal dispersions[6].

Computer simulations utilizing Monte Carlo methods have further shown that systems of hard spherocylinders exhibit not only the nematic phase but also, smectic, and different crystalline phases[8]. This phase diagram was experimentally evaluated by using hard rod systems (Se, FeOOH, and nickel dimethylglioxime particles) with a wide range of aspect ratio[9].

Recently, the interest in such systems is renewed due to fabrication of anisotropic nanoparticles (NPs) and improved techniques which provide nanometric control of materials and devices. Inorganic lyotropic liquid crystals have the potential to combine the typical features of liquid crystals, such as anisotropy and fluidity, with the electronic properties, such as electrical conductivity [10] or magnetism[11].

The formation of a liquid crystalline phase of rod-like NPs is often anticipated

from the observation of orientational and positional order in their assembly on the TEM grid[12]. This observation implies the formation of a liquid crystalline phase prior to complete evaporation of the solvent.

However, the most challenging problem in studying lyotropic LC phase formed by anisotropic NPs is to attain the critical concentration so as to obtain the critical concentration necessary to observe the phase transition predicted by Onsager. In the case of highly anisotropic (large L/d ratio) particles, concentrations of few percent by weight are usually necessary in order to observe such a transition. With particles of much lower aspect ratio, such as nanorods synthesized so far, much higher concentrations are required.

Meanwhile, the LC phase of suspensions of CdSe semi-conductor nanorods was explicitly demonstrated[13]. The suspension of CdSe NRs of aspect ratios tunable up to 15 shows schlieren textures in polarized light microscopy and displays spontaneous isotropic/nematic phase separation in a given range of concentration.

LC phase of gold NRs may provide a promising feature since it combines the typical properties of LC with the electro-optical response of colloidal dispersions[14].

There has been an attempt to show LC phases of gold NRs[15]. However, LC formation was not explicitly demonstrated.

8.1.2. Contact line deposits in an evaporating drop

When a drop of colloidal dispersion dries, the particles deposit in a ring at the periphery of the drop. The colloidal particles migrate to edge where the contact line of the drop gets pinned, and the evaporating fluid at the edge is replenished by a strong capillary driven flow that carries nearly all the solute to the edge. The solute becomes concentrated into a fraction of the perimeter during evaporation (Figure 8.1).

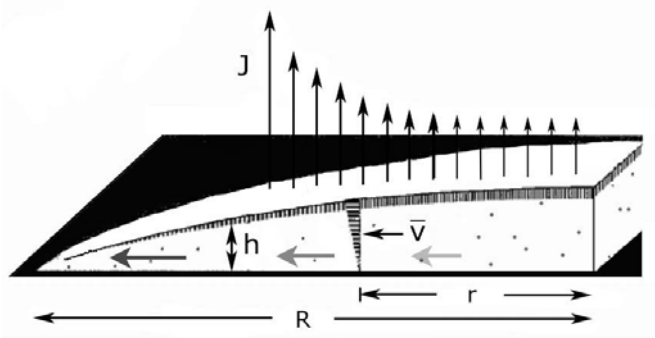

Figure 8.1. The factors leading to outward flow in a drop of fixed radius *R* slowly drying on a solid surface. The evaporative flux *J*(*r*) reduces the height *h*(*r*) at every point *r*. As its contact line is pinned, the radius of the drop cannot shrink. To prevent the shrinkage, liquid must flow outwards *v(r).* From the reference 16.

Deegan et al.[16] showed that these ring-like deposits can be observed whenever the surface is partially wet by the fluid irrespective of the chemical composition of the substrate. And they can be found with solutes ranging in size from the molecular to the colloidal. By treating the droplet as a symmetric lens of fluid about the substrate and making an analogy to electrostatics, the evaporative mass flux, J_s, is given by

$$J_s(r,t) \approx (R-r)^{-\lambda}$$

where $\lambda = (\pi - 2\theta_c)/(2\pi - \theta_c)$, R is the droplet radius, r is the radial coordinate, and θ_c is the contact angle.

Figure 8.2 shows a dried coffee stain[16] and a dried gold NRs solution. Since gold NRs solution leaves a ring shaped deposit on the substrate gold NRs, we rationalize that the outward flow carries gold NRs to the edge and the concentration of NRs at the edge becomes high enough to undergo the phase transition from isotropic to nematic liquid crystal.

a) b)

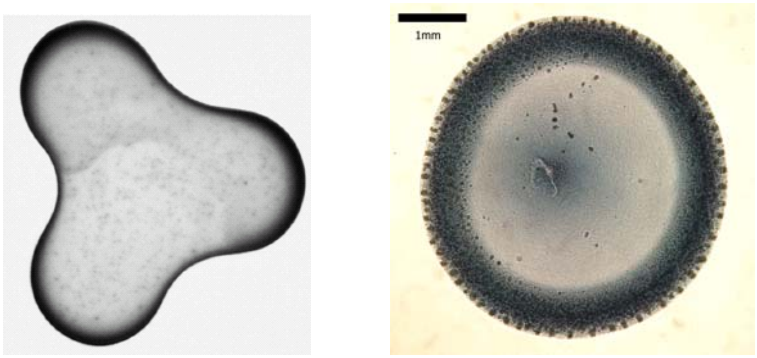

Figure 8.2. Images of a) a 2-cm-diameter drop of coffee from reference 16 and b) a 4-mm-diameter drop of colloidal gold NRs.

In this chapter, we accomplished the experimental observations of lyotropic liquid crystalline phases of colloidal gold NRs by achieving the phase transition volume fraction through the convective flow resulting from pinning of the evaporating drop.

8.2. Experimental

When NR suspension is treated as hard-rods[17] , the critical concentration for I-N phase transition is predicted to be 30 wt % for an aspect ratio of 10. Higher aspect ratio of gold NRs are usually produced in a low yield with large size distribution and byproduct (nanospheres and nanocubes). And it is relatively difficult to attain the solution concentration higher than the critical concentration. Thus, LC phase of gold NRs was not explicitly demonstrated.

We obtained spherocylindrical shape of gold NRs with controlled aspect ratio and with little byproduct (20%) by seeded growth procedure with binary surfactant solution according to procedures described in chapter 2. We successfully separated NRs from the nanocubes employing a single round of centrifugation (detailed in chapter 4). Excess surfactant was removed by additional centrifugation. Thus the final sample is almost pure NRs with low polydispersity (standard deviation of aspect ratio is less than 15%) and the volume fraction, Φ was 5×10^{-5}. The desired volume fraction is obtained by adding distilled water to the sample.

A specific amount of gold NR solution was deposited on a clean glass slide. The evaporating solution was observed using an optical microscope under crossed polarizers (Leica DMRX).

8.3. Results and discussion

8.3.1. The “coffee ring” of gold nanoparticle suspension.

We observed ring-like deposits from gold NR suspension as well as gold nanosphere solution. Rings were found in big drops (5mm in diameter) and in small drops (1mm in diameter) with the solute volume fraction ranging from 10^{-10} to 10^{-5}.

When placed on a glass slide, a drop of colloidal dispersion of gold NPs spreads quickly to its largest size. For example, a 2μl drop spreads to a maximum radius of 1.5 mm leaving the center height at approximately 62μm. The drop does not shrink after reaching its maximum size. In general, the evaporation occurs in two stages[18]. In the first stage, the contact line is pinned and the contact angle decreases until it reaches a critical value. In the second stage, the contact line starts to recede.

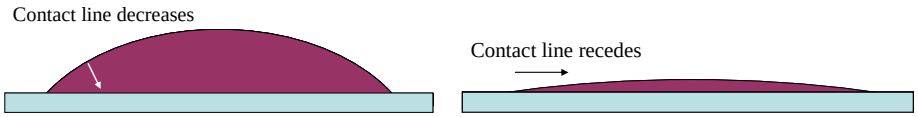

Scheme 8.2. A schematic of the droplet evaporation process[18].

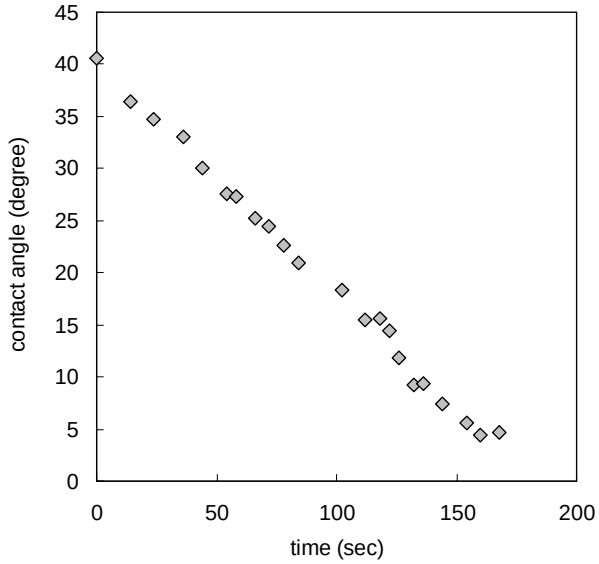

Figure 8.3. The contact angle of a drop of gold NR solution (1μl) on a glass substrate as a function of time.

Figure 8.3 shows the contact angle of a drop of gold NR solution on a glass substrate as a function of time during the drying process. The contact angle linearly decreases as water evaporates. When the contact angle becomes less than 5°, the contact line starts to recede and finally water evaporates completely. First stage occupies a substantial fraction of the drying time (1st stage ~168 sec and 2nd stage ~12 sec). The duration of this time is inversely proportional to the volume of the drop. During this stage, a flow generated from the evaporating drop causes the solutes to be carried to the edge resulting “coffee ring”. When the size of drop is the same, the width of the overall ring (band width) linearly increases as the solute concentration increases indicating that most of the particles are carried to the edge forming the ring (Figure 8.4).

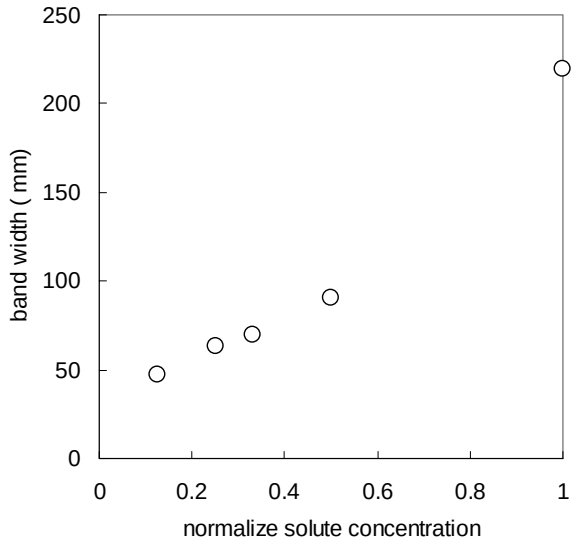

Figure 8.4. The band width is plotted as a function of normalized volume fraction of the gold NRs in the case of slow evaporation.

8.3.2. LC phase formed in an evaporating drop.

A simple way to identify a LC phase is to observe its texture using polarized light microscopy[19]. Since LC phases are birefringent, they interact with linearly polarized light, and can be observed between crossed polarizers.

We observed the coffee ring formation using polarized microscope. When the aspect ratio of gold NR is less than 4, the ring formed at the contact line but we didn't observe any birefringence from the evaporating solution. The birefringence from the surfactant crystal appears after water evaporates completely (Figure 8.5).

a) b)

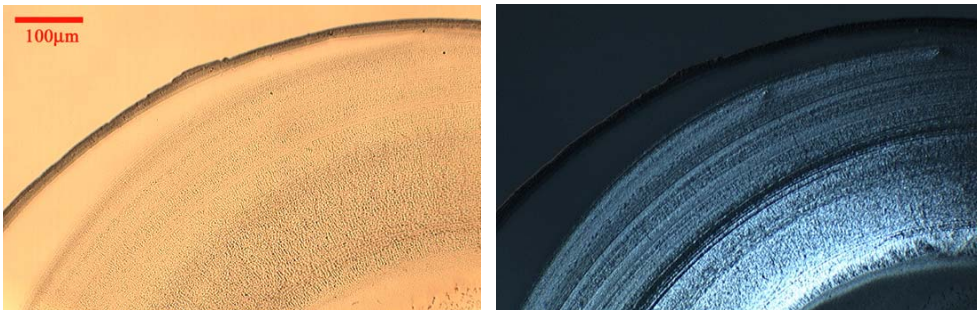

Figure 8.5. Optical microscope images of a dried drop of gold NRs with the aspect ratio of 3. a) Bright field image and b) polarized image at the edge. Birefringence is from the surfactant crystal.

When the aspect ratio is larger than 4, as the contact line is pinned, it becomes highly birefringent. Then birefringent droplets emerge from the interior and move towards the edge and join the existing birefringent contact line forming a ring. This bright band moves inward with droptlets joining at the same time. Meanwhile, the contact line separates from the outer edge and recedes inwards. After the contact line recedes, birefringence of the area behind the contact line becomes weaker due to the loss of fluidity. The formation of birefringent ring is shown in Figure 8.6.

The time to complete the evaporation is about 11min for a drop that is 2µm in diameter. The highly birefringent edge appears only after 3min. This period can be considered to be "self-pinning"[20]. Gold NRs wedge between the substrate and the contact line.

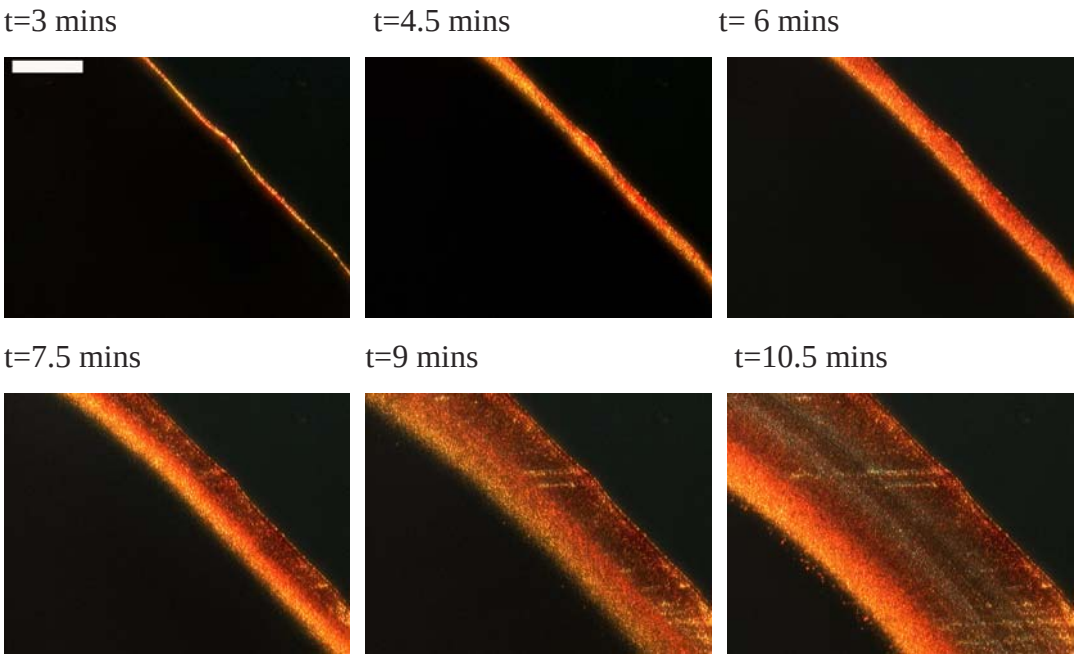

Figure 8.6. In this series of images the center of the drop is in the bottom left corner. The images of the drop of gold NRs solution during evaporation under optical microscope with cross polarizers, as described in the text. The scale bar is 30μm.

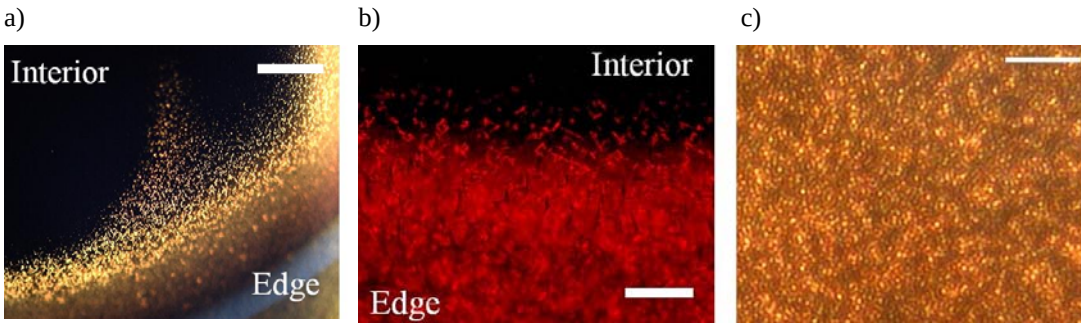

Figure 8.7. The images of the drop of gold NRs solution during evaporation under optical microscope with cross polarizers, as described in the text. a) Emerging liquid crystal domain from the interior near the edge and moving toward the edge. b) Magnified image showing the individual domain joins the existing structure. c) The assembly of liquid crystal domains before complete drying. The scale bar is 200 μm for a) and 20 μm for b) and c).

The droplets in Figure 8.7 c) are about 3-4 μm in diameter. From the birefringence and fluidity of the droplet, it is apparent that the droplets are domains of

liquid crystals[21]. Also the individual domain kept sparkling until the drop dried completely. The sparkling of the individual domains or droplets is due to the fluctuations of the optic axis of the nematic phase driven by thermal energy.

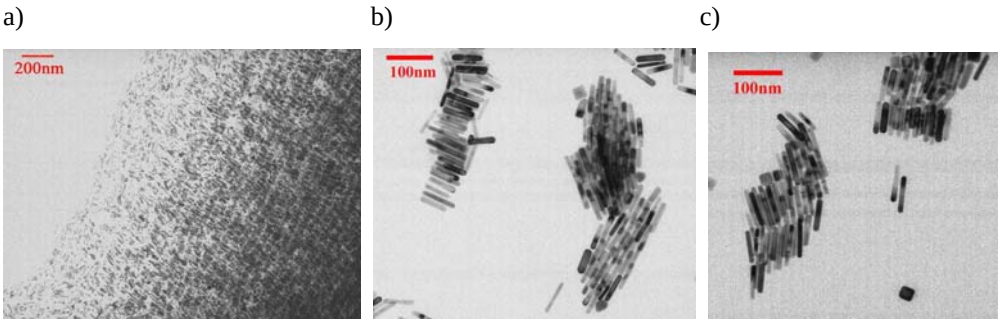

Figure 8.8. TEM images of a dried drop of gold NR solution. a) The edge of the drop showing smectic-like structure. b) and c) show the small size of nematic-like domain away from the edge.

The drop of gold NRs was evaporated on a TEM grid and taken to the TEM observation. Figure 8.8 shows the self assembly of gold NRs in a dried drop. The outer ege consists of monolayer of NRs and the NRs lie parallel to the interface of air and the solution. Moving towards inside, the thick layer of smectic-like structure of band width of a few hundred micrometers is found (a). Also, the reminiscence of the nematic domain is found as shown in (b) and (c) away from the edge. These self assemblies confirmed that as the concentration of gold NRs increases, NRs form a small domain of nematic phase as they are draged towards the edge and go through nematic-smectic transition as the domains join the existing structure.

Thus we observed the dynamic phase transition from isotropic to lyotropic liquid crystals. This phase transition was confirmed to be reversible by rewetting the dried sample. To our knowledge, the liquid crystalline phase of gold NRs as well as the coffee ring patterns formed by liquid crystals has never been reported.

The change of the orientation in assembly of gold NRs resembles disclinations in a nematic LC (Figure 8.9 (a) and (b)). Interestingly, when the observation was made at tilted angle, what appears to be nanosphere turns out to be NRs standing on the grid ((c) and (d)). Thus we were able to visualize the core of defect. Although no theory can describe the molecular configuration near the core of the defect[22], LC of gold NRs will be useful in solving the structure of the core of the defect.

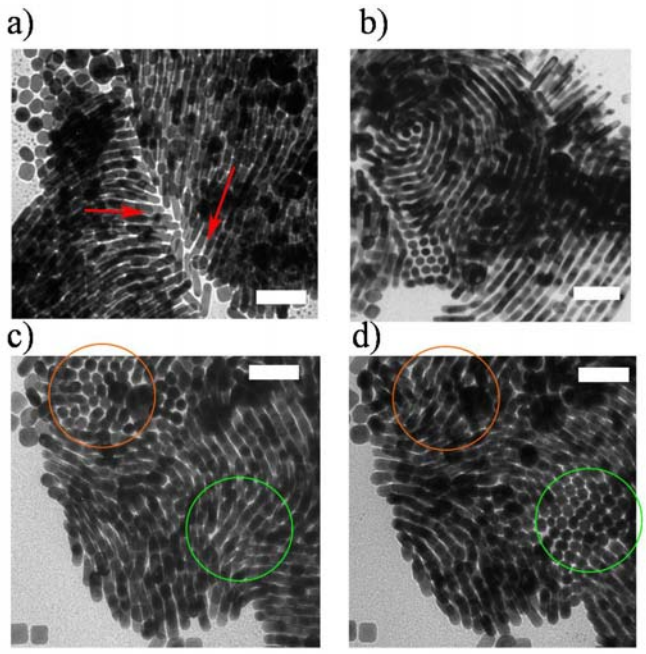

Figure 8.9. TEM images of assembly of gold NRs[23]. a) and b) show the change of the orientations in assembly of gold. c) and d) show the identical areas with tilted angle. The scale bar is 100nm.

8.3.3. Two dimensional phase transition observed in self assembly on a TEM

To examine NR assembly systematically by TEM, a drop of 4 μl gold NRs solution was deposited on a carbon coated copper TEM grids and the solution was slowly evaporated in a closed environment. Evaporation rate is further lowered by placing small beaker containing water inside the chamber. As the solvent evaporated, instead of forming the coffee ring stain, LC phase was uniformly formed on the grid (Figure 8.10).

a) b)

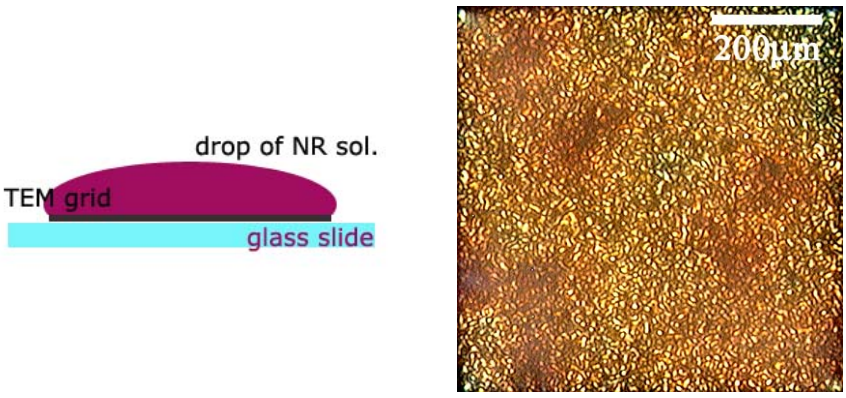

Figure 8.10. a) A schematic showing the preparation of a gold NR assembly on a TEM grid, b) A polarizing microscope image showing LC phase uniformly formed over the grid during the evaporation.

The completely dried sample was observed with TEM. Inhomogenity of local concentration of gold NR solution caused the different self assembly of NRs on the substrate (Figure 8.11). At low number density, 2 to 4 NRs form aggregates and exist sparsely in an isotropic state. As the number density increases, NRs start to

form a monolayer of partially nematic-like phase. With further increase of number density, NRs form smectic-like phase. For short NRs (aspect ratio is 3), the smectic-like assembly showing both orientational and positional order was observed (Figure 8.12). The ordered assembly was observed for the very long NRs (aspect ratio is 14). In this case, even though the suspension contains some of the spherical byproducts, phase transition from isotropic to nematic and smectic phase can be confirmed by the self assembly of dried suspension (Figure 8.13).

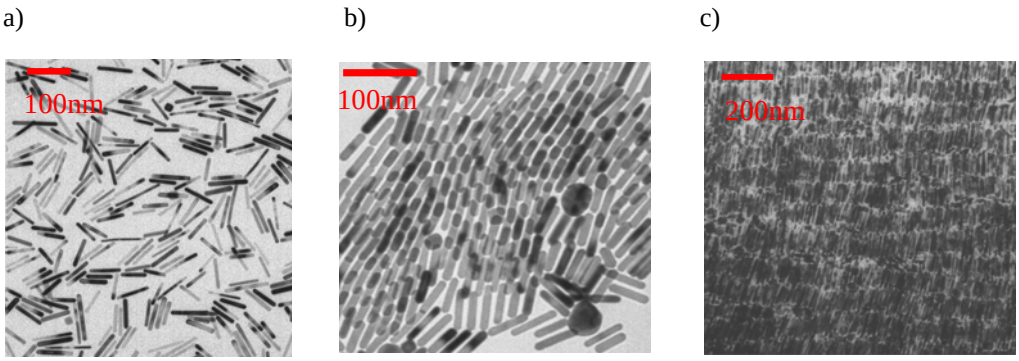

Figure 8.11. TEM images of gold NR assembly. Aspect ratio is 6. a) Isotropic phase b) nematic-like assembly, and c) smectic-like assembly.

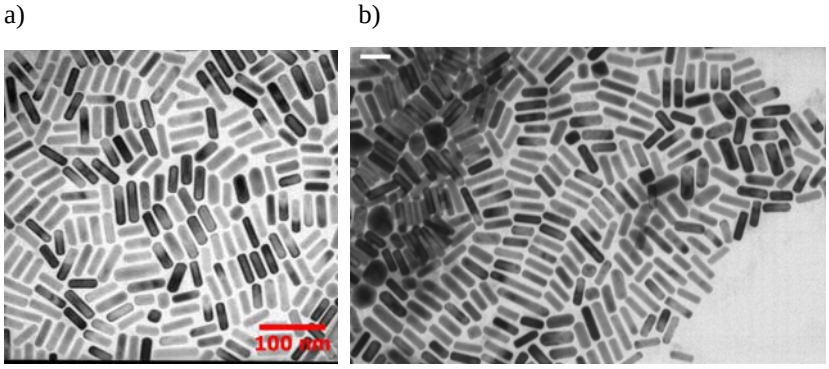

Figure 8.12. TEM images of gold NRs assembly. Aspect ratio is 3. a) Isotropic phase and b) transition from isotropic to smectic-like assembly.

a) b)

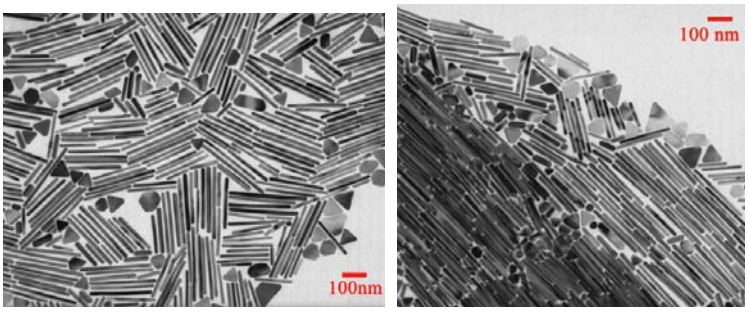

Figure 8.13. TEM images of gold NRs assembly. Aspect ratio is 14. a) Isotropic phase and b) nematic-like assembly.

The order parameter was measured to characterize the liquid crystalline phase. The angle between the director and the long axis of each rod was measured and the 2 dimensional order parameter, $S = \langle \cos 2\theta \rangle$ was calculated for NRs of two different aspect ratios (L/d=3 and 6) and plotted as a function of number density (

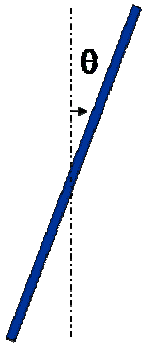

Figure 8.14).

a) b)

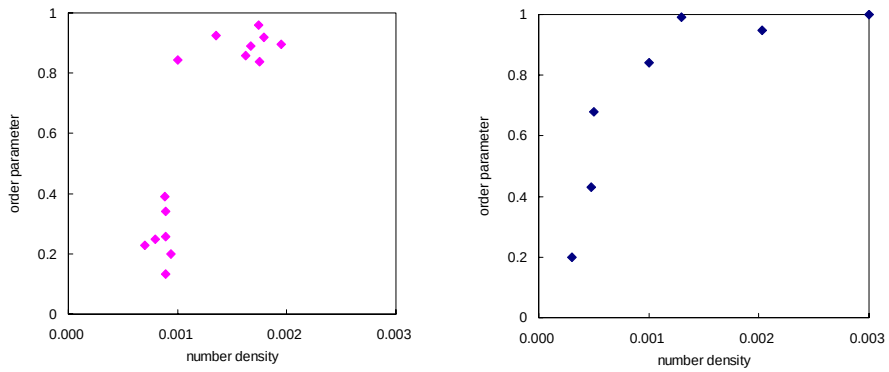

Figure 8.14. Measured values of the gold NRs number density and the order parameter, S. (a) The aspect ratio is 3 and (b) the aspect ratioj is 6. Number density was calculated by counting the number of NRs per 10000nm^2.

Bates el al. studied two-dimensional hard rod fluids consisting of spherocylinders confined to lie in a plane using Monte Carlo simulations[24]. For long rods, a 2D nematic phase is observed at high density. The transition from this phase to the low density isotropic phase is continuous. For short rods the nematic phase disappears so that, the solid phase undergoes a first order transition directly from smectic to an isotropic phase. We found in our experiments that transition from isotropic to higher order structure is continuous for longer NRs but for shorter NRs isotropic phase undergoes a first order transition directly to an smectic phase. These results are in good agreement with the simulations.

8.3.4. Patterns formed by LC in evaporating solution.

Figure 8.15 shows the deposit resulting from dried drops of different initial volume fraction of gold NRs (aspect ratio 6) and evaporation conditions arranged left to right in order of decreasing volume fraction of gold NRs. For each image, a drop of 2μl gold NR solution was placed on the glass slide, which resulted in fluid films of 3mm in diameter on the substrate.

The upper row shows the images of dried deposit from the slow evaporation. In this case, the substrate was kept in a closed environment. It takes 1hr for the drop

to be completely dried. We only observed the formation of single ring/band at the contact line regardless of the volume fraction of the solute. The width of the band decreases as the volume fraction of NRs decreases.

The bottom row shows the images of dried deposit from the fast evaporation. In this case, the substrate was kept in open environment until the water evaporates completely. The time to complete the evaporation is about 11mins. In (f) there is a dark ring formed at the edge. As the volume fraction decreases, we observed multiple rings formed interior of this ring while the width of the ring also slightly decreased (g, h and i). Upon further decreasing concentration, very thin ring was formed without additional rings inside (h).

The patterns formed by various concentrations can be visualized by polarized optical microscopy because of the birefringence of ordered assembly of gold NRs, and is shown in Figure 8.16.

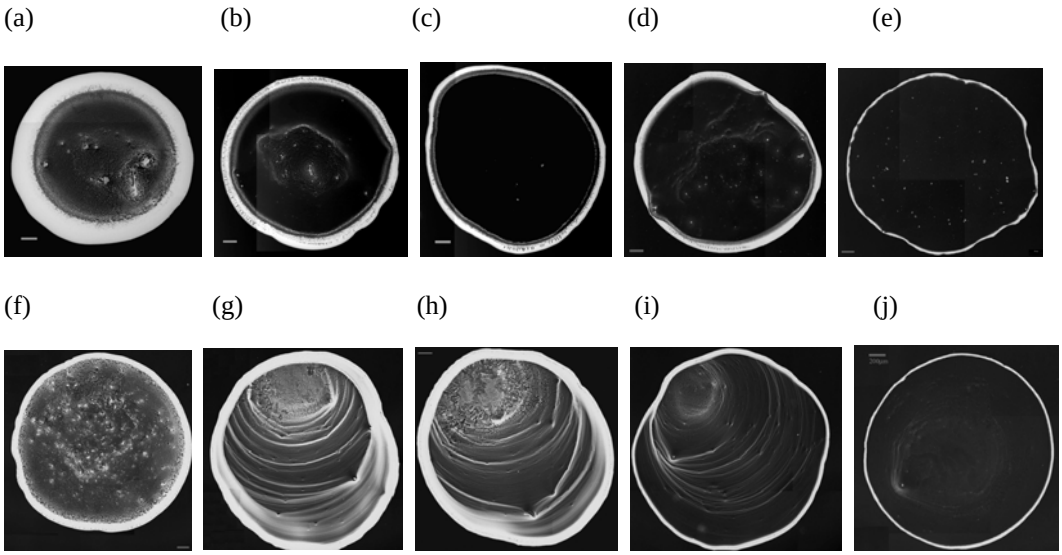

Figure 8.15. "Coffee stain" formed by drying drops of gold NR solution. The images in the upper row show the drying drops from slow evaporation. The volume fraction decreases from left to right: a) 1×10^{-5} , b) 5×10^{-6} ,c) 3.3×10^{-6} d) 2.5×10^{-6} and f) 1.25×10^{-6}. The images at the bottom row are from fast evaporation. The volume fraction of the drops in the same column is identical. The scale bar is 200μm.

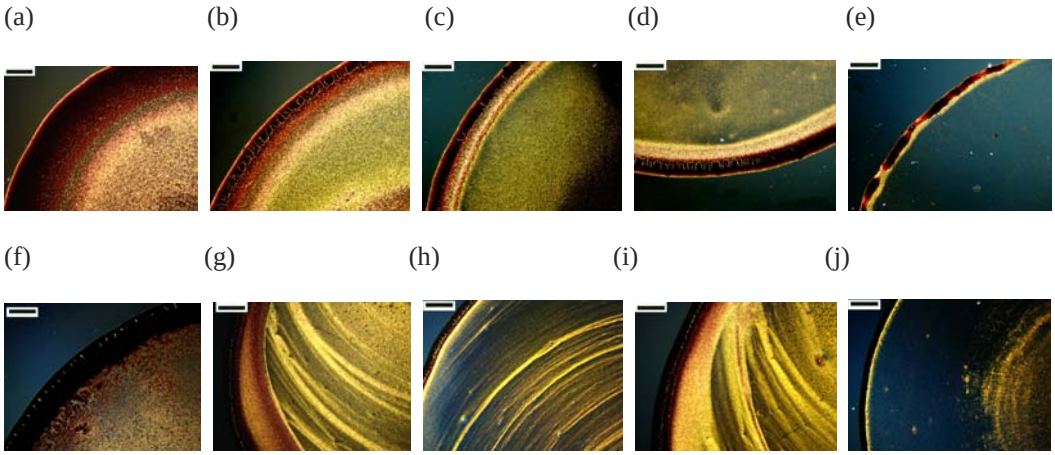

Figure 8.16. The patterns formed by various concentrations and different evaporation condition were visualized by polarized optical microscopy for the samples shown in Figure 8.15. Only the edge areas are illustrated. The scale bar is 200μm.

The multiple ring pattern formation has been observed when a suspension droplet dries on a solid substrate[25-28]. It can be understood by a similar mechanism to that of the "coffee stain" formation and closely related to the receding of contact line. A suspension of latex particles has been usually chosen to investigate this phenomenon. Adachi et al.[25] examined the drying process and found that the droplet contact line shrinks toward the center of the droplet with an oscillatory motion causing generation of particle array film at the contact line. Deegan[26] further studied the parameters affecting the patterns of dried drops and found that depending on the concentration and the size of the drop, multiple rings with different sub-structure were formed. Recently, this mechanism has been adapted to prepare ordered structure of NPs and biomolecules[27,28].

The particles assemble to form a ring at the droplet contact line due to the convective flow induced by the evaporation of water from the filmsurface near the contact line. In the case of gold NRs, the observation of the drop through polarized microscopy gives the opportunity to examine the dynamic process of assembly due to the formation of LC phase. While the birefringent contact line grows to a band with the emerging LC droplets from the interior, the contact line shrinks toward the center. The area where the contact line passes, birefringence becomes weaker. The bright band seems to move inward because only the leading edge shows intense

birefringence. The relation between a change in the velocity of particles and that of the shrinking contact line is the key to understand the various patterns observed.

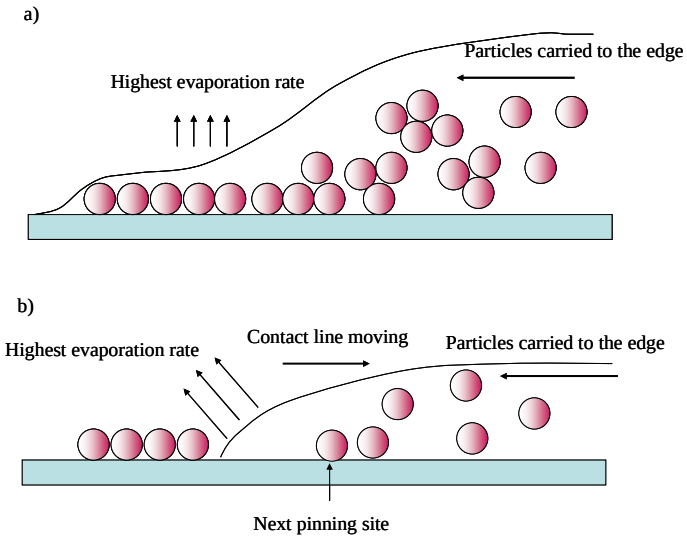

Figure 8.17. a) A schematic shows the accumulation of gold NRs at the contact line in the case of slow evaporation. Most of the particles can be carried to the edge forming a single dark ring. b) In the case of fast evaporation, contact line starts to recede while the particles move toward the edge resulting in the space between pinning sites.

When the evaporation is slower, the contact line is pinned long enough that a large contact line deposit can form resulting in a single ring which contains most of the particles in solution. And the width of the ring depends on the initial concentration of gold NRs. When the evaporation is faster, the contact line starts to shrink before enough amount of gold NRs accumulate at the outer edge leaving the spaces between the rings. And the shinking contact line drags the particle toward to the center. The contact line is arrested again when considerable amount of particles accumulates and the rings chronicle the moments of arrested contact line motion (Figure 8.17).

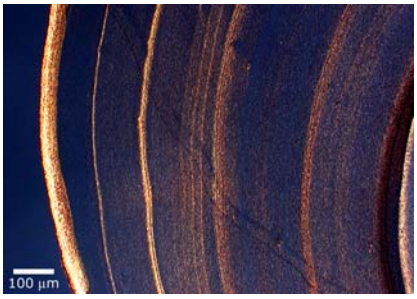

Figure 8.18. The well defined concentric multiple ring pattern formed by diluted gold NR solution. The image is taken under optical microscope with cross polarizers. The scale bar is 100 µm.

Figure 8.18 shows the well defined concentric multiple ring pattern that forms on evaporation. The distance between the contact lines as well as the time between pinning and sticking events do not show periodicity. Therefore the motion of the contact line can not be described as a simple sinusoidal response. We believe that with precise control of the drop size, roughness of the substrate and evaporation condition (inadvertent liquid heating caused by droplet illumination), one might obtain better data to conduct more systematic analysis of the multiple ring patterns.

8.4. Conclusions

We presented experimental results on the observation of lyotropic LC phase of gold NRs. The dynamic phase transition was observed by evaporating drops of gold NR solution on a glass slide. As the solution evaporates, the particles are carried toward the contact line causing the local concentration near the contact line to become higher than transition concentration. The evaporation rate and concentration of the

solute play an important role in determining not only the pattern of "coffee stain" but also the multiple ring formation. We found that the pinning/depinning motion of the contact line is responsible of this phenomena. But in our observation, the motion of the contact line is essentially stochastic. We believe that the ability to deposit a ring and multiple rings of gold NRs on a solid substrate provide potential for surface-patterning applications.

References

[1] Zocher, H. “Uber freiwillige Strukturbildung in Solen (Eine neue Art anisotrop flqssiger Medien) ” *Z. Anorg. Allg. Chem.* **1925,** *147,* 91.

[2] Langmuir, I. “The role of attractive and repulsive forces in the formation of tactoids, thixotropic gels, protein crystals and coacervates”, *J. Chem. Phys.* **1938**, *6*, 873.

[3] Bawden,F.C.; Piries,N.W.; Bernal, J.D.; Fankuchen, I. “Liquid crystalline substances from virusinfected plants” *Nature* **1936**, *138*, 1051.

[4] Buining, P. A.; Philipse, A. P.; Lekkerkerker, H. N.W. “Phase Behavior of Aqueous Dispersions of Colloidal Boehmite Rods” *Langmuir* **1994**, *10*, 2106.

[5] Maeda, H.; Maeda,Y. “An Atomic Force Microscopy Study of Surface Structures of Colloidal α-FeOOH Particles Forming Smectic Layers” *Nano Lett.* **2002**, *2*, 1073

[6] Vroege, G. J.; Lekkerkerker, H. N. W. **“**Phase transitions in lyotropic colloidal and polymer liquid crystals” *Rep. Prog. Phys.* **1992,** *55*, 1241.

[7] Onsager, L. “The effects of shape on the interaction of colloidal particles” *Ann. N. Y. Acad. Sci.* **1949**, *51,* 627.

[8] Bolhuis,P.; Frenkel,D. “Tracing the phase boundaries of hard spherocylinders” *J. Chem. Phys.* **1997**, *106* , 666.

[9] Maeda, H.; Maeda,Y. “Liquid Crystal Formation in Suspensions of Hard Rodlike Colloidal Particles: Direct Observation of Particle Arrangement and Self-Ordering Behavior” *Phys. Rev. Lett*. **2003**, *90*, 018303.

[10] Lamarque-Forget, S.; Pelletier,O.; Dozov, I.; Davidson,P.; Martinot-Lagarde,P.; and Livage,J. “Electrooptic Effects in the Nematic and Isotropic Phases of Aqueous V_2O_5 Suspensions” *Adv. Mater*. **2000**, *12,* 1267.

[11] Lemaire, B.J.; Davidson, P.; Ferre, J.; Jamet, J.P.; Panine, P.; Dozov, I.; Jolivet, J.P. “Outstanding magnetic properties of nematic suspensions of goethite (alpha-FeOOH) nanorods” *Phys. Rev. Lett*. **2002**, *88*, 125507.

[12] a) Kim, F.; Kwan, S.; Akana, J.; Yang, P. “Langmuir-Blodgett Nanorod Assembly”

J.Am.Chem.Soc. **2001**, *123*, 4360, b) Nikoobakht, B; El-Sayed, M. A. "Self Assembly of Gold Nanorods" *J.Phys.Chem. B.* **2000**, 104, 8635 c) Sau,T.K.; Murphy,C.J. "Self-Assembly Patterns Formed upon Solvent Evaporation of Aqueous Cetyltrimethylammonium Bromide-Coated Gold Nanoparticles of Various Shapes" *Langmuir* **2005**, *21,* 2923.

[13] a) Li,L.; Walda, J.;Manna, L.;Alivisato,A.P. "Semiconductor Nanorod Liquid Crystals" *Nano lett.* **2002**, *2*, 557 b) Li,L.; Alivisato,A.P. "Semiconductor nanorod liquid crystals and their assembly on a substrate" *Adv. Mater*. **2003**, *15*, 408 c) Li,L.; Marjanska,M.; Park, G.H.J.; Pines,A.; Alivisato,A.P. "Isotropic-liquid crystalline phase diagram of a CdSe nanorod solution" *J. Chem.Phys*. **2004**, *120*, 1149 d) Talapin, D.V.; Shevchenko, E.V.; Murray, C.B.; Kornowski, A.; Förster, S.; Weller, H. "CdSe and CdSe/CdS Nanorod Solids" *J. Am. Chem. Soc*. **2004**, *126*, 12984.

[14] van der Zande,B.M.I.; Koper, G.J.M.; Lekkerkerker, H.N.W. "Alignment of Rod-Shaped Gold Particles by Electric Fields" *J. Phys. Chem. B* **1999**, *103,* 5754.

[15] Jana, N. R.; Gearheart, L. A.; Obare, S. O.; Johnson C. J.; Edler, K.J.; Mann, S.; Murphy, C. J. "Liquid crystalline assemblies of ordered gold nanorods" *J. Mater. Chem*. **2002** , *12*, 2909.

[16] R.D. Deegan, R.D.; O. Bakajin, O.; T.F. Dupont, T.F.; G.Huber, G. ;S.R.Nagel, S.R.; Witten, T.A. "Capillary flow as the cause of ring stains from dried liquid drops" *Nature* **1997**, *389*, 827.

[17] Lee, S.J. "A numerical inverstigation of nematic ordering based on a simple hard-rod model", *J. Chem.Phys*. **1987**,*87*,4972.

[18] Hu, H.; Larson, R. G. "Analysis of the Microfluid Flow in an Evaporating Sessile Droplet" *Langmuir* 2005, 21, 3963.

[19] Dierking,I. "Textures of Liquid Crystals" 2003, Wiley-VCH, Weinheim, Chapter 3.

[20] Deegan,R.D. "Pattern formation in drying drops" *Phys.Rev.E* **2000,** *61,* 475

[21] De Gennes, P.G. "The Physics of liquid Crystals" **1974**, Oxford Univ. Press, Oxford, Chapter 3.

[22] Zasadzinski, J.A.N.; Meyer, R.B. “Molecular Imaging of Tobacco Mosaic Virus Lyotropic Nematic Phases” *Phys.Rev.Lett.* **1986,** *56*, 636.

[23] The images of a,c and d were taken by Dr. H.J.Lee at Korea Research Institute of Standards and Science using one of the gold NRs prepared in our study.

[24] Bates, M.A.; Frenkel, D. “Phase behavior of two-dimensional hard rod fluids” *J. Chem. Phys.* **2000**, *112*, 10034.

[25] Adachi,E.; Dimitrov,A.S.; Nagayama,K. “Slip stick Stripe Patterns Formed on a Glass Surface during Droplet Evaporation” *Langmuir* **1995,** *11,* 1057.

[26] Deegan,R.D., “Pattern formation in drying drops” *Phys.Rev.E* **2000,** *61,* 475.

[27] Small,W.R.; Walton,C.D.; Loos, J.; Panhuis, M. “Carbon Nanotube Network Formation from Evaporating Sessile Drops” *J. Phys. Chem. B* **2006**, *110,* 13029

[28] Smalyukh,I.I.; Zribi,O.V.; Butler,J.C.; Lavrentovich,O.D.; Wong,J.C.L. “Structure and Dynamics of Liquid Crystalline Pattern Formation in Drying Droplets of DNA” *Phys.Rev.Lett.* **2006,** *96*, 177801.

Chapter IX

Conclusions and Recommendations for the Future Work

9.1. Conclusions

The major findings of the work are summarized below:

We have shown that the morphology of gold nanorods(NRs) is controlled by manuplating the reduction rate of gold ion and the adsorption kinetics of the surfactant on the surface of gold nanoparticle. We prepared gold NRs with low polydispersity and byproducts using improved seed mediated method. With modifying the reduction steps, higher aspect ratio of gold NRs can be obtained.

We found that centrifugation can be the method of choice for the separation when the synthesis results in particles with different sizes and shapes. Different sizes and shapes of particles result in sufficiently different sedimentation coefficients leading to efficient separation of particles. Thus, the efficient separation of gold NRs from mixture of shapes was achieved by understanding the hydrodynamics of NRs and nanospheres undergoing centrifugation. The purity of the NRs is higher than 99% and the yield of separation through a round of centrifugation can be achieved up to 78% by increasing CTAB concentration which affects the colloidal interaction.

The optical properties of resulting refined gold nanorods were compared to the predictions of existing theories, and the main parameters affecting them such as aspect ratio and the dielectric properties of the environment were discussed.

Gold NRs with well defined aspect ratio were introduced into a PVA matrix by means of solution-casting techniques. The film was drawn to induce the uniaxial alignment of gold NRs to be used as color polarizing filters. We observed strong optical dichroism in the visible as well as near – IR region which can be utilized to make polarizers over a large range of wavelengths.

The various patterns of self assembly were formed by deposition of gold NR solution on a TEM grid. The different patterns can be explained by drying mediated self assembly where the coverage ratio and evaporation condition are among the important factors to determine the characteristics of the pattern.

The phase transition to a liquid crystalline phase was observed by evaporating the drop of gold NR solution on a glass microscope slide. As the solution evaporates, the particles are carried toward the contact line causing the local concentration to become higher than the concentration required for the phase transition. The evaporation rate and concentration of the solute play an important role to result in not only the pattern of the “coffee stain” but also the multiple ring formation. We

found that the pinning/depinning motion of the contact line is responsible for this phenomenon.

9.2. Recommendations for future works.

In nanomaterial research, there is rapidly growing interest in the bulk fabrication of hybrid nanostructures with discrete domains of different materials arranged in a controlled fashion. The unique characteristics of such structures are the ability to independently optimize the dimension and composition of the individual components and thus providing entirely novel properties via the coupling between components[1].

Possible routes to fabricate the building blocks for these structures include the synthesis of compositionally heterogeneous nanoparticles (usually by the growth of the 2nd component on the surface of an as-made nanoparticle), bi-phase interfacial modifications, or phase separation of bi-component mixtures on a nanoparticle surface[2,3]. Optimally, theses building blocks are designed to naturally assemble into the final structure through asymmetric particle-particle interaction. This assembly can be further directed by providing predetermined “instructions” for assembly, such as by modifying the nanoparticle surface with biomacromolecules[4].

Considering the fact that the successful applications of nanoparticles require

the ability to tune their properties by controlling size, shape and surface modifications, gold NPs are an excellent foundation to expand, given the substantial progress in the synthesis of complex shapes in the past few years[5].

We have demonstrated that different shapes of Au NPs besides nanorods can be prepared by controlling the various parameters that affect the growth kinetics. The unique surface plasmon resonance of these complex shapes endows many interesting properties such as color tunablity, enhanced fluorescence, and surface-enhanced Raman scattering. Combined, these properties make metal nanoparticles valuable candidates for future nanoelectronics and nanophotonic applications once appropriate techniques are developed to allow the controlled generation of artificial assemblies.

We suggest combining several routes to fabricate hybrid NPs including the generation of heterogeneous nanoparticles and the phase separation of bi-component mixtures on a nanoparticle surface. Fabrication of hybrid NP will involve these steps: (1) synthesis of gold NP with different morphologies (2) epitaxial growth of 2nd component on the pre-made Au NPs to generate hybrid NPs, and (3) modification of the hybrid NP surface utilizing pattern formation (phase separation) of multicomponent oligomer/polymer on the surface of the particles. These structures will be utilized in developing negative index materials and hybrid piezoelectric sensors.

References

[1] Perro,A.;Reculusa,S.;Ravaine,S.;Bourgeat-Lami,E.;Duguet, E., "Design and synthesis of Janus micro- and nanoparticles", *J.Mat.Chem*. **2005**, *15*, 3745.

[2] Roan, J. "Soft Nanopolyhedra as a Route to Multivalent Nanoparticles" *Phys.Rev.Lett*. **2006**, *96*, 248301.

[3] Glogowski, E.; He,J.; Russell, T.P.; Emrick,T. "Mixed monolayer coverage on gold nanoparticles for interfacial stabilization of immiscible fluids" *Chem. Commun*. **2005**, 4050.

[4] Park, S.Y.;Lee,J.; Georganopoulou, D.; Mirkin, C.A.;Schatz,G.C. "Structures of DNA-Linked Nanoparticle Aggregates" *J. Phys. Chem. B* **2006,** *110*, 12673.

[5] Pérez-Juste,J.; Pastoriza-Santos ,I.; Liz-Marzán ,L.M.; Mulvaney, P. "Gold nanorods: Synthesis, characterization and applications" *Coordination Chemistry Reviews* **2005**, *249*, 1870 and referencestherein.